



UNIVERSITY
OF TRENTO - Italy

Department of Materials Engineering
and Industrial Technologies

Doctoral School in Materials Engineering - XXII cycle

Synthesis and Characterization of Luminescent Nanostructured SiOC Thin Films

Aylin Karakuşcu

Tutor: Prof. Gian Domenico Sorarù



January 2010

Doctoral Thesis

**Synthesis and Characterization of Luminescent
Nanostructured SiOC Thin Films**

Aylin Karakuşcu

Tutor

Prof. Gian Domenico Sorarù

Doctoral Committee:

Prof. Alberto Molinari

Prof. Marjorie Olivier

Prof. Nikolaos E. Zafeiropoulos

Biricik Anneannem
Yasar Kidan'a,

Table of Contents

Abstract.....	i
Introduction.....	1
Chapter I. Literature Review.....	5
1.1. Polymer Derived Ceramics.....	5
1.1.1. Sol-Gel Method.....	6
1.1.2. Types of PDCs Produced by Sol-Gel Method	9
1.1.2.1. SiOCs	9
1.1.2.2. SiBOCs.....	13
1.1.3. Polymer Pyrolysis Method.....	14
1.1.4. Types of PDCs Produced by Polymer Derived Method.....	15
1.1.4.1. SiCNs and SiOCNs	15
1.2. Thin Film Production and Spin Coating.....	19
Chapter II. Characterization Techniques.....	22
2.1. Thermal and Structural Analysis	22
2.1.1. TGA.....	22
2.1.2. Dilatometer Measurements.....	22
2.1.3. FTIR	22
2.1.4. NMR	23
2.1.5. EPR	24
2.1.6. X-ray Diffraction (XRD)	26
2.1.7. Elemental Analysis	26
2.1.8. XPS	27
2.1.9. Mass Spectroscopy	27
2.2. Surface Properties and Thickness Analysis	28
2.2.1. SEM and FE-SEM	28
2.2.2. AFM	29
2.2.3. Profilometer	29
2.2.4. SIMS.....	29

2.2.5. Ellipsometer	30
2.3. Surface contact angle and Energy measurements	31
2.4. Optical Analysis of Materials	31
2.4.1. Photoluminescence	31
2.4.2. UV-Vis analysis	32
Chapter III. Synthesis and Characterization of SiOC gels and powders	33
3.1. Background information	33
3.2. Experimental details	34
3.3. Results	35
3.3.1. Gel characterization	35
3.3.2. Gel-to-Ceramic transformation	41
3.3.3. Structural characterization of the SiOC glasses	42
3.3.3.1. NMR Study	42
3.3.3.2. EPR Study	43
3.3.3.3. XRD study	48
3.3.3.4. Laser Ionization Time of Flight Mass Spectrometry Study	50
3.4. Discussion	50
3.5. Conclusions	52
Chapter IV. Processing and Characterization of SiOCs films	53
4.1. Background information	53
4.2. Experimental Details	54
4.3. Results And Discussion	55
4.4. Substrate Effect	82
4.5. Stability Measurements/ Weathering Resistance	89
4.6. Shrinkage behaviour of SiOC films and powders	91
4.6.1. Background information	91
4.6.2. Experimental	93
4.6.3. Results and Discussion	95
4.7. Conclusions	99
Chapter V. Other systems studied	101
5.1. SiBOC Ceramics	102

5.1.1. Experimental Details	102
5.1.2. Results And Discussion	103
5.2. SiBOC films	108
5.2.1. Experimental Details	108
5.2.2. Results And Discussion	109
5.3. SiOCN Films	117
5.3.1. Experimental Details	117
5.3.2. Results And Discussion	118
5.4. Conclusion	128
6. Conclusion on PhD study.....	130
References	133
Appendix	147
Part I. External Quantum Efficiency of SiOC samples	147
Part II. Lifetime measurements	155
Acknowledgement.....	159
CV.....	161

Abstract

A new approach to obtain visible luminescence from sol-gel derived SiOC films is proposed. This novel method is based on a simple processing route to produce nanostructured multicomponent ceramics. According to this route, hybrid sol-gel derived precursors are converted to ceramic materials by a pyrolysis process in controlled atmosphere at 800-1000°C. Higher temperatures lead to formation of Si-rich SiOC, C-rich SiOC or stoichiometric SiOC according to the starting composition. The final composition, which is relevant to line emission, can be easily controlled through a number of processing parameters like the composition of the preceramic gel and the heat treatment conditions. Thus, this new processing method seems very well suited for the production of white emitting materials since the Si- and C-based emission can be tuned across the visible spectral range from UV-blue to red by controlling film composition. A further advantage of this method is that the thin films can be formed on Si or quartz wafers and this can serve as starting material to process more complex photonic devices such as waveguides or LEDs.

In the amorphous state (800-1000°C), all SiOC films showed UV-blue luminescence peaking at about 410 nm, which is attributed to defect states present in the matrix such as dangling bonds. The increase of the pyrolysis temperature ($\geq 1100^\circ\text{C}$) led to the partition of SiOC and formation of SiC, C and Si phases. The intense green-yellow luminescence observed in stoichiometric SiOC films caused by the presence of SiC and very low amount of free C. On the other hand, Si rich SiOC film showed a very broad and extremely intense white luminescence peak centred at 620 nm covering almost all visible range (430 nm-900 nm) at 1200 °C. This behaviour is explained by the simultaneous presence of SiC, C and Si in the film. External quantum efficiency measurements yielded 11.5% and 5% efficiencies in Si rich SiOC and stoichiometric SiOC films, respectively, pyrolysed at 1200°C. On the other hand, C rich SiOC films did not show any noticeable improvement in PL, indicating that C excess in the SiOC system is detrimental for the luminescence behaviour.

Solutions which used in thin film production have been characterized extensively by means of several characterization properties. Moreover, the related powders and bulks

have been characterized for the sake of coherency and widen the study. In addition, a study on volumetric shrinkage of films and powders has been done. The results showed that the shrinkage in films happens almost 200°C earlier than powder and higher amount of siloxane release due to the low dimension, the shrinkage is higher than powders.

The last part of the study dedicated to two different systems, SiBOCs and SiOCNs, in order to understand the effect of the boron addition on SiOC system and study the optical properties of the SiOCN. Tunable (color emission change) SiOC films is obtained with high quantum efficiency by adding very few amount of boron in SiOC. Moreover, the processing temperature is decreased and very broad emission is obtained. Finally, results showed that SiOCN PDC gives very high emission in UV range and they are promising materials for UV-LEDs.

Introduction

Historically, the interest for the polymer pyrolysis route to advanced ceramics (PDC route) was driven by the search for ceramic fibers with high thermo-mechanical performance [Verbeek, 1973; S. Yajima, 1976]. A peculiar feature of the new processing route is the possibility of producing ceramics at lower temperatures compared to the classical ceramic production from powders. This property made the PDCs possible candidates for producing glow plugs for diesel engines, micro-gears, micro-cellular foams and brakes [R. Riedel, 1995]. The recent studies are focused on more complicated structures like MEMs [L.A. Liew, 2001]. Moreover, some unexpected properties were reported such as electrical, magnetic, optical properties and high temperature viscoelasticity [P. A. Ramakrishnan, 2001; A. Saha, 2003; J. C. Pivin, 2000; A. Scarmi, 2005].

In the literature optical properties of PDCs have been mentioned only few times but the preliminary results suggested that they can be good candidates for LEDs [J. C. Pivin, 2000, G. Das, 2008, G. D. Soraru, 2003]. However, almost none of the reported works focused only on optical properties of the PDCs but, indeed, the optical characterization was in general presented as a complementary result. Therefore, we aimed to perform a complete study on optical properties of PDCs.

In literature two classes of PDCs have been studied; SiOCs and SiCNs. SiOCs have been studied more by sol-gel method instead the SiCNs are produced by the polymer pyrolysis method [Greil, 2000]. Since most of the commercial precursors of SiCNs contain abundant amount of graphitic carbon, which are known to absorb visible light, in principle, they could not suit very well for optical application. On the other hand, many studies on SiOCs showed the possibility of varying the composition in a very wide range from Si rich SiOC system to stoichiometric SiOC (used to express that it contains very few amount of free carbon) or C rich SiOC [G. D. Sorarù, 1995]. It has been indicated that the compositional changes can be achieved just by changing few experimental details. Therefore, in our study we have focused on the sol-gel method to produce different types of SiOCs, with the aim of characterizing their optical behaviour and to correlate it with their nanostructure.

From a technological point of view, for many years worldwide research has been focused on finding Si based material to be used as LED due to mature technology of Si. Si has been investigated and several other matrixes or doping elements have been reported to increase the efficiency of the Si based LEDs. On the other hand, C, when it is in the cluster size, is known to give emission. Therefore, working on Si-rich and C-rich SiOC as well as stoichiometric will give a more complete vision about optical properties of the SiOCs.

Most of the LED fabrication is based on thin film production on a semiconductor substrate. This choice can be explained thinking that film production is faster and lower amount of material is required when we compare them with powders or bulk samples. Therefore, the study is based on production of the SiOC films. The film production consists of the following steps: (i) solution preparation and spin coating, which takes couple of hours and (ii) drying stage, which requires only 1 day at 80°C. After these two steps the films can be stored for several months. Since the resultant films are very thin (around 300 nm), only very low amount of material is required and very large areas can be coated easily. On the other hand, almost one month is necessary for bulk/powder preparation. Indeed, in these cases the gelation is slow and the drying step is quite longer compared to thin films.

Another key advantage of the films above bulk/powders is higher compositional/structural homogeneity which can be achieved due to the very low diffusion distance of the film compared to bulk/powders. It is well known that the long diffusion distance that the gases produced during pyrolysis have to go through to reach the sample surface may be the reason for the compositional gradient often found in bulk PDC [T. Rouxel, 2001]. Therefore, the limited thickness of the film should give us the possibility to decrease the diffusion distance and as a result, it is expected that thin film will show homogeneous and reproducible characteristic.

On the contrary, due to very low thickness, the films they are very difficult to characterize with by means of classical methods (SEM, XRD, NMR etc.). Especially the structural analyses are very hard to perform on films. Moreover, the SiCO films are expected to be amorphous and this reduces even more the range of characterization

techniques which can be successfully applied. Accordingly, several advanced characterization methods such as XPS, SIMS, ellipsometer, ATR-FTIR have been used to understand the films deeply. Sometimes to give more accurate information about one property several methods have been used and reported in this study (e.g. for thickness measurements ellipsometer, FE-SEM, profilometer have been used). As a result the SiOC films with different compositions have been characterized by means of several different characterization methods and it has been demonstrated that they are very promising materials for LED applications with their high efficiencies.

A part of this study has also been dedicated to the characterization of powder samples. The reason for this being the fact that powders can be characterized easier (with conventional techniques like XRD, TG/DTA, NMR etc) than thin films. However, we are aware of the fact that, due to the different diffusion distance of powders and thin films (less than 500 microns compared to less than 10 microns) the structure and composition of the two set of samples can be slightly different and this possible difference has always been taken in to account in our analysis. A particular study, aimed to find out possible differences in the pyrolytic conversion of thin films and bulk samples has been carried out comparing the shrinkage during pyrolysis of the two set of samples.

Finally, to widen the perspective of SiOCs, some other systems, SiBOC and SiOCN, have been examined. These studies have been performed to test the possibility to improve the optical properties. The study on boron added SiOC films is devoted to optical properties and it showed that different range of colors (tunable films) with high optical efficiency can be obtained by adding very small amount of boron. To clarify the effect of boron we have characterized the SiBOC structure on powdered samples.

Finally we have also performed the optical characterization of a SiOCN PDC system. In this case the material has been obtained by pyrolysis of a commercial polymer. Since this system is rich of free carbon the optical characterization has been limited to samples pyrolyzed at low temperatures, when the graphitic phase is not yet fully developed. Accordingly, we found that SiOCN PDC show very high emission in UV range and they are promising materials for UV-LEDs.

This thesis consists of six chapters and starts with a short literature survey aiming to explain in details the materials and their structure/properties, the production methods and the review of the work done until now. The following chapter (**Chapter 2**) gives the experimental details of the measurements performed during all through the PhD study. For the sake of the coherency, the study on SiOC gels and powders which is linked to SiOC films is reported in **Chapter 3**. In this chapter, SiOC gels, which are used to produce film and relevant powders pyrolysed at different temperatures, were characterized. The **Chapter 4**, which is the main part of the PhD study, focuses only on SiOC thin films with different compositions. Many different characterization methods have been reported in this section (AFM, SEM, FE-SEM, FTIR, DCA, profilometer, SIMS, XPS, GA-XRD, UV-VIS, PL measurements, Stability measurements-Weathering Resistance). This chapter ends with a comparison of two systems (film and bulk) by means of shrinkage during pyrolysis. Finally, **Chapter 5** is given as a collection of all the other studied systems (SiBOC and SiOCN). These chapters are completed by the conclusion of PhD study and references.

Chapter I. Literature Review

1.1. Polymer Derived Ceramics

Polymer Derived Ceramics (PDCs) have been proposed over 30 years ago as precursors for the fabrication of mainly Si-based advanced ceramics. Advanced non-oxide Si-based materials such as Si_3N_4 , or SiC are commonly produced by inorganic solid state reactions at high temperatures. For instance SiC is synthesized by the reaction of silica with carbon according to the Acheson process at 2200°C . Furthermore, silicon nitride is fabricated either by the reaction of the elements or by the nitridation of silica in the presence of carbon at the 1500°C . Moreover, to get a compact product from these powders, high sintering temperatures in the range of $1700\text{-}2100^\circ\text{C}$ and the addition of sintering aids have to be used because of their predominantly covalent nature.

In the early 70s, the first works appeared in the literature which showed that highly refractory SiC ceramics could be produced at much lower temperature $800\text{-}1200^\circ\text{C}$ by thermal decomposition of organosilicon preceramic polymers polymer [Verbeek, 1974; G. Winter, 1975]. In 1976 the pioneering work of Yajima [S. Yajima, 1976] in Japan showed that SiC ceramic fibers with excellent high thermal stability could be produced by pyrolysis in inert atmosphere of polycarbosilane precursor fibers. This process is called preceramic polymer pyrolysis and recently several groups has been working on this subject in order to improve the processing as well as finding new application fields [R. Riedel, 1995].

Polymer Derived Ceramics (PDCs) can be considered as a new family of nanostructured ceramic materials derived from inorganic polymeric precursors [R. Raj, 2001]. According to this route, the pre-ceramic polymer is shaped, cross-linked and pyrolyzed in controlled atmosphere (inert or reactive) at temperature exceeding 800°C and converted into self-similar ceramic devices and components [X. Liu, 2009]. PDCs have shown extraordinary properties, especially at ultra-high temperature such as oxidation and creep resistance [S. Modena, 2005; L. An, 1998], chemical durability [G.D. Soraru, 2002], electrical conductivity (from insulating up to semiconducting behaviour) [S. Trassl, 2003] and photo and electro-luminescence [Loner, 2001]. Such unusual

properties originate from the very peculiar nanostructure of these ceramics in which various nanocrystalline phases grow in-situ into an amorphous C-containing matrix [A. Saha, 2006; G. Gregori, 2006].

Nowadays, polymer derived method has been used not only to process ceramic fibers but also to produce some complex Si-C-O, Si-(E)-C-O, Si-C-N and Si-(E)-C-N (E = B, Al, Ti etc.) ceramic systems (polymer derived ceramics, PDCs) which can not be synthesized *via* other methods [A. Quaranta, 2009]. A large variety of precursors for ceramic products in the compositional systems such as Si-N, Si-C-N, Si-O-C, Si-C-Al-O-N have already been synthesized, most of them in laboratory scale. **Figure 1.1** presents a scheme of major silicon containing preceramic polymer systems [Greil, 2000].

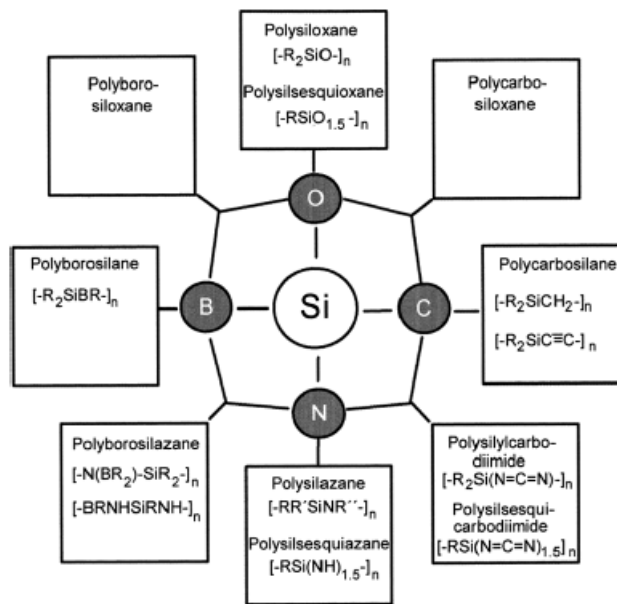


Figure 1.1. Preceramic polymer compositions in the system Si-O-C-N-B [Greil, 2000].

1.1.1. Sol-Gel Method

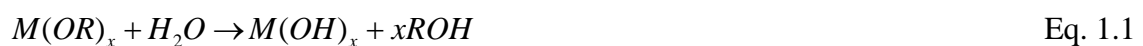
The sol-gel method is relevant in the PDCs technology since it allows the synthesis of pre-ceramic networks with tailored chemical composition which can be subsequently pyrolyzed to get SiOC glasses with controlled composition and nanostructure.

Sol-gel process can be categorized into three routes. The first one called “colloidal” method involves the dispersion of colloidal particles in a liquid to form a sol and then the destabilization of the sol to produce a gel which is subsequently dried, to form a porous ceramic, and fired to crystallize and/or densify the material [J.D. Mackenzie, 1988]. The second method involves the production of powders precipitated from the sol. The resulting powders are then dried and processed using traditional ceramic processing techniques. The third approach is the polymerization of organometallic compounds such as alkoxides to produce a gel with a continuous network [Mehrotra, 1990].

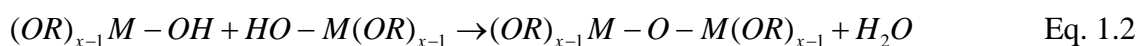
A “colloid” is a suspension in which the dispersed phase is so small that gravitational forces are negligible and interactions are dominated by short-range forces, such as van der Waals attractions and surface charges. The inertia of dispersed phase is so small that it exhibits Brownian motion, a random walk driven by momentum imparted by molecules of the suspending medium. A “sol” is a colloidal suspension of solid particles in a liquid [C.J. Brinker, 1990].

Most typical sol-gel precursors are metal alkoxides. Metal alkoxides have the general formula $M(OR)_x$ where M is a metal or a metalloid element and R is an alkyl or related group. The applicability of metal alkoxides for the sol-gel technique is determined by their solubility, volatility (in order to purify the precursors) and their oligomerization capability. Oligomerization of the metal alkoxides affects the homogeneity of the final product.

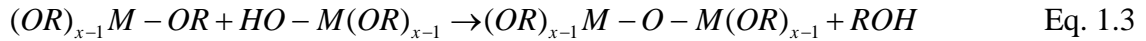
In general, sol-gel technique is based on the hydrolysis of the metaloxide and further condensation reactions of the fully and/or partially hydrolysed alkoxides to corresponding oligomeric species. The reaction is called hydrolysis, because a hydroxyl ion becomes attached to the metal atom



Two partially hydrolyzed molecules can link together in a condensation, such as



or



These reactions cause the formation of a metal-oxygen-metal bridge, which constitutes the backbone of any oxide ceramic structure. Continued condensation leads to an increase in the density of metal-oxygen-metal cross-links until eventually gelation or precipitation occurs [J. B. Wachtman, 1993].

The basic principle of the sol-gel process is to form a solution of the elements of the desired compounds in an organic solvent, polymerize the solution to form a gel, and dry and fire this gel to displace the organic components and form a final inorganic oxide.

Important and typical precursors for making sol-gel solutions are alkoxides of the general composition $M(O-R)_n$, where R is an alkyl radical (CH_3 , C_2H_5 , etc.). Their properties and reactions affect the preparation process and determine the product features. Inorganic and organic salts can also be used for introducing some oxides into multicomponent systems. The precursors are dissolved in a suitable organic solvent to form the solution. In order to get the solution with a high concentration of necessary components and proper viscosity, surface tension and boiling point, the solvent must be carefully selected.

In order to obtain a suitable solution for making films, various properties of solution are adjusted. Different precursors show a wide range of reactivity toward H_2O which makes the preparation of multicomponent homogeneous systems difficult and also presents difficulties with premature gelation during film processing. The gelation of a solution means the formation of a network in the solution. The hydrolysis and polycondensation of organometallic compounds such as alkoxides leads gelation. During the drying stage the wet coating is converted to a relatively dry, harder coating and considerable shrinkage of the coating occurs. It is at this stage that problems related to film cracking and surface smoothness in the final film become most acute. The annealing step converts the gel coating into a densified complex oxide film. This process includes the removal of residual $-OH$ or $-OR$ groups by polycondensation reactions, pyrolysis of the

organic compounds or groups left in the film into carbon, oxidation of the carbon, and gradual densification of the film [Karakuscu, 2006].

1.1.2. Types of PDCs Produced by Sol-Gel Method

1.1.2.1. SiOCs

Silicon oxycarbide glasses are amorphous solids derived from the structure of silica glass in which part of the divalent oxygen atoms have been replaced with tetracoordinated carbon atoms. The ideal composition of a silicon oxycarbide phase consisting only of Si-O and Si-C bonds, with no Si-Si, C-O, and C-C bonds, is $\text{SiC}_x\text{O}_{2(1-x)}$, in which one tetravalent carbon atom substitutes for two divalent oxygen atoms. This substitution leads to the presence, in the amorphous network, of carbidic carbon units, $[\text{C}(\text{Si})_4]$, which strengthen the structure by increasing its bond density. Thus, all of the physical and chemical properties directly related to the structure of the amorphous network, such as the elastic modulus, hardness, density, viscosity, glass transition temperature, and chemical durability, are expected to increase with the amount of incorporated carbon. Moreover, it is possible to have nano-sized SiC from the oxycarbide glass by in situ formation at high temperatures ($\geq 1400^\circ\text{C}$). Silicon oxycarbide glasses can be produced by pyrolysis in an inert atmosphere of polysiloxanes. These precursors can be synthesized via the sol-gel route starting from organically modified silicon alkoxides, $\text{R}'_x\text{-Si}(\text{OR})_{4-x}$. R' is usually a methyl group. However, other organic groups containing more C atoms were introduced in silica gels such as ethyl, propyl, phenyl or vinyl. In contrast, with phenyl or unsaturated side chains, the residual C content is much higher and leads to the formation of an important free carbon phase. Methyl-substituted silica gels thus appear as the most suitable precursors for silicon oxycarbide glasses [G. D. Sorarù, 1995].

The composition regimes of SiOC system are shown in the composition diagram in **Figure 1.2**. Amorphous phase is generally formed in carbon-rich regimes, relative to the stoichiometric mixtures of the crystalline forms. The possibility of synthesizing PDC of different composition in the ternary Si-C-O phase diagram depends from the possibility of synthesizing pre-ceramic precursors with tailored architecture and chemical composition [S. Dirè, 1999; Sorarù, 1994]. Accordingly, stoichiometric silicon

oxycarbide glasses, whose composition lies on the tie line between SiC and SiO₂ (indicated with arrow in **Figure 1.2**), have been obtained from pre-ceramic polymers with tailored composition [G. D. Sorarù, 1995]. This result has been achieved using the sol-gel method for the synthesis of the pre-ceramic network. Indeed, the sol-gel process gives the possibility, through the use of different molecular precursors, to precisely tailor the composition of the resulting polymeric network [G. D. Sorarù, 1995(b)]. Moreover, the sol-gel method allowed the formation of PDC compositions inside the Si-SiO₂-SiC compatibility triangle [H. Bréquel, 2004] and even in the binary Si-SiO₂ system [D'Andrea, 1995]. These last compositions are actually used for the synthesis of Si/SiC nanocrystals and of Si nanocrystals embedded into an amorphous SiO₂ matrix, respectively [A. Karakuscu, 2009].

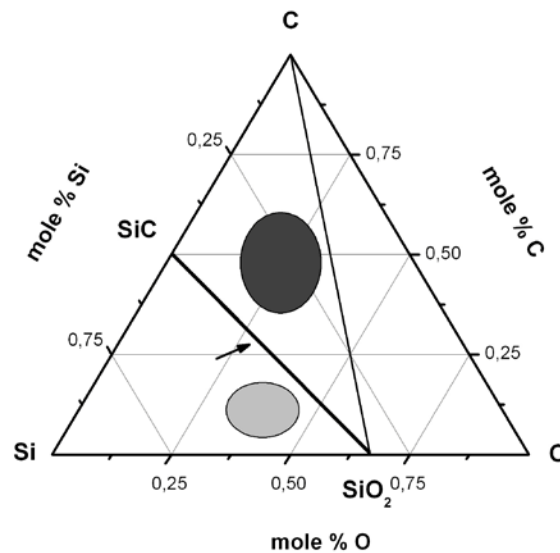


Figure 1.2. Composition regime for polymer-derived ceramic (PDC) silicon oxycarbides. Circles with dark gray color represent the well studied area in the literature. The circle with light gray color indicates the Si-rich SiOC region and the arrow shows the stoichiometric SiOC line [A. Karakuscu, 2009].

PDCs are intrinsically fairly complex systems, as they undergo profound modifications, when exposed to temperatures higher than the usual pyrolysis conditions (1000°C). At elevated temperature, a devitrification process of the initial amorphous network leads to a local crystallization of different phases. This process is linked to the redistribution of the chemical bonds, phase separation and finally nucleation and growth of nanocrystals.

The modifications occurring within these amorphous materials strongly depend on the starting composition. Nevertheless, some major common aspects can be recognized: (i) during annealing, the entire bulk of these materials undergo a phase separation process; (ii) the free carbon phase-when present undergoes a graphitization process; (iii) with increasing temperature, the local formation of nanocrystals is typically observed [Greil, 2000].

The modelling of SiOC system is a very recent subject. Although some models are proposed, there are still some open points in the literature about the structure of SiOC. Kroll modelled the “free carbon” phase in silicon oxycarbide glasses using a low-density structure of a-SiOC, into which a part of the graphite structure is embedded. This work based on comparing stoichiometric SiOC ($\text{SiC}_{0.33}\text{O}_{1.33}$) with SiOC containing “free carbon” ($\text{SiC}_{0.33}\text{O}_{1.33} + 0.62\text{C}$) (**Figure 1.3**). A treatment at 800°C shows the reaction of the “free carbon” phase with the surrounding a-SiOC host by multiple bond formation, resulting in a decrease of the total energy. Further annealing at 1600°C decreases the energy further, but the more radical conditions also create a particular interface structure between segregation and host. The weakness of the modelling lies on the fact that H is not involved in the modelling and it has been known that H release in SiOCs may continue till high pyrolysis temperatures ($\geq 1200^\circ\text{C}$) [Kroll, 2005].

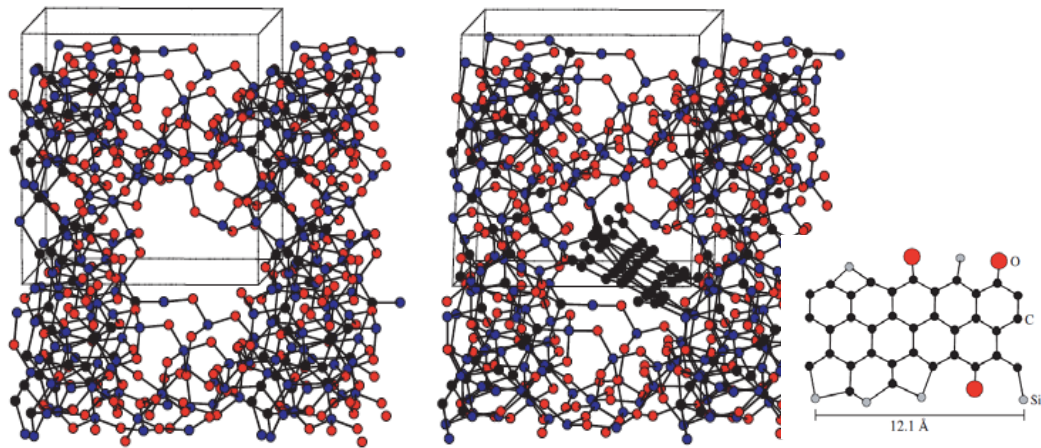


Figure 1.3. Left: The initial structure of $\text{Si}_{48}\text{C}_{16}\text{O}_{64}$. Right: The model of a-SiOC: Cf , $\text{Si}_{48}\text{C}_{16}\text{O}_{64} + 30\text{C}$, with the carbon strip inserted into the pore after the annealing at elevated temperatures (3 ps at $T = 800^\circ\text{C}$ and 5 ps at $T = 1600^\circ\text{C}$). For both structure the simulation box is outlined. **Inset.** The bonding environment of the graphitic segregation of the model of a-SiOC: Cf . The periodicity and the length of the simulation box in the direction of the carbon strip is indicated [Kroll, 2005].

Another model is proposed for the nanodomains in polymer-derived SiOC. This model is constructed from three constituents: clusters of silica tetrahedra that form the heart of the domain, the surrounding monolayer of mixed bonds of the type $\text{SiC}_n\text{O}_{4-n}$ where n gives the fourfold coordination of silicon to carbon and oxygen, and the graphene cage-like network that encases the domains. The carbon bonded to silicon is called sp^3 or carbidic carbon and the carbon in graphene is sp^2 or graphitic carbon. A conceptual molecular make up of such a structure is drawn in **Figure 1.4** [A. Saha, 2006].

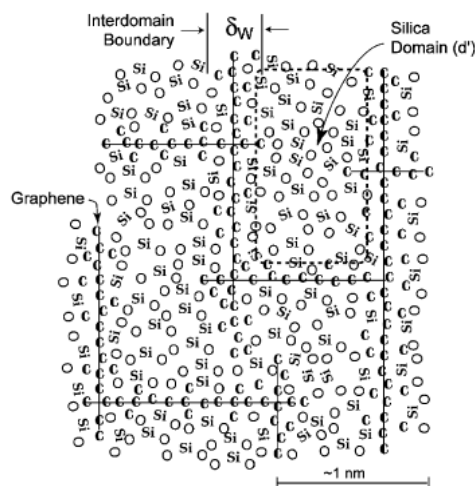


Figure 1.4. A concept of the molecular make-up of the nanodomains. Note that the interdomain boundary consists of graphene layers with mixed Si–C–O bonds forming the interface with the silica domains [A. Saha, 2006].

The model predicts the domain size as a function of the carbon content. These predictions found to be in reasonable agreement with the measurements of the nanodomains in SiOC synthesized with varying carbon contents. However, similar to previous model, it is only based on high temperature behavior of the ceramic and do not contain hydrogen contribution at lower temperatures. Meanwhile, this model is the most accepted model on high temperature behavior of the SiOC recently.

1.1.2.2. SiBOCs

SiBOC system is a very recent subject which has been first mentioned in 1998 [G. D. Soraru F. B., 1998]. Studies in the literature showed that, when boron is introduced in SiOC system, β -SiC crystallization is enhanced while it inhibits the formation of crystalline SiO₂. Thus, the matrix and surface cracking associated with the phase transformation of cristobalite during cooling and heating, which could deteriorate the mechanical strength, can be avoided. Boron also promotes the formation of the borosilicate clusters in terms of amounts and size.

At $T \geq 1500$ °C, boron was found to enhance the growth of segregated sp²-carbon nanocrystals. Nanocrystalline sp² C forms thicker graphite nanocrystals in SiBOC

system. Therefore, SiBOC system has been proposed as a possible candidate for Li ion batteries since highly porous SiBOC with ordered graphite nanocrystals can be obtained after etching [R. Peña-Alonso, 2007]. However, limited studies have been found in literature on SiBOC system and therefore, it remains as an open field with undiscovered properties and applications.

1.1.3. Polymer Pyrolysis Method

Polymer pyrolysis method starts with the synthesis of the precursor polymers or oligomers from monomer units. The precursors are then cross-linked in order to form organometallic pre-ceramic networks three dimensions. The organometallic networks are transformed into amorphous covalent ceramics by heat treatment (organic/inorganic transition) in controlled atmosphere (Ar, He, N₂, etc.). Additionally, the amorphous ceramics can be crystallized by further annealing at high temperature. **Figure 1.5** describes a flow chart for the standard preparation process of precursor-derived ceramics [Peng, 2002].

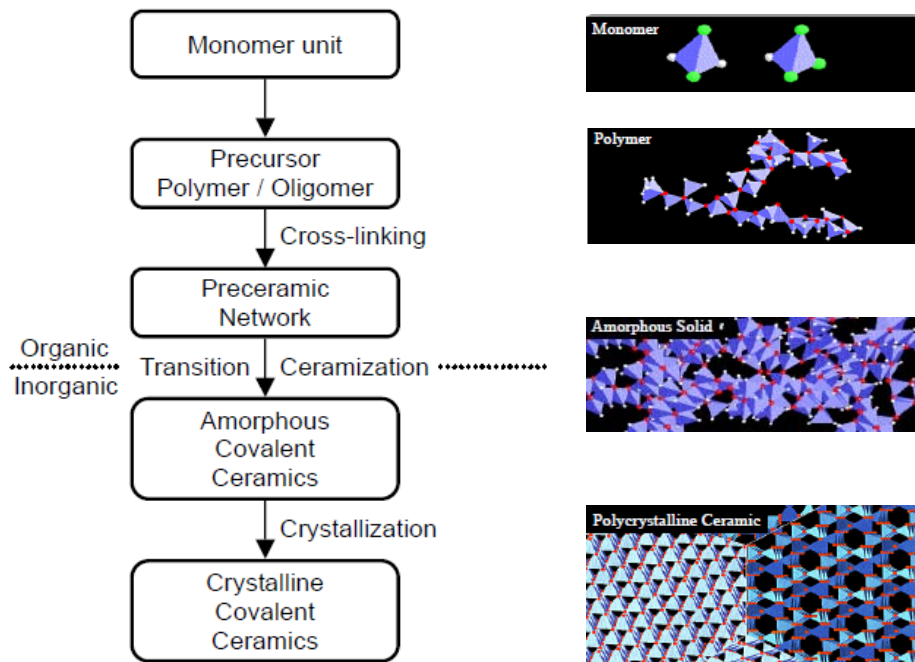


Figure 1.5. A flow chart for the preparation of precursor-derived ceramics [Peng, 2002].

Typical reactions during the polymer pyrolysis are shown as follows to produce SiN or SiN/SiC composite from polysilazane [R. Riedel, 1995]:

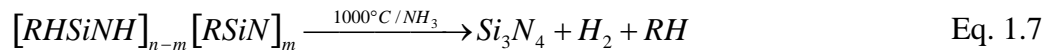
- i. Synthesis of Si-based oligomers or polymers from low molecular weight compounds:



- ii. Enhanced chemical or thermal cross-linking of the as-synthesized polymers giving high molecular weight compounds suitable for polymer-to-ceramic transformation with high yields:



- iii. Finally, pyrolysis of the cross-linked polymer providing the desired ceramic material:



1.1.4. Types of PDCs Produced by Polymer Derived Method

1.1.4.1. SiCNs and SiOCNs

In SiCN system, upon pyrolysis at 1000°C, the structure of these amorphous materials can be generally described as a random network of Si–C–N atoms. However, if the carbon fraction present in the starting precursor is high enough, then, upon pyrolysis, part of it remains excluded from the “silicon backbone” constituting the amorphous network and creates the so-called (excess) free carbon phase. Further thermal treatments at temperatures above 1000°C induce the rearrangement of the amorphous network the main aspects of the structural evolution of PDCs upon annealing at temperatures

exceeding 1000°C [M. Monthieux, 1996]. It has been reported via TEM analysis that free carbon was the first phase to crystallize, irrespective of the Si/C ratio in the considered system, giving origin to the basic structural units (BSUs) of graphitic carbon. The excess of carbon seemed to stabilize the network hindering the nucleation of SiC crystals. However, at 1484°C (N₂-atmosphere, 1 atm), the carbothermal reduction of silicon nitride occurs:



which is generally considered as the onset of the material degradation.

Carbothermal reaction and the compositional changes during the heat treatment of SiCNs is given in **Figure 1.6**. The general composition of polysilazane-derived ceramics can be given as Si_{3+x}C_{x+y}N₄, which is shown as **A** in **Figure 1.6-a**, remains metastable at T<1440°C. Above this temperature (T>1440°C) SiCNs give off nitrogen till the system reaches the tie line composition as Si_{3+x}C_xN₄, which is shown as **B** in **Figure 1.6-b**, and finally crystallises to give Si₃N₄ and SiC [D. Galusek, 1999].

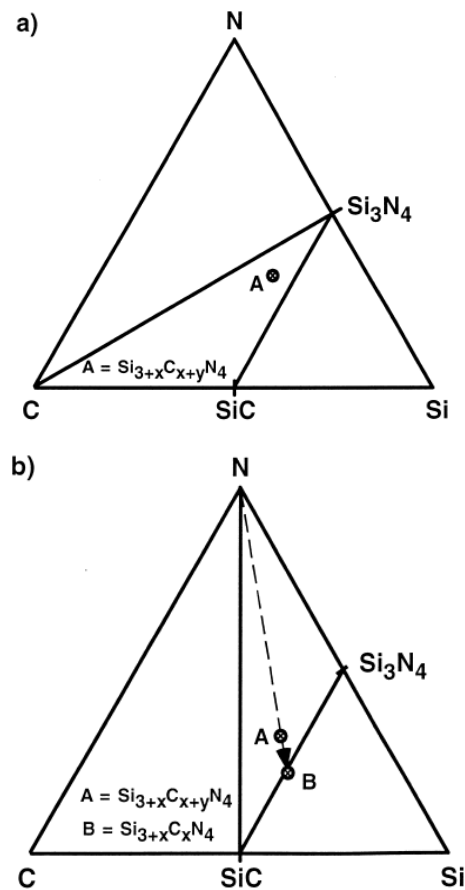
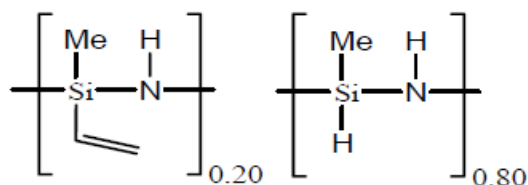


Figure 1.6. Schematic illustration of amorphous poly(hydridomethyl)silazane derived SiCN after pyrolysis at (a) $T \leq 1440^\circ\text{C}$ and (b) its crystallisation path at $T > 1440^\circ\text{C}$, in respective isothermal sections of the ternary SiCN phase diagram. Compositions are given in atom% and the oxygen content in amorphous SiCN is neglected [D. Galusek, 1999].

In the literature, usually no differentiation has been done between SiCN and SiOCN due to the experimental difficulties to avoid oxygen contaminations during the synthesis of SiCN system. Therefore, SiCNs nearly always contain significant amounts of oxygen [T. J. Cross, 2006]. Due to this, many experiments on SiCN (even not always mentioned) have been done in glove box system and treated under very pure atmospheres. Correspondingly, ammonia atmosphere has found to be the only proper atmosphere to produce pure SiCN without oxidation [T. Cross, 2006(b)]. However, this property of polysilazanes makes the processing complicated and lowers the commercialization. Therefore, in our work, we aimed to produce SiOCN films in laboratory conditions with stable oxidation to simplify the production process and

compare the optical properties with the SiOC system. For this purpose, we have used a commercial polysilazene namely Ceraset® (KiON) having relatively low reactivity toward oxygen. Its chemical structure is shown in **Figure 1.7** [Ceraset®].



KiON Ceraset Polysilazane 20

Figure 1.7. Chemical structure of the polysilazane, Ceraset®-KiON [Ceraset®].

Ceraset Polysilazane is versatile, low viscosity liquid thermosetting resin. It has been patented and known as “KiON Ceraset Polysilazane 20”. This polysilazane contains repeat units in which silicon and nitrogen atoms are bonded in an alternating sequence and cyclic and linear features exist.

According to the studies in literature, the cross-linking solidification of CerasetTM takes place around 250°C by hydrosilylation of vinyl groups followed by a transamination reaction between 280°C and 400°C [Y.-L. Li, 2001]. During the subsequent ceramization step, the major thermolysis reaction involves dehydrogenation between Si-H and N-H groups, and condensation of Si-CH₃ and N-H groups around 600-800 °C. These reactions yield an amorphous Si-C-N ceramic accompanied by the formation of the gaseous by-products of hydrogen and methane. Further heat treatment at high temperature induces the Si-C-N ceramics to crystallize into nano-sized silicon carbide and silicon nitride [H. Schmidt, 2004].

Curing can be achieved at lower temperatures through the addition of a small quantity of a free radical generator, typically peroxide. Typically 0.1 wt% to 5 wt% of the peroxide are sufficient to initiate curing. Dicumyl peroxide is soluble in the liquid polymer and typically about 0.5 – 1wt% peroxide based on the weight of the polymer is used. This peroxide/polymer solution is stable at room temperature for at least six months. Heating the peroxide/polymer solution causes the peroxide to undergo decomposition into radical species which initiate the thermosetting reaction. At

temperatures above 150°C the thermosetting is rapid and may be extremely exothermic. This converts liquid polysilazane based resins to a solid, cross-linked polymer.

1.2. Thin Film Production and Spin Coating

In recent years, thin film science has grown world-wide into a major research area. The importance of coatings and the synthesis of new materials for industry have resulted in a tremendous increase of innovative thin film processing technologies. Currently, this development goes hand-in-hand with the explosion of scientific and technological breakthroughs in microelectronics, optics and nanotechnology [R.W. Siegel, 1997]. Presently, rapidly changing needs for thin film materials and devices are creating new opportunities for the development of new processes, materials and technologies.

There exists a huge variety of thin film deposition processes and technologies which originate from purely physical or purely chemical processes. The more important thin film processes are based on liquid phase chemical techniques, gas phase chemical processes, glow discharge processes and evaporation methods [D. A. Glocker, 1998]. Conventional CVD and PVD processes are used routinely to synthesize thin film systems. Such process technologies are rather complex and expensive. On the other hand, sol-gel is inexpensive and enables the synthesis of thin film materials with complex chemical compositions. The main advantage of sol-gel method is the high degree of compositional control, inherent with other solution synthesis routes for multi-element, inorganic materials. Therefore, it is proposed to be one of the key technologies to synthesize epitaxial oxide, nitride and carbide films for a variety of different applications, e.g. opto-electronic device applications, hard coatings and dielectric thin films [Wegner, 2000].

Spin coating method is widely used to prepare thin films from sol-gel or polymer solutions. In general, four distinct stages of the spin coating process are reported to be crucial for homogeneity of the films [D.E. Bornside, 1987]. As it is shown in **Figure 1.8**, the first stage is the deposition of the coating fluid onto the substrate. Usually this dispense stage provides a substantial excess of coating solution compared to the amount that will ultimately be required in the final coating thickness. For many solutions it is often beneficial to dispense through a sub-micron sized filter to eliminate particles that

could lead to flaws. Indeed, in our studies we have used a filter with 0.2 μm pore size to overcome this problem as well as avoid the impurities. Another potentially important issue is whether the solution wets the surface completely during the dispense stage. If not, then incomplete coverage can result.

The second stage is when the substrate is accelerated up to its final desired rotation speed. This stage is usually characterized by aggressive fluid expulsion from the substrate surface by the rotational motion. The third stage is when the substrate is spinning at a constant rate and fluid viscous forces dominate fluid thinning behaviour. This stage is characterized by gradual fluid thinning. Fluid thinning is generally quite uniform, though with solutions containing volatile solvents; it is often possible to see interference colours “spinning off”, and doing so progressively more slowly as the coating thickness is reduced. Edge effects are often seen because the fluid flows uniformly outward, but must form droplets at the edge to be flung off. Thus, depending on the surface tension, viscosity, rotation rate, etc., there may be a small bead of coating thickness difference around the rim of the final substrate.

The fourth stage is when the substrate is spinning at a constant rate and solvent evaporation dominates the coating thinning behaviour. As the prior stage advances, the fluid thickness reaches a point where the viscosity effects yield only rather minor net fluid flow. At this point, the evaporation of any volatile solvent species will become the dominant process occurring in the coating. In fact, at this point the coating effectively “gels” because as these solvents are removed the viscosity of the remaining solution will likely rise.

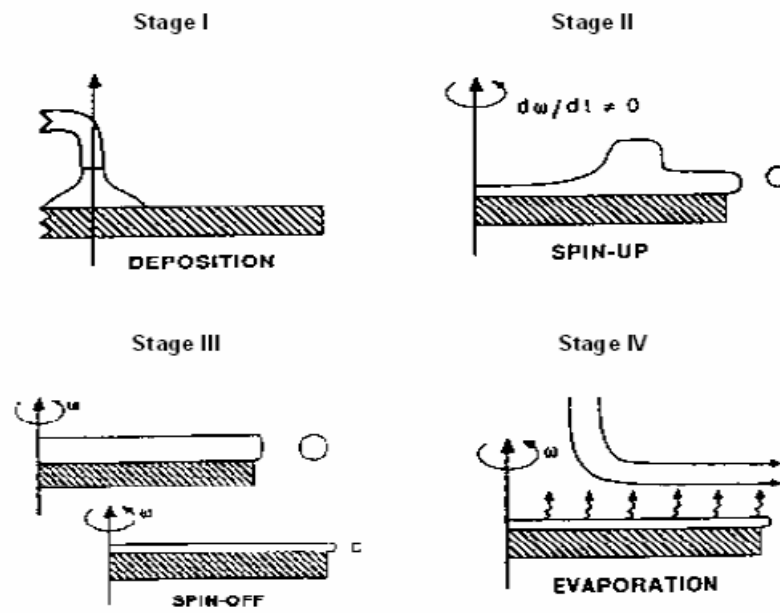


Figure 1.8. Stages of the spin coating process [D.E. Bornside, 1987].

The third stage is when the substrate is spinning at a constant rate and fluid viscous forces dominate fluid thinning behaviour. This stage is characterized by gradual fluid thinning. Fluid thinning is generally quite uniform, though with solutions containing volatile solvents; it is often possible to see interference colours “spinning off”, and doing so progressively more slowly as the coating thickness is reduced. Edge effects are often seen because the fluid flows uniformly outward, but must form droplets at the edge to be flung off. Thus, depending on the surface tension, viscosity, rotation rate, etc., there may be a small bead of coating thickness difference around the rim of the final substrate. The fourth stage is when the substrate is spinning at a constant rate and solvent evaporation dominates the coating thinning behaviour. As the prior stage advances, the fluid thickness reaches a point where the viscosity effects yield only rather minor net fluid flow. At this point, the evaporation of any volatile solvent species will become the dominant process occurring in the coating. In fact, at this point the coating effectively “gels” because as these solvents are removed the viscosity of the remaining solution will likely rise.

Chapter II. Characterization Techniques

2.1. Thermal and Structural Analysis

2.1.1. TGA

Weight loss of the powdered sample was followed by thermogravimetric analysis (TGA) in a STA 409 Netzsch apparatus. It should be noted that, weight loss of the samples gives valuable information about not only the temperature stability but also the pyrolysis nature (decomposition, reactions and ceramic yield, etc.) of the sample. TGA method is one of the most crucial methods for the PDCs due to the importance of the ceramic yield.

In the TGA experiments, inert gas (Ar and N₂) was used in order to avoid oxidation. Experiments were performed under Ar flow of 100 ml/min with a heating rate of 10°C/min. Sample weight losses were examined up to 1500°C in order to see the high temperature stability of the investigated systems.

2.1.2. Dilatometer Measurements

Dilatometric experiments were performed in order to investigate the thermal expansion of the gel. By this method, total shrinkage during pyrolysis in inert atmosphere up to 1400°C has been studied. Disc samples having approximately 1.5 mm thickness and 7.7 mm diameter were obtained by cutting and polishing of a dried gel rod. Samples were loaded into Netzsch 402/E dilatometer and the expansion and contraction of the sample along its diameter was recorded as a function of temperature. Experiments were performed under Ar (100 ml/min) with a heating rate of 5°C/min.

2.1.3. FTIR

Bonding structure of the films, gels and pyrolysed samples were investigated by Fourier-Transform Infrared Spectroscopy (FTIR). Fittings of the possible components were done by dmfit program [D.Massiot, 2002]. Nicolet Avatar 330 FTIR was used in

transmission mode to follow the structural evolution with increasing pyrolysis temperature for the all samples on Si substrate. For the films made on SiO₂ substrate, reflectance mode of FTIR (Attenuated total reflection-FTIR, ATR-FTIR) was used. In this method, a single ZnSe crystal has been used and the typical measurement condition is shown in **Figure 2.1**. In this method an infrared beam is directed onto an optically dense crystal with a high refractive index at a certain angle. This internal reflectance creates a transient wave that extends beyond the surface of the crystal into the sample held in contact with the crystal. This transient wave protrudes only a few microns (0.5 μ - 5 μ) beyond the crystal surface and into the sample [PerkinElmer, 2009].

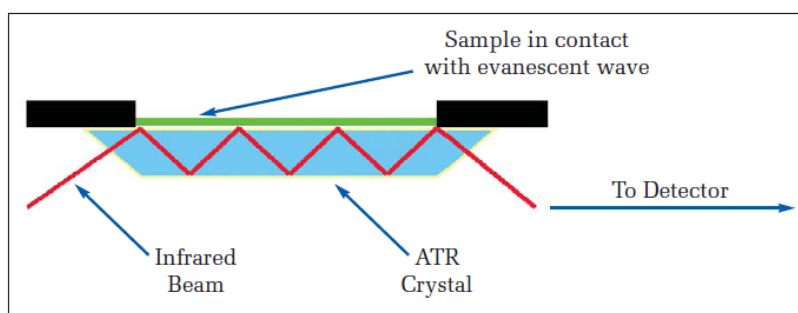


Figure 2.1. Schematic of experimental set up of Attenuated total reflection-FTIR (ATR-FTIR) [PerkinElmer, 2009].

2.1.4. NMR

²⁹Si and ¹³C solid-state NMR were employed to study the structure of the gels and pyrolysed samples. The investigations are primarily focused on the characterization of the amorphous gel structure, where NMR has been known to be very suitable. In addition, NMR data are provided for the transformation from the organic (gel) to inorganic (powder pyrolysed at 1000°C) state.

Solid State NMR experiments were carried out on a Bruker Avance 400 WB spectrometer, operating at 79.493 MHz for ²⁹Si and 100.145 MHz for ¹³C. Samples were packed in 4 mm diameter zirconia rotors. Experimental conditions for ²⁹Si MAS was 4.3 μs 90° pulse, -2dB power, 20s for recycle delay, and 8 kHz of rotating speed. Q8M8 was used as primary shift scale references for ²⁹Si. For ¹³C NMR, CP with proton

decoupling, -0.5 db of power and 4 us of power length, rotating speed of 8 kHz, 15 s of recycle delay and 200 scans was used.

2.1.5. EPR

The EPR spectra are conventionally detected by modulating the applied magnetic field with an oscillating magnetic field (lock-in detection), which makes spectrum looks like the first derivative of the EPR absorption. Bruker Elexsys E500 equipped with a Bruker SHQ resonator is used in all measurements. All the measurements were performed at room temperature and quartz sample tubes were used. The acquisition parameters are very important for EPR measurements. The modulation frequency kept at 100 kHz and the modulation amplitude depended on the spectrum and is specified for each sample. the analog-digital conversion time (ADCT), which determined the vertical resolution and the amplitude of the signal, was set to 10 ms. the receiver time constant (time constant of a filter in the acquisition system), determined the signal-to-noise ratio by filtering out the high frequency noise- the larger the time constant, the higher the SNR- was set to 1.28 ms.

The intensity I is the surface under the absorption spectrum, therefore it is the double integral of the EPR spectrum and it is calculated by numerical double integration of the EPR spectrum.

$$I = \int_{-\infty}^{+\infty} dB_0 \int_{-\infty}^{B_0} f(B_0') dB_0' \quad \text{Eq. 2.1}$$

The intensity is proportional to the absolute quantity of spins in the sample tube. To be comparable, the intensities of different EPR spectra must normalized with respect to instrumental parameters and to sample mass:

$$I_{norm} = \frac{I}{ADCT \times \text{modulation amplitude} \times \sqrt{\text{microwave power} \times 10^{\text{receiver gain} / 20} \times \text{sample mass} \times \text{nb of scans}}} \quad \text{Eq. 2.2}$$

Sample dependent parameters have been given in the following table (**Table 2.1**) to report the details of the EPR measurements of all samples. Analyses were done in

Laboratoire de Chimie de la Matière Condensée de Paris, France, under supervision of Dr. Laurent Binet.

Table 2.1. EPR measurement details

Sample	Temperature	Modulation amplitude (G)	Microwave power (mW)	Receiver gain (dB)
T ^H D ^H ₁	800°C	0.2	0.016	55
	1000°C	0.2	0.032	40
	1200°C	0.2	0.032	30
	1400°C	0.2	0.127	50
T ^H D ^H ₂	800°C	0.5	0.02	50
	1000°C	0.5	0.12	30
	1200°C	0.5	0.12	30
	1400°C	0.2	0.12	20
T ^H	800°C	0.2	0.05	50
	1000°C	0.2	0.05	40
	1200°C	0.2	0.05	60
	1400°C	0.5	0.05	60

Experimental ESR spectra represent absorption derivative with respect to the magnetic field. All spectra were normalized with sample mass and with respect to relevant experimental parameters (receiver gain, modulation amplitude, microwave power, ADC conversion time), so that the intensities of the spectra are comparable. The magnetic fields were also rescaled to a common microwave frequency: 9.385634 GHz, so that the line positions are also comparable. *g*-values were calculated by following equation:

$$g = \frac{714.484 \times 9.385634(\text{GHz})}{\text{resonance field (Gauss)}} \quad \text{Eq. 2.3}$$

The resonance field (absorption maximum) is measured at the intercept with the baseline. Spin concentrations were calculated from the ESR intensity (= double integral of the ESR spectrum). A DPPH standard sample containing a known spin quantity was used to calibrate the ESR intensity.

2.1.6. X-ray Diffraction (XRD)

Glancing angle mode was used for the XRD analysis of films since this method gave the possibility to get more information from the film rather than substrate which is most of the time amorphous SiO₂. X-ray diffractometer (Bruker D8 Advance Super Speed) is equipped with Cu rotating anode (wavelength 0.154 nm) and Goebel mirror (horizontal divergence 0.03° FWHM) yielding 10⁹ photons/s in the primary beam. Analyses were performed in Institute of Inorganic Chemistry of Slovak Academy of Sciences, Bratislava, Slovakia.

On the other hand, focusing method of XRD was used for powdered sample characterization. X-Ray diffraction analysis was conducted (Model D/Max-B, Rigaku Co., Tokyo, Japan) at 40 kV and 30 mA with CuK α radiation ($\lambda=0.15418$ nm) and a graphite monochromator. The data collection was conducted in the range $2\Theta = 10^\circ$ - 90° with a step of 0.1 and an acquisition time of 20 sec. X-ray characterization yielded not only the information about the microstructure of the samples but also the information about the particle sizes. The evaluation of crystalline particle size was estimated by Scherer formula.

2.1.7. Elemental Analysis

The quantitative analysis of oxygen and hydrogen was performed with ELTRA ONH 2000 instrument. The elements N, H and O can be analyzed individually or simultaneously over a wide range of sample matrixes and concentrations. The basic principle of quantitative analysis is high temperature combustion of organic and many inorganic solid or liquid samples. The gaseous combustion products are purified, separated into their various components and analyzed with an Infrared detector (IR) in the case of oxygen and Thermo conductivity detector (TCD) in the case of nitrogen and hydrogen.

Quantitative determination of carbon was done using ELTRA CS 800 C/S instrument. This system is the capable instrument based on combustion technique for the rapid simultaneous or individual determination of carbon and sulphur in steel, metals, alloys, ores, ceramics, minerals, etc. This instrument can be supplied with up to four

independent infrared cells. The respective cells with the appropriate path length and sensitivity can be individually selected to offer optimum precision for the analysis of high and low levels of both sulphur and carbon. Elemental analysis of SiOC powders were performed in University of Stuttgart, Max Planck Institute for Metals Research (Germany).

2.1.8. XPS

XPS analyses have been devoted to obtain the surface concentration for the elements of interested and a possible difference in chemical bonding. XPS analysis depth is around 10 nm. Surface chemistry of the films deposited on silica was examined by X-ray photoelectron spectroscopy (XPS), SPECS analyser Phoibos100 with 5 channeltrons detection working at 2.10-10 Torr, equipped with an Xray gun non monochromated Mg K α source (1253.6 eV). XPS analyses were performed in ITC-irst, Center for Scientific and Technological Research, Trento (Italy).

2.1.9. Mass Spectroscopy

Laser Ionization Time of Flight Mass Spectrometry (LITOF-MS) was performed to get structural information on SiOC glasses. This method is a quite recent method and it is especially suitable for investigation of the intermediate-range order in glasses, where it can measure the presence and relative abundance of mesounits composed of 7–20 or more atoms [D. Stentz, 2000]. These measurements were performed in Physics departments of Coe College, Iowa (USA). The sketch of the experimental set-up is given in **Figure 2.2**.

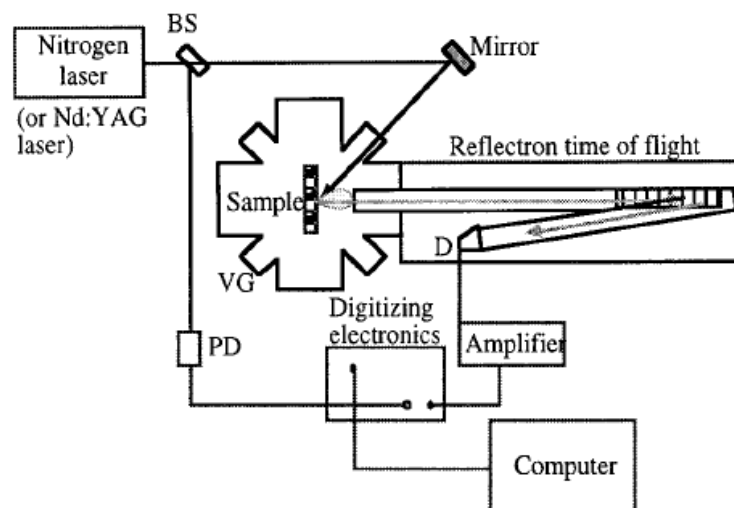


Figure 2.2. Sketch of the experimental arrangement of the LITOF mass spectrometer. Not shown are the camera trained on the sample and the sample insertion rod. The source region is conical to allow better access for the laser beam [D. Stentz, 2000].

2.2. Surface Properties and Thickness Analysis

2.2.1. SEM and FE-SEM

The surface and morphological feature of the films has been investigated by Jeol JSM-5500 Scanning Electron Microscopy (SEM). Since SEM is an easy and fast method to detect the surface quality, it has been used to optimize the films (homogeneity, defect, crack free morphology, etc.), especially early stage of the study.

Additionally, field emission SEM is used on some samples to understand the surface morphology in more details. The microscope is an ESEM-FEG XL-30, FEI Company, NL, equipped with a Field Emission Gun and EDAX X-ray microanalysis. The images were acquired in High-Vacuum mode at 15-20 kV. The analyses were performed at the Microbiology and Virology Laboratory, S. Chiara Hospital, Trento (Italy).

2.2.2. AFM

Surface qualities and roughness of the films were investigated by NT-MDT P47H Atomic Force Microscopy (AFM), with a scanning size of 50 μm . AFM was used also in some thickness measurements. AFM measurements were done in physics department, university of Trento (Italy).

2.2.3. Profilometer

Film thicknesses were determined by using a Hommel tester T8000 profilometer. In the measurement the depth of a scratch created with a razor blade in the coating is measured both as coated and pyrolysed films. The sensitivity of the profilometer measurements was rather low below 400 nm. Therefore, several thickness measurements by different characterization methods were done in this study. However, due to easiness of this method, most of the reported thickness measurements were done by profilometer.

2.2.4. SIMS

Elemental profile variations through the cross section of the films were studied by Cameca SC-Ultra Secondary Ion Mass Spectrometry (SIMS). SIMS analyses are focused on the depth profiling of hydrogen, carbon, oxygen and silicon. In particular these profiles aim at identifying possible out diffusion of C and H, as consequence of pyrolysis and films densification. A gold capping layer -about 20nm thick- has been deposited on the samples surface. This conductive capping layer and an electron beam are used to compensate the electronic charge on the sample surface.

As coated films showed different response to sputtering, compared to the pyrolyzed ones due to polymeric features of the as coated films. Therefore, the profile was corrected according to the etching rate after the measurements. All the depth profiles have been aligned on Y axis (in counts per second) to the signal of each species in the SiO_2 substrate and the profiles depth has been measured for each sputtered crater with a mechanical profilometer Tencor P15. SIMS measurements were performed in ITC-Irst, Center for Scientific and Technological Research, Trento (Italy).

2.2.5. Ellipsometer

Shrinkage of the films during pyrolysis was followed up to 800°C by in-situ thermal ellipsometric analysis. Ellipsometry measurements were performed on UV-Vis variable angle spectroscopic ellipsometer (VASE) from Woollam, and data analysis was performed with the WVase32 software. Measurements were fitted over the transparent range (550-1000 nm). A single Cauchy layer was used to model the deposited films, asymmetric optical properties emanating from unidirectional contraction were not observed, and therefore, no correction was applied. Gradients in the thickness were also not observed, as previously reported. For in-situ ellipsometric analysis, the ellipsometer was fitted with a home-built covered heating unit connected to a programmable temperature regulator (developed in conjunction with SOPRA). Small holes were present to allow a thermocouple and beam access to the sample as well as gas flow. The pyrolysis environment was adjusted by Ar flow between 1 and 5 L/min of through the sample stage at. Ellipsometer measurements were performed in Laboratoire de Chimie de la Matière Condensée de Paris Université, Pierre et Marie Curie Paris (France).

2.3. Surface contact angle and Energy measurements

The experiments were performed using a Cahn microbalance DCA 322 which is able to collect data at a speed of 1 Hz. (It has to be noted that the low speed in collecting data can work as a kind of low band filter with respect to the effective force values, due to the higher frequency of the used acoustic vibration.) To the balance it was added a vibration apparatus composed by a loudspeaker (diameter 6 cm, nominal impedance 8 Ω , 0.250 W) driven by a function generator (model MK 1050 by Mitek). Upon the vibrating diaphragm, it was placed a plastic ring to hook a 4 cm Teflon beaker filled with the measure liquid. In this way, the vibrating parts were made close together to avoid unwanted or accidental movements of the beaker. All the DCA runs were performed at room temperature ($22 \pm 2^\circ\text{C}$) [C. Della Volpe, 2001].

As a measure liquid, ultrapure water ($18.5 \text{ M}\Omega \text{ cm}^{-1}$ produced by a Millipore Milli-Q device) was employed, using only fresh liquid for each experiment. The ethylene glycol ($\text{C}_2\text{H}_6\text{O}_2$) and Bromonaphtalene ($\alpha\text{Br-C}_{10}\text{H}_7$) were also used for the surface energy measurements. Measurements were done in the supervision of Prof. C. Della Volpe.

2.4. Optical Analysis of Materials

2.4.1. Photoluminescence

Photoluminescence measurements (PL) were recorded at room temperature using a spectrometer operating with an Argon Laser (365nm) as excitation source with a 2 mW power on the sample. The fluorescence light was collected from the front face of the samples in reflection mode. Interferential filters were used to clean the excitation wavelength in order to minimize the scattered stray light. All the spectra were corrected for the wavelength dependent response of the detection system. To have a quantitative indication of the PL intensity two approaches were used: (i) PL intensities of the films were compared with a reference film with Si nanocrystals as a benchmark and (ii) relative External Quantum Efficiencies (EQEs) of the films pyrolysed at 1200°C were calculated. As for the first approach, reference silicon nanocrystals have been produced by thermal annealing silicon-rich silicon oxide (SiO_x) films prepared by PECVD (plasma enhanced chemical vapour deposition) in order to obtain strong room-temperature photoluminescence (200 nm thickness, 42% atomic Si content, 1100°C and 1 hr annealing conditions). The reference gave red emission at 820 nm due to Si nanocrystals as it is described in previous works [F. Iacona, 2000; N. Dalbosso, 2007].

In the second approach, EQE, defined as the ratio of the number of photons emitted by the sample to the number of photoexcited electron-hole pairs, is a relevant figure of merit for LED applications. To measure the photon flux emitted from our samples, we calibrated the collection system (collecting lenses, monochromator, photomultiplier, photon counting unit) with a red LED whose EQE is known. By using this calibration, we measured the spectrally integrated luminescence intensity emitted by our films under photo-excitation and converted it into an emitted photon flux. The so-evaluated photon flux was corrected by the numerical aperture of the collecting system by assuming that the film is a lambertian point source. Then we measured the total absorbed power by the film by measuring with a standard power-meter calibrated at 365 nm, the total laser power incident on the sample, the power transmitted by the sample, the power reflected by the sample and the power absorbed by the quartz substrate. The difference among these quantities gives the power absorbed by the film, and knowing the wavelength of

the laser we deduced the absorbed photon flux. The ratio between the emitted and the absorbed photon fluxes yields the external quantum efficiency of the film [R. Guider, 2009; see **Appendix I**].

For the last part of the study (**Chapter 5**), PL measurements were recorded on Cary Eclipse in air, Varian Spectrophotometer using a Xenon lamp as the excitation source, sensitive across the whole wavelength range. Several different excitation wavelengths have been used to analyze the PL properties of SiOCN films.

2.4.2. UV-Vis analysis

The transmission spectra of the SiOC films were recorded over the region 190–800 nm using a Carry 3, UV–Vis spectrophotometer. Absorption spectra were used to determine the absorption optical band–gaps of the films (Tauc band–gap).

The transmittance of the films exhibited characteristic of inter-band transitions. The band-to-band transitions are described by the relation [Pankove, 1971];

$$\alpha(h\nu) = A(h\nu - E_g)^n \quad \text{Eq. 2.4}$$

where $\alpha(h\nu)$ is the absorption coefficient, A is a constant, which does not depend on photon energy, n depends on the nature of optical transition, $h\nu$ the photon energy and E_g is the band gap. The absorption coefficient in the fundamental absorption region was determined from the transmission spectra as a function of frequency ν using the relation:

$$\alpha(h\nu) = \left(\frac{1}{t}\right) \ln\left(\frac{1}{T}\right) \quad \text{Eq. 2.5}$$

where t is the film thickness and T the transmittance of the film [N. F. Mott, 1971]. All optical measurements of the films and powdered samples were done in physics department, University of Trento (Italy).

Chapter III. Synthesis and Characterization of SiOC gels and powders

Solutions which used in thin film production have been characterized extensively by means of several characterization properties. More specific methods like EPR and LITOF-MS have been performed to get a more detailed understanding of the formation and the structural change of the free-carbon phase. Moreover, the related powders and bulks have been characterized for the sake of coherency and widen the study and they are reported here in this chapter.

In this chapter, gels prepared from Triethoxysilane (T^H) precursor are extensively studied because this system is the least studied among all SiOCs in literature. Moreover, some preliminary studies of the films of this precursor showed promising optical properties [Modena, 2004]. Therefore, although characterization of the stoichiometric SiOC, prepared from a mixture of triethoxysilane and methyldiethoxysilane ($T^H D^H_2$) has been mentioned in this chapter, the study has been more focused on T^H system (Si rich).

3.1. Background information

In the literature, SiOC gels obtained from cohydrolysis of triethoxysilane, $HSi(OEt)_3$, (T^H) and methyldiethoxysilane, $HMe-Si(OEt)_2$, (D^H) give the possibility of precisely controlling the oxygen and carbon content in the gel by varying the relative amount of the two alkoxides. **Figure 3.1** is given to illustrate the compositions discussed in this chapter. For these compositions, the amount of carbon is related to the amount of oxygen according to the solid line in **Figure 3.1** and it ranges from 0 (pure T^H) to 1 ($T^H/D^H=1$) [G. D. Sorarù, 1995(b)]. In the figure, the dotted line shows the relationship between the C and O contents in the stoichiometric oxycarbide phase. The two lines cross each other for a value of $O/Si = 1.33$, corresponding to a T^H/D^H molar ratio of 2. In this case, the carbon content of the gel matches the carbon amount of the corresponding oxycarbide phase and therefore this composition (B in **Figure 3.1**) has been selected for the synthesis of stoichiometric SiOC composition. If the T^H/D^H molar ratio is higher than 2 (sample C), the corresponding SiOC glass contains Si-Si bonds,

while if the T^H/D^H ratio is lower than 2, such as in sample A, the final SiOC network contains C-C bonds and shows the tendency to form a free carbon phase. Gel precursors obtained from pure T^H lead to the formation of silica-based network with Si-Si bonds and considerably low amount of Si-C bonds. This system is considered as Si rich SiOC system [A. Karakuscu, 2009].

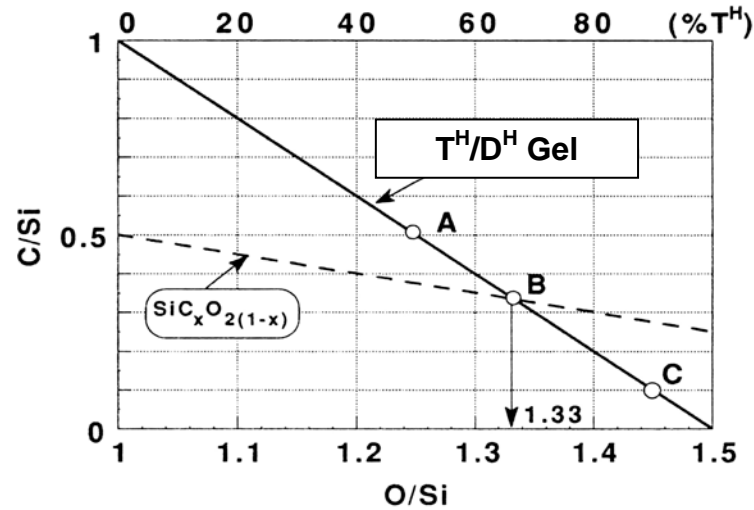


Figure 3.1. C/Si vs O/Si for gel samples obtained from cohydrolysis of triethoxysilane (T^H) and methyldiethoxysilane (D^H) (solid line) and for the stoichiometric oxycarbide phase (dotted line). The compositions of the studied gels (A, B, and C) are also reported. [G. D. Sorarù, 1995(b)]

3.2. Experimental details

Polymer pyrolysis method from sol-gel derived triethoxysilane (T^H) and methyldiethoxysilane (D^H) precursors have been used to produce gels. Powders with stoichiometric and Si rich SiOC compositions have prepared by $T^H/D^H=2$ and T^H ratios, respectively. For the easiness, the precursor ratios are given as sample labels. Triethoxysilane, $HSi(OEt)_3$, and methyldiethoxysilane, $HMe-Si(OEt)_2$, have been purchased from ABCR (97% pure) and used without further purification. Ethanol has been used as solvent with a molar ratio of $EtOH/Si=2$. Water amount and pH have been chosen in order to obtain a gelation time of a couple of hours ($pH=4.5$, HCl). Wet gels were dried at temperatures changing from RT to $110^\circ C$ for a month in order to give time for gelation. Cylindrical specimens with a diameter of ca 7-8 mm and few cm long

were accordingly obtained from dried gels. Before pyrolysis gel powders were grinded using an agata mortar. In order to check the structural evaluation through the pyrolysis, powders kept in a C-furnace under Ar flow (100 ml/min) with a heating rate of 5°C/min at different temperatures, in the range 800-1500°C with 1 hour holding time at the maximum temperature.

Gel samples and selected pyrolyzed SiOC powders were analyzed for oxygen, carbon, and hydrogen composition. Weight loss of the gel powders was followed by TGA. Fourier-Transform Infrared (FTIR) analyses of powder samples, before and after pyrolysis, were studied in the range of 4000-400 cm⁻¹. ²⁹Si MAS NMR and ¹³C MAS NMR were performed on gel and pyrolysed samples. EPR measurements were performed on all the set of the samples in order to compare the results of the powders from Si rich to C rich SiOC system. XRD analyses were done to detect the crystallization behaviour during pyrolysis. The evaluation of crystalline particle size was also carried on X-ray patterns according to the Scherer's formula.

3.3. Results

3.3.1. Gel characterization

Elemental analysis results are reported in **Table 3.1**. For the T^H gel, C/Si ratio was found to be 0.2 which indicates that the network is not fully condensed and some residual ethoxy groups are present. Since each ethoxy group bears 2 carbon atoms the chemical analysis indicates that, as an average, 10% of Si sites have one non hydrolyzed ethoxy group. On the other hand, the elemental analysis of T^HD^H2 gave elemental compositions close to theoretical values showing that di-functional group (methyldiethoxysilane) addition decreased the non hydrolysed group and no unexpected increase in C is observed due to non hydrolysed groups.

Table 3.1. Elemental analysis of powdered T^H samples gel and pyrolysed at 1000°C and 1400°C

Sample	Si (wt. %)	C (wt. %)	O (wt. %)	H (wt. %)	Empirical formula
Gel	42.6 ± 0.6	3.7 ± 0.1	51.3 ± 0.5	2.4 ± 0.1	SiO _{2.1} C _{0.2} H _{1.6}
1000 °C	47.2 ± 0.6	3.0 ± 0.1	49.7 ± 0.5	0.1 ± 0.05	SiO _{1.8} C _{0.1} H _{0.1}
1400 °C	46.2 ± 0.6	2.4 ± 0.1	51.4 ± 0.5	ND	SiO _{1.9} C _{0.1}

Table 3.2. Elemental analysis of powdered T^HD^H2 samples gel and pyrolysed at 1400°C.

Sample	Si (wt. %)	C (wt. %)	O (wt. %)	H (wt. %)	Empirical formula
Gel	52 ± 0.6	8.8 ± 0.2	35.2 ± 0.4	4 ± 0.1	SiO _{1.18} C _{0.39} H _{1.93}
1000°C	52.9 ± 0.6	7.4 ± 0.3	39.7 ± 0.6	<0.03	SiO _{1.31} C _{0.33}
1200 °C	48.2 ± 0.6	7.5 ± 0.2	44.3 ± 0.5	<0.01	SiO _{1.61} C _{0.36}

The gels were also characterized by FT-IR spectroscopy (see **Figure 3.2**) in order to get insights in the chemical bonding of its structure. The presence of Si-H bonds gives rise to the bands at 2256 cm⁻¹ (Si-H stretching), 2180 cm⁻¹ (Si-H stretching) and 830 cm⁻¹ (Si-H bending) [G.D. Soraru, 1995(c)]. Peaks at 1150, 1070 and 460 cm⁻¹ are related to the Si-O vibration of the siloxane network. Si-CH₃ (bending) bands at 1265 and 760 cm⁻¹ are attributed to the presence of D^H (methyldiethoxysilane) in solution (**Figure 3.2-a**). Vibration of residual Si-OEt groups should give a band at 1100 cm⁻¹, which is not clearly present in the FT-IR spectrum of the gel, probably due to their low concentration.

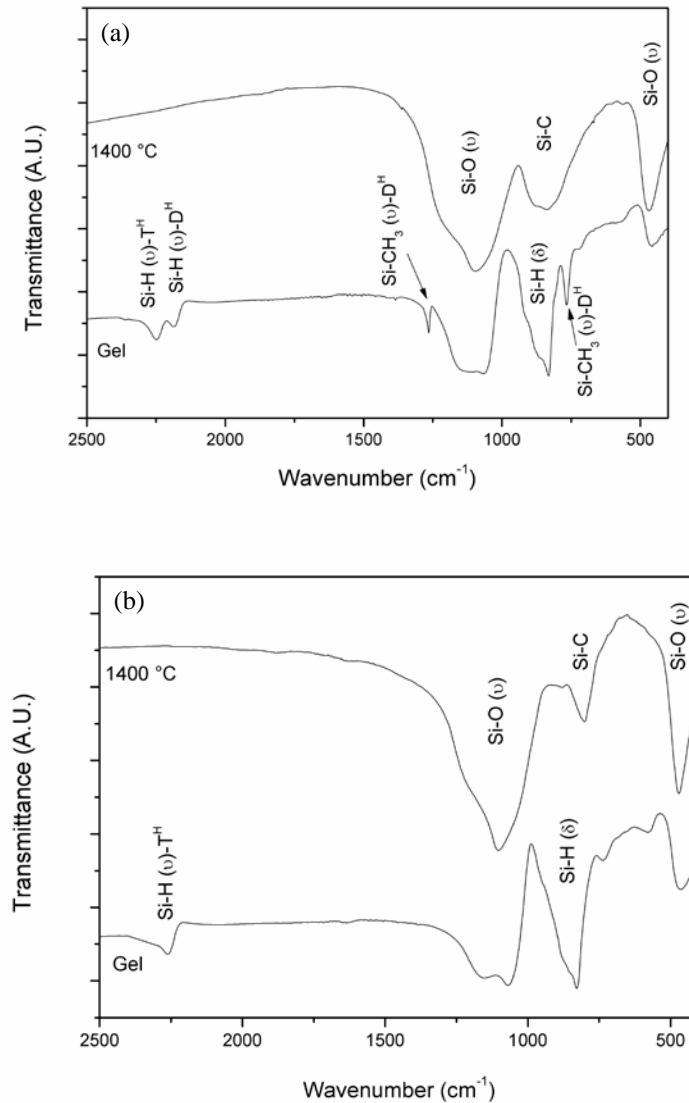


Figure 3.2. FTIR spectra of gel and pyrolysed (a) T^HD^H2 and (b) T^H samples. Corresponding bands are shown on the figure.

The ²⁹Si MAS NMR of the T^H gel sample is reported in **Figure 3.3**. The spectrum shows peaks in two distinct regions: around -82 ppm due to silicon atoms bonded to 3 oxygen atoms and one H atom, HSiO_{1.5} also known as T^H units, and in the range -100-110 ppm typical of silicon atoms bonded to four oxygen atoms such as those of silica glass, SiO₄ also known as Q units. The presence of Q units is due to a partial oxidation of Si-H bonds during the sol-gel reaction with formation of new Si-O bonds. In the Q unit region the component at low field (peak at -108 ppm) can be assigned to silicon sites with four bridging oxygen known as Q₄ sites, and the peak at -99 ppm to silicon

atoms bearing three bridging and one terminal oxygen, known as Q₃ sites, Si(OSi)₃OX, X = H or Et [H. El Rassy, 2005]. The spectrum has been simulated to extract the percentage of the various silicon sites (see **Table 3.3**). Q₃ units are around the 14% of the total Si units. This value is close to the value estimated by chemical analysis (10%) assuming that the terminal groups are mainly due to non hydrolyzed ethoxy moieties. The presence of Si-OEt group in the siloxane network has been also verified by ¹³C CP-MAS NMR (see **Figure 3.4**). In this spectrum the Si-OCH₂CH₃ groups give rise to the peak at 59.9 ppm (-OCH₂- units) and at 16.7 ppm (-CH₃) groups.

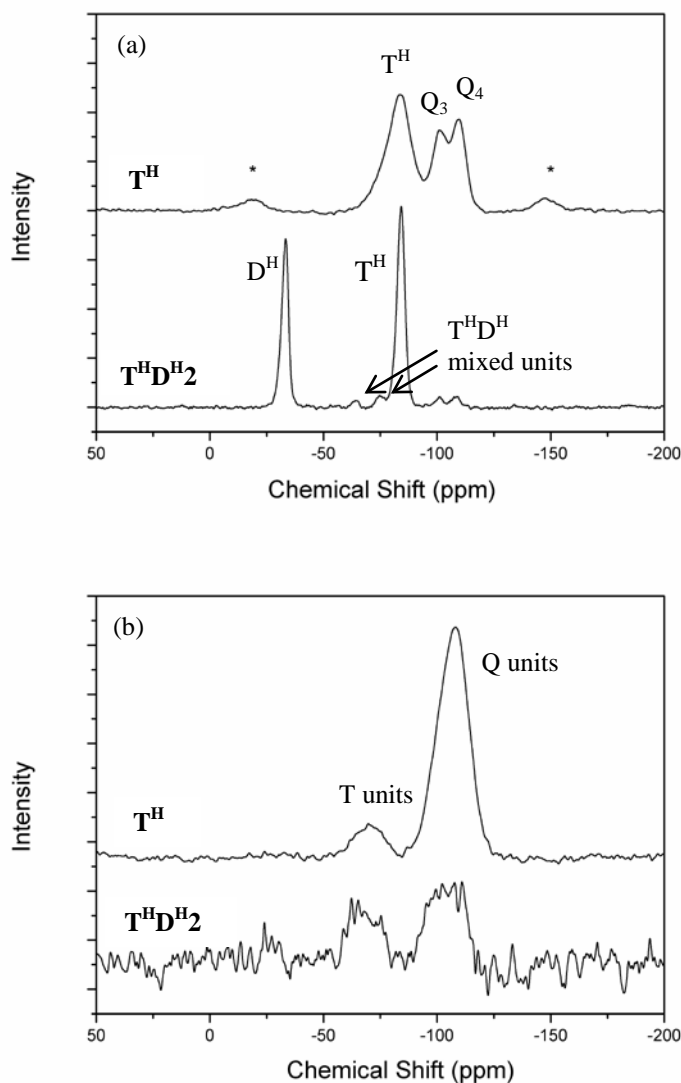


Figure 3.3. ²⁹Si NMR of T^H and T^HD^H₂ samples as (a) gel and (b) pyrolysed at 1000°C.

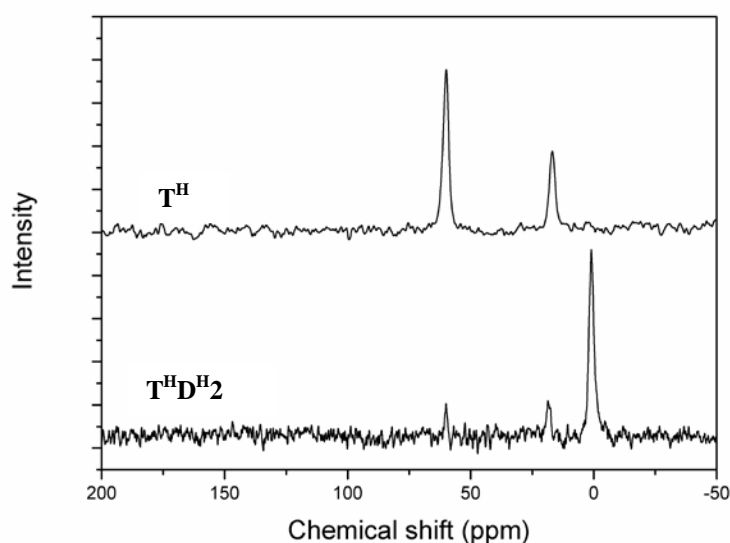


Figure 3.4. ^{13}C CP-NMR of $\text{T}^{\text{H}}\text{D}^{\text{H}2}$ and T^{H} gels.

^{29}Si MAS NMR and ^{13}C CP-MAS NMR of the THDH2 gel showed very low amount of non hydrolysed ethoxy groups. Namely, only 3 % of Q_3 units were detected in ^{29}Si NMR of the gel. The main two peaks at 84 ppm and 64 ppm belong to the precursors T^{H} unit from triethoxysilane (T^{H}) and D^{H} from methyldiethoxysilane (D^{H}) precursor, respectively. Moreover, very small amount of Q_4 units were also detected in similar studies on the same gel [G. D. Sorarù, 1995].

In the ^{13}C MAS NMR spectrum of the $\text{T}^{\text{H}}\text{D}^{\text{H}2}$ sample the only peak present is at 1 ppm due to methyl groups bonded to silicon, Si-CH_3 , of the D^{H} units. The other alkoxy group peaks, which were present in the NMR spectrum of the T^{H} sample, are not evident in the ^{13}C NMR spectrum [G. Trimmel, 2003]. Therefore, it is verified by elemental analysis and NMR that the addition of difunctional alkoxides to the T^{H} system favours the complete hydrolysis leading to a gel free of residual alkoxy groups.

Table 3.3. Quantitative analysis of the ^{29}Si NMR spectra of $\text{T}^{\text{H}}\text{D}^{\text{H}2}$ and T^{H} gels.

Sample	SiO_4		$\text{Si}(\text{OSi}\equiv)_3(\text{OX})$		HSiO_3		Mixed $\text{T}^{\text{H}}\text{-D}^{\text{H}}$ bonds				HSiCO_2	
	δ (ppm)	%	δ (ppm)	%	δ (ppm)	%	$\text{T}^{\text{H}}_1\text{-}(\text{D}^{\text{H}})$		$(\text{D}^{\text{H}})\text{-T}^{\text{H}}_2\text{-}(\text{D}^{\text{H}})$		δ (ppm)	%
Gel $\text{T}^{\text{H}}\text{D}^{\text{H}2}$	108.6	3	101.3	3	83.9	50	74.9	6	64.1	2	33.5	36
T^{H}	109.3	63	101.2	14	83.9	23	-		-		-	

Table 3.4. Quantitative analysis of the ^{29}Si NMR spectra of the $\text{T}^{\text{H}}\text{D}^{\text{H}2}$ and T^{H} powders pyrolysed at 1000°C .

Sample	SiO_4		CSiO_3		SiC_2O_2	
	δ (ppm)	%	δ (ppm)	%	δ (ppm)	%
1000°C $\text{T}^{\text{H}}\text{D}^{\text{H}2}$	107.7	60	65.3	36	27.2	4
T^{H}	108.2	87	70.1	13	-	

3.3.2. Gel-to-Ceramic transformation

TGA and dilatometer analysis are given in **Figure 3.5**. TGA analysis reveals a continuous weight loss from 200 up to 800°C in both SiOC samples. No significant weight loss can be observed above 800°C. The total weight loss for Si rich SiOC system (T^H) is only 3.1 % which is among the lowest weight loss reported for the SiOC system [P. Colombo, 1994]. However, stoichiometric SiOC ($T^H D^{H_2}$) gel showed 6.5 % of weight loss due to higher release of H_2 and CH_4 .

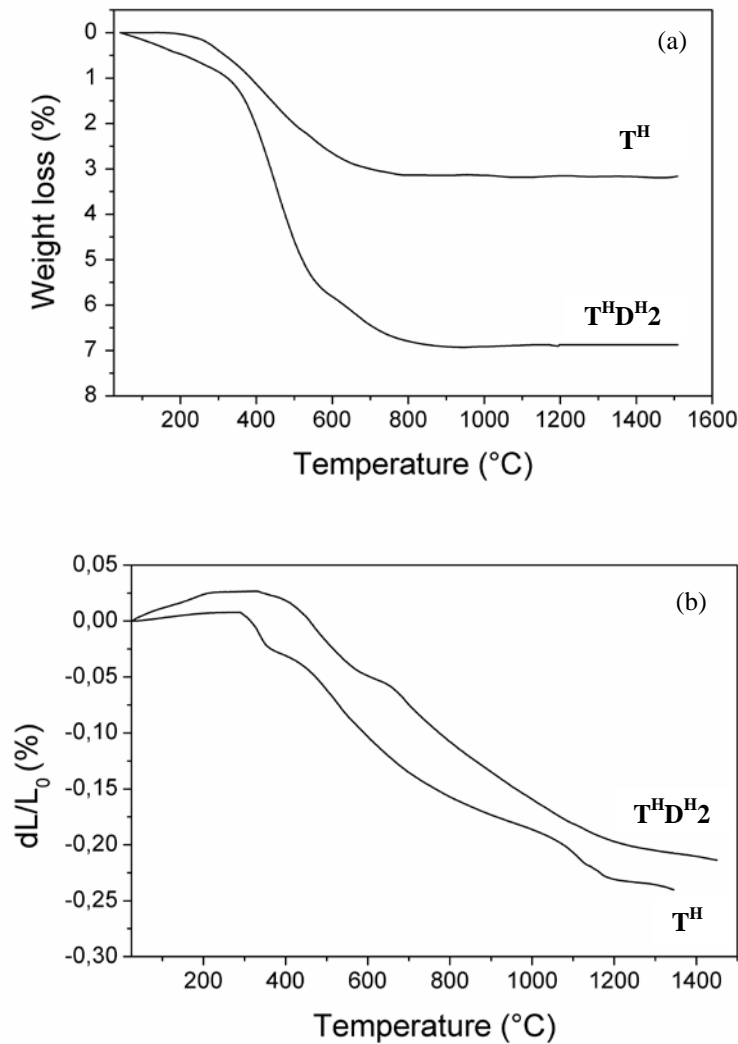


Figure 3.5. TGA and dilatometer measurements of gel samples.

Dilatometer measurements give complementary information to the TGA analysis. Gel samples expand till $\approx 300^\circ\text{C}$ then they shrink up to 1200°C with a total linear shrinkage

of $\approx 25\%$. For the T^H sample, unlike the TGA, which shows a continuous transformation from 200 to 800°C, the dilatometry analysis reveals three distinct shrinkage steps: from 300 to 400 °C, from 400 up to 1100°C and from 1100 to 1200°C. The low temperature event may be related to the reactivity of the residual ethoxy groups (already detected by ^{13}C MAS NMR and chemical analysis) and/or hydroxyl moieties which are known to be the first units to react during gel pyrolysis [R. Camprostrini, 1995]. The second event, from 400 up to 1100°C spans over the temperature range typical for the ceramization process and in this case could be related to the evolution of hydrogen and low molecular weight species such as SiH_4 [Mutin, 2002; R. Camprostrini, 1995]. It is worth of noticing that the shrinkage continues even above 800°C when the TGA does not show any weight loss. This phenomenon could be associated to the completion of the evolution of hydrogen, H_2 , which occurs without appreciable weight loss but results into a significant densification of the matrix [G.D. Sorarù, 1990]. Above 1000°C the residual hydrogen in the silica-based network is quite low (see **Table 3.1**) and the shrinkage step from 1100 to 1200°C is probably associated to a different mechanism: a viscous sintering process of the porous glass. Indeed, it is known that triethoxysilane-derived glasses are still porous at 1000°C [G.D.Sorarù, 1996], with a specific surface area up to $70 \text{ m}^2/\text{g}$, and they can viscous sinter when the temperature becomes close to the glass transition temperature, which is, for SiO_2 -based glasses around 1100-1150 °C. A similar sintering phenomenon was already reported for a SiOC glass in the temperature range 1200-1300°C [G.D.Sorarù, 2000].

3.3.3. Structural characterization of the SiOC glasses

Chemical analysis of the SiOC glasses pyrolyzed at 1000 and 1400°C reveal that C is still present in the glass structure and that above 1000°C the composition is stable up to 1400°C (see **Table 3.1 and 3.2**).

3.3.3.1. NMR Study

Characterization of the amorphous T^H glass obtained at 1000°C has been performed by ^{29}Si MAS NMR (see **Figure 3.3**) and the percentage of the various silicon sites, as obtained from the simulation of the spectrum, are reported in **Table 3.4**. The spectrum shows one main peak at -108 ppm assigned to SiO_4 sites (87%) and a smaller

component (13%) at -70 ppm that could be assigned to Si atoms bonded to three O atoms and one C atom forming $\text{CSiO}_{1.5}$ sites (T units). However the peak at -70 ppm could also be compatible with the existence of Si-Si bonds belonging to mixed silicon units such as $\text{Si}(\text{Si}_x\text{C}_y\text{O}_z)$ with $x+y+z=4$ [G. D. Sorarù, 1995(b)]. Indeed, the NMR resonance at -70 ppm is very broad and spans over a chemical shift range from -60 up to -85 ppm which include the chemical shift for metallic silicon at -80 ppm [J. S. Hartman, 1987]. Similarly, ^{29}Si NMR of the $\text{T}^{\text{H}}\text{D}^{\text{H}2}$ sample showed rather large two peaks centred at 107 ppm corresponding to SiO_4 and 65 ppm related to SiCO_3 units. Although the spectrum is rather noisy, another peak at around 27 ppm can be seen and it is attributed to SiC_2O_2 units.

In conclusion, the NMR study confirmed, for the $\text{T}^{\text{H}}\text{D}^{\text{H}2}$ sample, the formation of a silicon oxycarbide glass in which mixed silicon oxycarbide units containing 1 and 2 Si-C bonds per Si atoms, are present. For the T^{H} composition, the NMR investigations revealed the presence, of Si-C bonds belonging to CSiO_3 units, while the presence of Si-Si bonds cannot be clearly either confirmed or disproved.

3.3.3.2. EPR Study

EPR is widely used to detect the presence of defect states, namely dangling bonds in the structure. It is known that during polymer-to-ceramic transformation in PDCs, bond cleavage and recombination processes occur and this causes formation of dangling bonds such as radicals [S. Trassl, 2002; I. Menapace, 2008; G.D. Sorarù, 1990]. The relation between these radicals and optical properties have been discussed in literature for Si/SiO₂ [M. Baran, 2004]. Therefore, for the sake of the optical characterization of SiOC films, the EPR study is very essential.

C dangling bonds, which is known to be present in most of the SiOCs, have been studied in the literature extensively by EPR. It is known that very low amount of free C can be detected in almost all the SiOCs eventhough no graphitic carbon can be detected by XRD at higher temperature. Relatively, in our work $\text{T}^{\text{H}}\text{D}^{\text{H}2}$ is considered as stoichiometric glass and, theoretically, it does not contain free carbon. Indeed the experimental composition of this sample was found to be close to the theoretical one.

However, the traces of the carbon or other possible defect states are expected to be present in T^H as well as $T^H D^H_2$. Therefore, EPR study has been done for both systems.

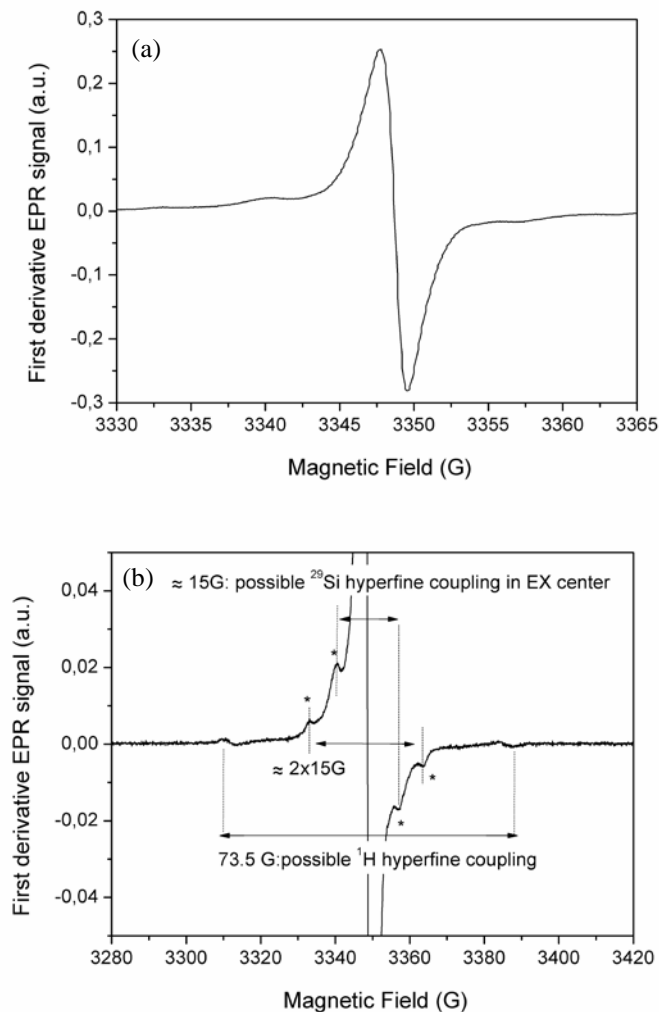


Figure 3.6.(a) EPR spectra of $T^H D^H_2$ pyrolysed at 800 °C. (b) higher magnification of the spectrum is shown with the possible components.

The EPR spectrum of $T^H D^H_2$ sample pyrolysed at 800°C (**Figure 3.6-a**) showed one main intense line at $g=2.0026$ which is assigned to C radicals [A. Stesmans, 2008; S. I. Andronenko, 2006]. However, in higher magnification some interesting features, coming from other possible defect centers, are observed in EPR spectrum (**Figure 3.6-b**).

The presence of features (peaks marked by a star and doublet with 73.5G splitting) flanking symmetrically may suggest another interpretation for the origin of the EPR

peak as well as C dangling bonds. Actually, a similar line with the same g-value and with two peaks separated by $\approx 15\text{G}$ on both sides of the line has already been reported in SiO_2 [A. Stesmans, 1995, A. Stesmans, 1994] and assigned to the so-called EX center (Si vacancy) in SiO_2 . The two peaks separated by 15G are attributed by these authors to hyperfine coupling with ^{29}Si ($I=1/2$).

Moreover, the four peaks marked by a star could be part of a same ESR signal. The particular ratio of 2 between the splitting of the outer peaks and the splitting of the inner peaks is unlikely a coincidence. The signal could then be the signature of 2 EX centers coupled by magnetic dipolar interaction. The splitting D of the inner peaks is then related to the distance between the two centers by the equation 3.1. From $D = 15\text{G}$, the distance R between the two centers is found as $R \approx 1\text{ nm}$.

$$D = \frac{\mu_0 g\beta}{4\pi R^3} \quad \text{Eq. 3.1}$$

The peaks separated by 73.5 G were already observed in silica and were assigned to the hyperfine coupling with a proton in an E' center (oxygen vacancy in SiO_2) [A. Stesmans, 2008]. However, since the g-value 2.0026 in our case does not match that reported for the E' center, we interpreted that these two peaks correspond to the coupling with a proton in the EX center.

On the other hand, T^{H} spectrum exhibits several signals different from $\text{T}^{\text{H}}\text{D}^{\text{H}2}$ (**Figure 3.7**). There are at least four detected signals at $g=2.0008$, at $g=2.0028$, at $g=2.0045$ and $g=2.0063$. The peak at $g=2.0028$ can be assigned to C radicals while the peak at $g=2.0008$ can be assigned to O vacancies in silica, which is discussed before as E' center. The presence of E' center in this sample is reasonable since TH is oxygen deficient compared to silica.

The assignment of the last two peaks is not so straightforward. Either they correspond to the same specie with axial g-tensor ($g_{\parallel}=2.0063$ and $g_{\perp}=2.0045$), or they belong to two different species. In the literature the signal at $g=2.0045$ is mentioned as indication of oxygenated carbonaceous radicals whereas signal at $g=2.0063$ is reported as carbon- vacancy related defects in SiC [N. T. Son, 1999].

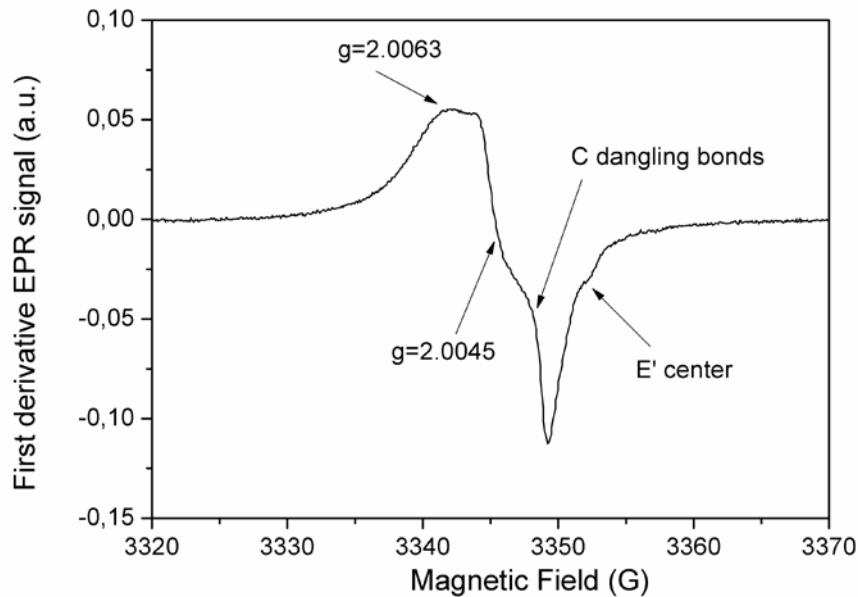


Figure 3.7. EPR spectra of T^H sample pyrolysed at 800 °C. Possible defect states are indicated.

To understand the evolution of the radical species during pyrolysis, EPR analyses were performed on samples pyrolysed at different temperatures in the range 800-1400 °C and the results are shown in **Figure 3.8**. To understand better the evolution of the defect states in the samples, g factors as well as spin concentrations have been calculated from EPR spectra since both of them (g factors and spin concentrations) are very important indications for the formation of radicals. The total spin concentration changes with temperature are plotted for both samples ($T^H D^{H2}$ and T^H) and reported in **Figure 3.9**.

$T^H D^{H2}$ showed only C-related radicals with a g value around $g=2.0025$ up to the maximum pyrolysis temperature. On the other hand, the EPR spectra recorded on T^H sample showed a very complex structure at every pyrolysis temperature (**Figure 3.8-b**). It should be noted that the total spin concentration is radically decreasing and at 1400°C reaching minimum (namely, $\sim 10^{17}$), indicating that the defect states concentration is very low at this temperature. Whereas, in all the EPR spectra of T^H two components at $g=2.0028$ (C dangling bonds) and at $g=2.0008$ (E' center (oxygen vacancy in SiO_2)) are clearly visible. In addition, other EPR peaks are also present in the T^H spectra which make the full assignment quite difficult and not yet complete at this time.

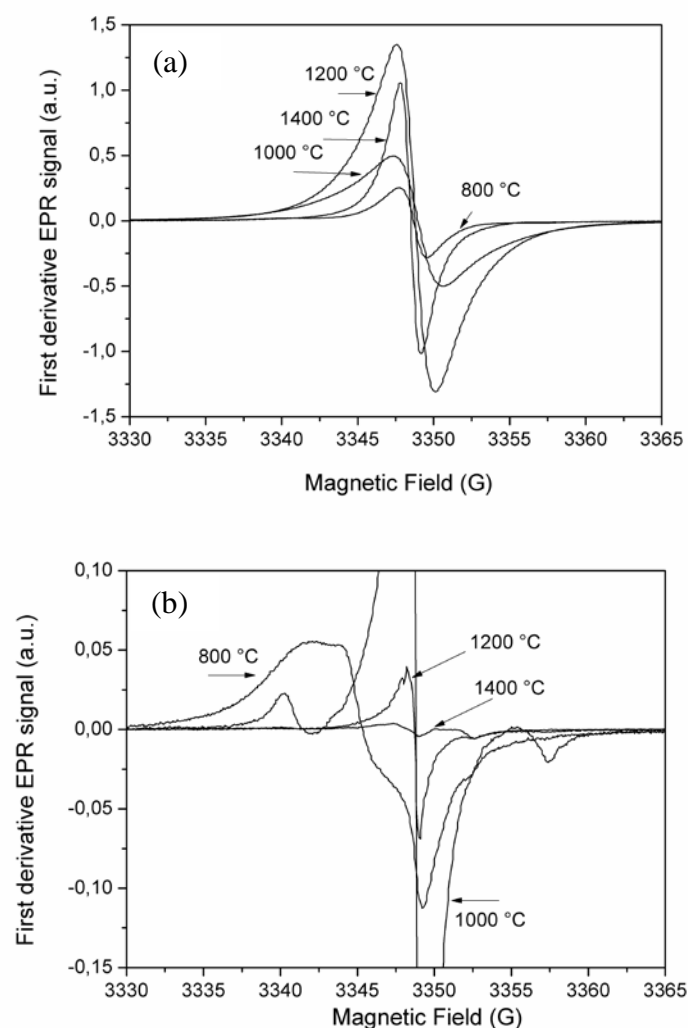


Figure 3.8. EPR spectra of carbon related dangling bonds in (a) $T^H D^H 2$ and (b) T^H powders pyrolysed at different temperatures (800-1400°C).

Both samples at 800 °C showed the same amount of total radical concentration (2.5×10^{18} - 3.3×10^{18} spin/gram) (**Figure 3.9**). However, for the $T^H D^H 2$ composition the radical concentration increases with the temperature up to 1200 °C while for the T^H sample continuously decreases. This result agrees with the literature data showing, for polycarbosilane-derived PDC, a maximum of C-dangling bonds at 1200°C [S. Trassl G. M., 2002]. On the other hand, T^H sample shows only a decrease in the total radical concentration with the pyrolysis temperature, which is a different behaviour from common PDCs.

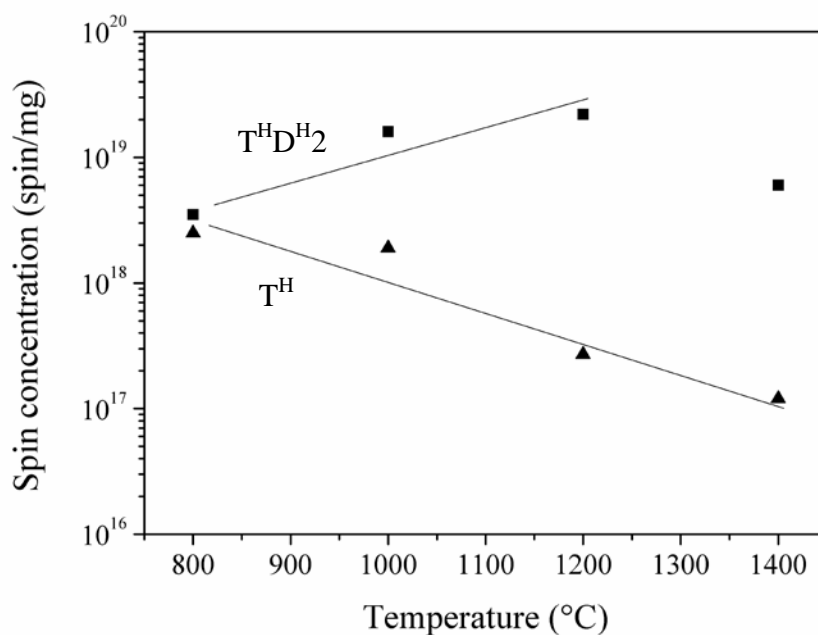


Figure 3.9. Dangling bonds concentration as a function of temperature for sample $T^H D^H 2$ and T^H . (spin concentration is shown exponential).

3.3.3.3. XRD study

The evolution of the XRD spectra recorded on T^H and $T^H D^H 2$ glasses pyrolyzed at different temperatures in the range of 1000-1500°C are shown in **Figure 3.10**. In T^H sample, the likely presence of Si-Si bonds at low temperatures (1000-1200°C) leads to the crystallization of elemental silicon at higher temperatures (1300-1500°C) (see **Figure 3.10-b**). Up to 1200°C the system is totally amorphous and at 1300°C, Si crystallization starts as shown by the diffraction peaks at 28°, 47° and 57°. A very broad component around 35°, which belongs to β -SiC phase, starts to become visible at 1400°C and develops into a clear peak at 1500°C. The β -SiC crystal size has been estimated ~ 7 nm by the Scherer formula. Although the existence of wide particle size distribution is known, to have a general idea about particle size changes as a function of temperatures, particle sizes for the all crystalline phases present in the system are estimated in the **Table 3.5**. The concomitant presence of Si and SiC crystals is a clear evidence that the pyrolysis product obtained in this study from a triethoxysilane-derived gel is indeed a Si-rich SiOC glass and not only a Si-rich SiO_2 glass.

Similar to literature results, T^HD^H2 sample did not show evidence of crystallization until 1300°C, and then the diffraction peaks related to SiC start to appear and its crystalline size increased quite gradually (**Figure 3.10-a**). However, even at 1500°C very broad peak suggests that there is wide distribution of crystalline size. Another relevant difference between the two studied SiOC glasses consists in the crystallization of cristobalite for the T^H glass pyrolyzed at 1500°C while for the SiOC with higher amount of C silica crystallization is prevented (**Figure 3.10** and **Table 3.5**).

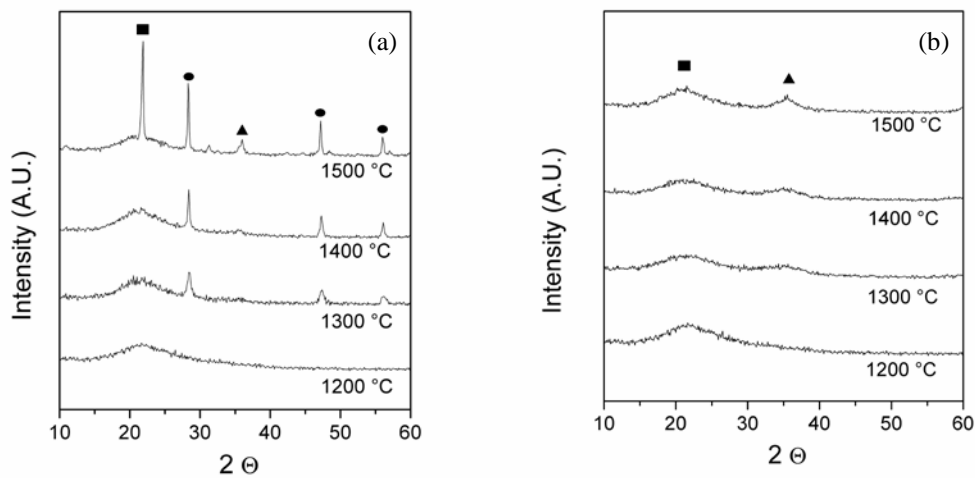


Figure 3.10. X-ray spectra of (a) T^HD^H2 (stoichiometric SiOC) (b) T^H (Si rich SiOC) samples pyrolysed at different temperatures (1200 -1500°C). Crystalline phases have been indicated above the spectra (■ SiO₂, ▲ SiC and ● Si).

Table 3.5. Estimated particle sizes (mean value) of phases present in the SiOC samples by using Scherer formula.

Sample	Particle size (nm)			
	Stoichiometric SiOC-T ^H D ^H 2	Si rich SiOC-T ^H		
	β-SiC [111]	SiO ₂ [111]	Si [111]	SiC [111]
1300°C	0.5	-	8.1	1.1
1400°C	0.8	-	14.5	1.1
1500°C	1.6	21.7	21.9	7.5

3.3.3.4. Laser Ionization Time of Flight Mass Spectrometry Study

The structure of amorphous ceramics such as glasses is composed of short-range units (nanounits) which interlink to form larger, intermediate-range components (mesounits). These mesounits are essential in determining the overall properties of the glass, but they are very difficult to investigate. Often, they are characterized by studying crystalline compounds with the same stoichiometries. Vibrational techniques such as Raman spectroscopy unambiguously identify these groups, but Raman is not able to quantify their presence, which remains an open and important question in glass studies. To understand the structure of mesounits in SiOCs, high-resolution time-of-flight mass spectroscopy driven by laser ionization (LITOF-MS) has been used. To simplify the experiments and obtain comparable results, well known, stoichiometric SiOC ($T^H D^H_2$) is studied at different pyrolysis temperatures (800 and 1400°C).

In all samples SiO_2 units was detected and its intensity increased drastically from 800°C to 1400°C by a factor of 5. Meanwhile, Si_3C_6 and C_4 units were detected only at 1400°C. These can be due to the phase separation of SiC, SiO_2 and C at higher temperatures. The only mixed units detected at 800°C were Si_2C_2O and Si_2C_3O . As the time increases other mixed units were detected such as SiC_2O_2 , SiC_5O_2 , Si_2C_5O , SiC_5O_3 , SiC_7O_2 and $Si_2C_3O_4$. However, some of these units overlapped other mixed units that have the same mass and distribution like $Si_2C_3O_4$ is overlapping with SiC_8O_2 and Si_2C_7O . Therefore this method gave us an idea of the some possible mixed units but it is not possible to define the exact structure of the mesounits (especially the large ones). More interestingly, presence of mixed C_3O_6 , which were not reported in SiOCs, is detected in SiOC sample at 1400°C.

3.4. Discussion

Thermal analysis (TGA) showed us that organic-to-inorganic transformation is a continuous process which ends around 800°C and no other major weight losses are detected above this temperature. Therefore, the pyrolysis temperature of the films is decided to start from 800°C.

Si rich SiOC formation from pure triethoxysilane is for the first time reported here. Triethoxysilane is a silicon alkoxide precursor which leads, upon hydrolysis and condensation (sol-gel process) to Si-H containing silica gels [M. Pauthe, 1989; G.D. Soraru, 1995(b)]. Heat treatment of these gels in inert atmosphere results in the formation of silicon-rich silica system which is known as sub-stoichiometric silica (SiO_x) [V. Belot, 1992]. The pyrolytic transformation from the Si-H containing gel to the Si-containing SiO_2 occurs with the condensation of Si-H moieties forming Si-Si bonds and gaseous H_2 [Mutin, 2002]. The final product, Si-rich SiO_2 , has been reported in literature with its unique photoluminescence properties [G. D. Soraru, 2003].

It is well known in the sol-gel science that residual, non hydrolyzed alkoxy groups are usually present in alkoxide-derived silica gels and that these moieties act like a C source during the pyrolysis in inert atmosphere [C.J. Brinker, 1990]. Accordingly, pure Si/ SiO_2 materials can be obtained only if the amount of residual organic groups is minimized. On the other hand, the small but not negligible presence of alkoxy groups in the starting gel can offer the opportunity to synthesized Si-rich SiOC. The non-hydrolysed groups are shown by NMR and formation of SiC at high temperatures is reported by means of several other characterization methods. Therefore, we have decided to use this precursor to produce Si rich SiOC films. Additionally, films with different compositions (stoichiometric and C rich) are produced by using triethoxysilane and methyldiethoxysilane with different ratios.

Meanwhile, several other structural characterization methods (i.e. EPR and LITOF-MS) are done to understand better the amorphous structure at low temperatures. The further optical studies, which will be discussed in **Chapter 4**, can be done in the light of these results. As a general perspective, it has been already reported in literature that the defect states in PDCs causes high luminescence and one of the few methods to study defect states is EPR. Relatively new results coming from LITOF-MS showed the interesting mesounits which can not be seen by other methods and gave valuable information about structure.

3.5. Conclusions

It is known that there are limited numbers of techniques which are available for the characterization of thin films, whereas many different characterizations can be performed on powders. This was the main reason for us to study the T^H and $T^H D^{H2}$ SiOC glasses in the powder form and to get insights into their amorphous/nanostructure. This information can be valuable hints to understand luminescent behaviours of these glasses either in the form of bulk and thin films.

Structural study on T^H precursor showed many important facts about this precursor. In our study, triethoxysilane has been chosen as precursor for Si-rich SiOC glasses. During the hydrolysis and condensation, Si-OR groups are first replaced by Si-OH and then condensations reactions form Si-O-Si bonds. Si-H bonding leads, during pyrolysis, to Si-Si bonding. Due to lack of full condensation the presence of residual alkoxy group have been observed in the gel sample by FTIR and ^{13}C NMR. Degree of condensation has been also calculated as 97.5, from ^{29}Si MAS-NMR. A similar degree of condensation has been reported in the literature and it was explained by the low mobility of trifunctional groups [R. Campostrini, 1996]. At high temperatures ($\geq 1000^\circ C$) the very few residual alkoxy groups produced C in the system that can react with excess Si and forms SiC which has been shown by XRD. Therefore, the resultant ceramic became Si rich SiOC and with an increase in pyrolysis temperature $Si_{nc}+SiC_{nc}/SiO_2$ has been achieved.

Chapter IV. Processing and Characterization of SiOCs films

4.1. Background information

Light Emitting Diodes (LEDs) are currently studied with the aim of increasing the efficiency and reducing the cost of lighting systems for several applications, such as automotive or domestic applications. Among the different inorganic materials, Si-based LEDs show many potential advantages since silicon is a cheap and abundant element and has a mature processing technology. Moreover, if Si is used in combination with SiC and/or C, it could provide a suitable heat-resistant material for white light applications. The most encouraging results have been obtained when Si, SiC and C have a cluster size of few nanometers [S. Y. Seo, 2004; A. Perez-Rodriguez, 2003]. However, production of Si, SiC and C nanoclusters embedded in a dielectric matrix such as SiO₂ is not straightforward and the most widely used approach is ion implantation [A. Perez-Rodriguez, 2003; S. Y. Seo, 2004; G. R. Lin, 2005].

In our study, the SiOC films produced from pyrolysis of sol-gel derived silane precursors are proposed to produce white emitting materials. This novel method is based on a simple processing route to produce nanostructured multicomponent ceramics [R. Raj, 2001]. According to this route, sol-gel derived precursors are converted to ceramic materials by a pyrolysis process in controlled atmosphere at 800-1000°C. Higher temperatures lead to formation of Si-rich SiOC, C-rich SiOC or stoichiometric SiOC according to the starting composition. At temperatures higher than 1200°C, formation of SiC inside SiO₂ matrix is expected due to the phase separation of multicomponent SiOC [H. Bréquel, 2004]. The final composition, which is relevant to line emission, can be easily controlled through a number of processing parameters like the composition of the preceramic gel and the heat treatment conditions. Thus, this new processing method seems very well suited for the production of white emitting materials since the Si- and C-based emission can be tuned across the visible spectral range from UV-blue to red by controlling film composition. A further advantage of this method is that the thin films can be formed on Si or quartz wafers and this can serve as starting material to process more complex photonic devices such as waveguides or LEDs.

4.2. Experimental Details

SiOC thin films with three different chemical compositions were produced by the polymer pyrolysis method from sol-gel derived precursors. To understand the effect of Si and C on the luminescence behaviour of the SiOC system, precursor compositions were chosen to give C-rich, stoichiometric and Si-rich SiOC films. Accordingly, to obtain C-rich SiOC and stoichiometric SiOC films triethoxysilane (T^H) and methyldiethoxysilane (D^H) were used with T^H/D^H molar ratios of 1 and 2, respectively [H. Bréquel, 2004]. On the other hand, two different Si-rich SiOC films were prepared by T^H/D^H ratio of 9 and from T^H without any addition of D^H . To seek of clarity, the precursor ratios will be used to label the samples and they are shown in the phase diagram, **Figure 4.1**.

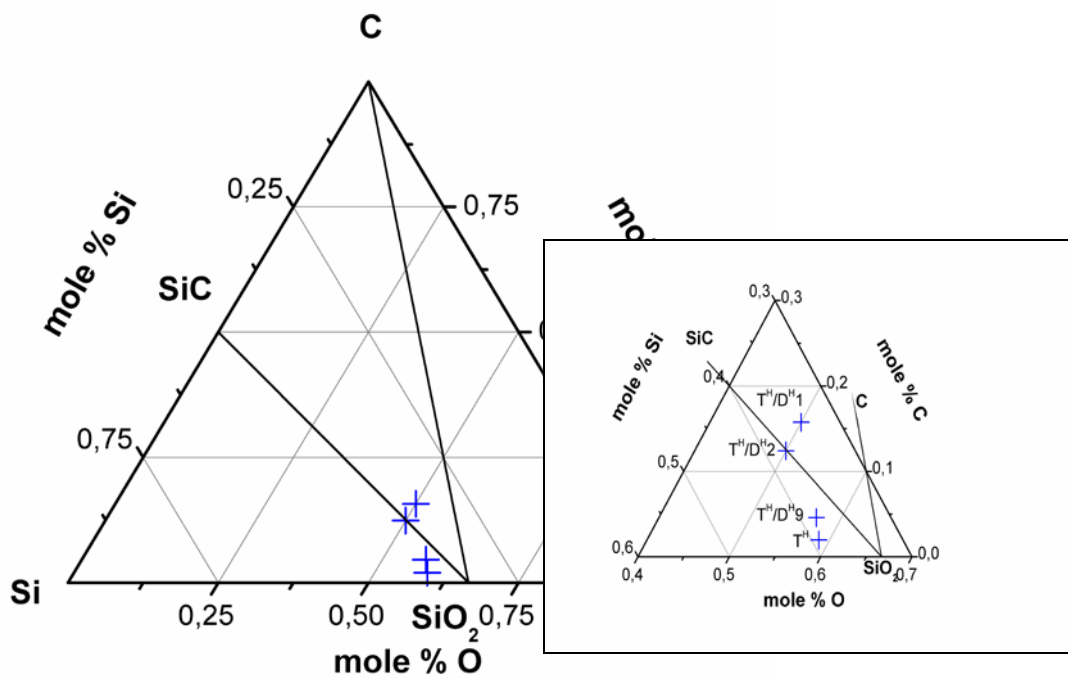


Figure 4.1. Phase diagram of Si-C-O. **Inset.** Studied compositions have been shown with the corresponding precursor ratios used for labelling.

For all compositions, ethanol was used as solvent with a ratio of EtOH/Si=2. Proper amount of H_2O (pH =4.5, HCl) was added to the alkoxide solutions in order to induce hydrolysis and to have a gelling period long enough to allow sufficient time for film

production. The selected solution was spun at 3000 rpm for 1 minute on ultrasonically cleaned SiO₂ (Heraeus -HSQ300) and Si (n-type) substrates. The gel films were stabilized at 80°C for 24 hours before pyrolysis. The pyrolysis process was carried out in a C-furnace under Ar flow (100 ml/min) with a heating rate of 5°C/min at different temperatures, in the range 800-1250°C with 1 hour holding time at the maximum temperature.

Surface quality of the films was investigated by SEM and AFM. Surface properties of the films were examined by Wilhelmy technique. The method gave important information not only about the change in hydrophobicity of the sample during the polymer to ceramic transformation but also the surface energy of the films by measuring advancing and receding contact angles. Elemental profile variations through the cross section of the films were studied by SIMS. Profilometer measurements were performed to investigate the film thicknesses. Chemical composition of the films was examined by XPS. The chemical nature of bonds present in the film was studied by XPS and FTIR. Photoluminescence measurements (PL) were recorded and evaluated according to the experimental details given in **Chapter 2.4.1**. The time-resolved photoluminescence (TRPL) technique is used to measure lifetime of the films (For further details see **Appendix II**). The transmission spectra of the SiOC films were recorded in order to determine the absorption optical band-gaps of the films (Tauc band-gap).

4.3. Results And Discussion

Surface morphology and of the films were examined by SEM and AFM. SEM analysis shows that at every pyrolysis temperature homogeneous and crack free films are produced even at the edges. Average roughnesses were measured from the AFM images and falls in the range 0.5 – 2.5 nm. The roughness increases up to 1100°C and then it stabilizes. Optimized surface properties have been obtained after adding a drying step at 80°C for 24h. **Figure 4.2** shows the SEM and AFM images for films deposited without (**Figure 4.2-a**) and with (**Figure 4.2-b**) the drying step. Large cracks were present in the film in **Figure 4.2-a** which were completely disappeared in **Figure 4.2-b** after drying step.

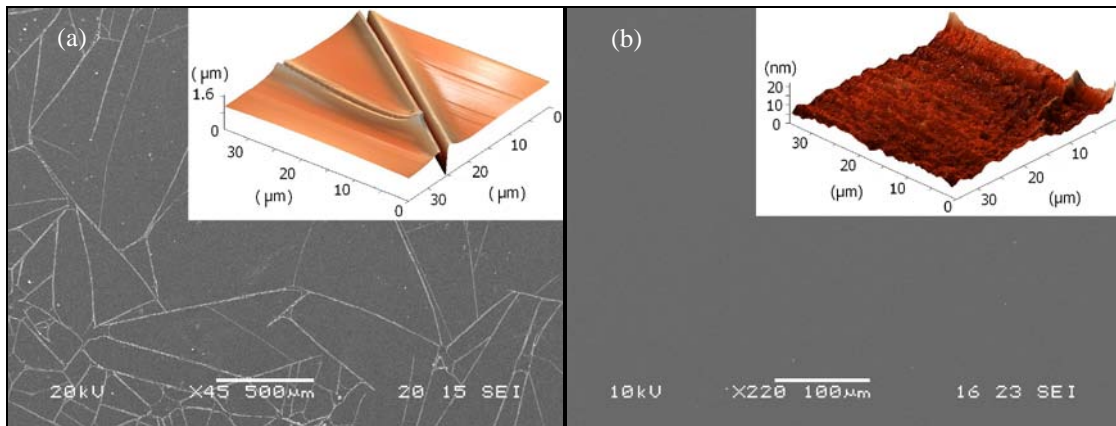


Figure 4.2. SEM images of samples annealed at 1200°C before (a) and after (b) optimisation. **The inset** shows AFM images of the same samples

FTIR spectra of the sol-gel derived, pre-ceramic films are given in **Figure 4.3**. Si-H bonds from triethoxysilane (T^H) gave rise to peaks at 2243 cm^{-1} (ν (stretching)) and at 831 cm^{-1} (δ (bending)). Similarly, Si-H bonds from D^H lead to bands at 2173 cm^{-1} (ν) and at 760 cm^{-1} (rocking). Si-CH₃ stretching vibrations were associated with the peak at 1261 cm^{-1} . In particular, Si-H peaks at 2180 and 2250 cm^{-1} confirmed the presence of both silicon precursors in the $T^H D^H$ films. Moreover, the FTIR spectrum of the $T^H D^H 1$ film shows a higher intensity of the 2173 cm^{-1} peak in agreement with $T^H D^H$ ratio used for the synthesis. Si-O stretching peaks are present in the range $1140\text{-}1065\text{ cm}^{-1}$ [A. Karakuscu, 2008; G.D. Soraru, 1995]. Finally, the peak observed at 610 cm^{-1} is caused by the Si substrate.

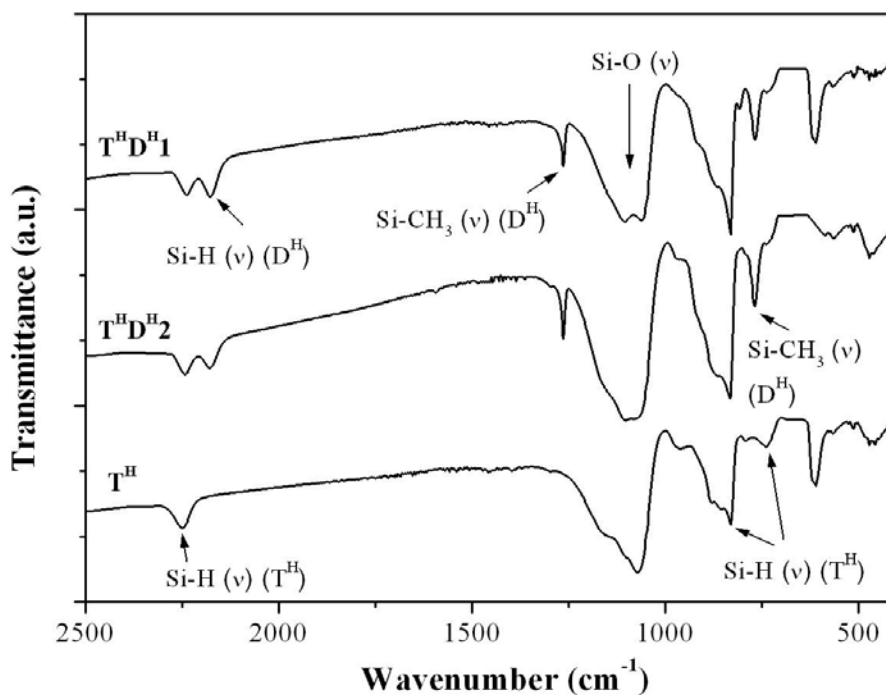


Figure 4.3. FTIR spectra of as-coated SiOC films with different compositions. Corresponding bands are shown on the figure with possible relevant precursor.

In order to understand the change in the bonding structure of the films during the pyrolysis, stoichiometric SiOC films pyrolysed at different temperatures were analysed by FTIR. The FTIR in transmittance mode have been used to analysis the films on Si substrate. However, due to the reaction between the SiOC film and the Si substrate at high temperatures ($\geq 1200^{\circ}\text{C}$), results were given only up to 1100°C (see **Chapter 4.4**). **Figure 4.4** shows the corresponding results from the samples as deposited and annealed at 800°C , 1000°C and 1100°C , respectively. The intensities of the bands at 450 and 1090 cm^{-1} belong to Si-O-Si rocking and stretching vibrations of SiO_2 increased with the increase in pyrolysis temperature [G. Das, 2007]. The peaks at 831 cm^{-1} and 2243 cm^{-1} , due to Si-H bonds from triethoxysilane (T^{H}), vanished as the pyrolysis temperature increase. Similarly, Si-H bonds from D^{H} at 760 cm^{-1} , 1250 cm^{-1} and 2173 cm^{-1} disappeared at 800°C . For pyrolysis temperatures higher than 800°C , a band at 820 cm^{-1} appeared. This vibration is related to Si-C bonding and its intensity increased radically with the annealing temperature [G. D. Sorarù, 1996]. Finally the film pyrolysed at 1100°C , basically showed two vibrations at 450 cm^{-1} belonging to Si-O and at 820 cm^{-1} related to Si-C vibration. The wide band centred at 1084 cm^{-1} with a

shoulder at 1220 cm^{-1} is a combination of many bonding and considered as a complex range of Si-O and Si-O-C vibrations [G. Das, 2007].

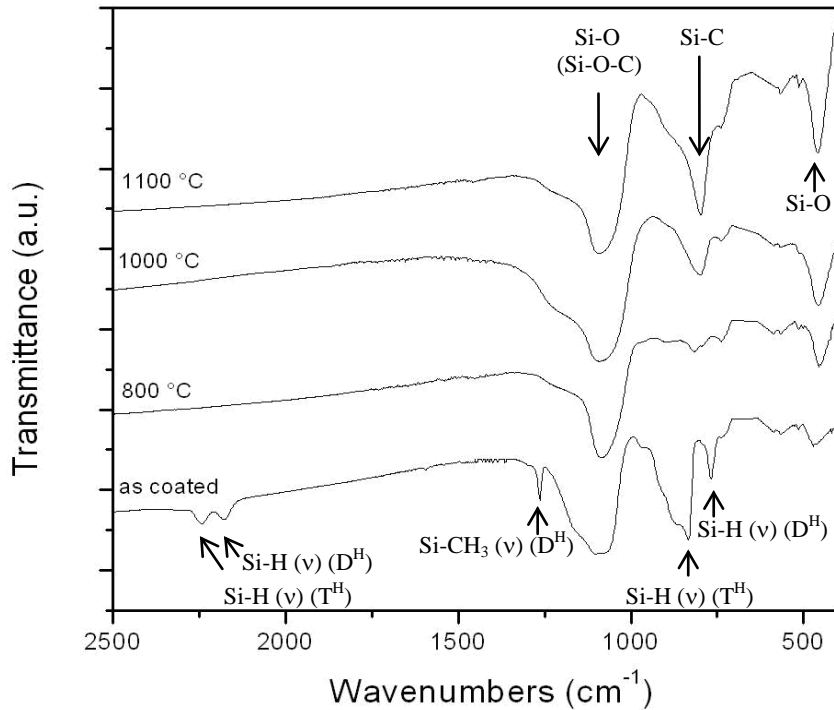


Figure 4.4. FTIR spectra of as deposited and annealed stoichiometric SiOC films ($T^H D^H2$).

Since the FTIR measurements in transmittance mode could not give more information on the bonding state of the films pyrolysed at high temperatures ($\geq 1200^\circ\text{C}$), some FTIR-ATR measurements were performed for the films coated on SiO_2 substrate and given in **Figure 4.5**. We need to remind that the knowledge of the bonding structure of the films on SiO_2 was crucial for the study, since we performed all the following optical characterization on films on SiO_2 substrate. Moreover, as it will be discussed later on, the Si substrate could not be used for pyrolysis temperatures higher than 1200°C . Therefore, ATR-FTIR measurements were performed to complement the transmittance FTIR measurements.

In the spectra of as-coated film (**Figure 4.5**), Si-H bonds of the T^H precursor gave rise to peaks at 2243 cm^{-1} and 831 cm^{-1} while Si-H bonds of D^H units led to a corresponding band at 2173 cm^{-1} [G. D. Sorarù, 1996]. Si- CH_3 stretching and rocking vibrations were

revealed by the peaks at 1261 cm^{-1} and 760 cm^{-1} . Peak at 1065 cm^{-1} with a shoulder at 1140 cm^{-1} was assigned as Si-O bonds in the siloxane network similar to transmittance FTIR.

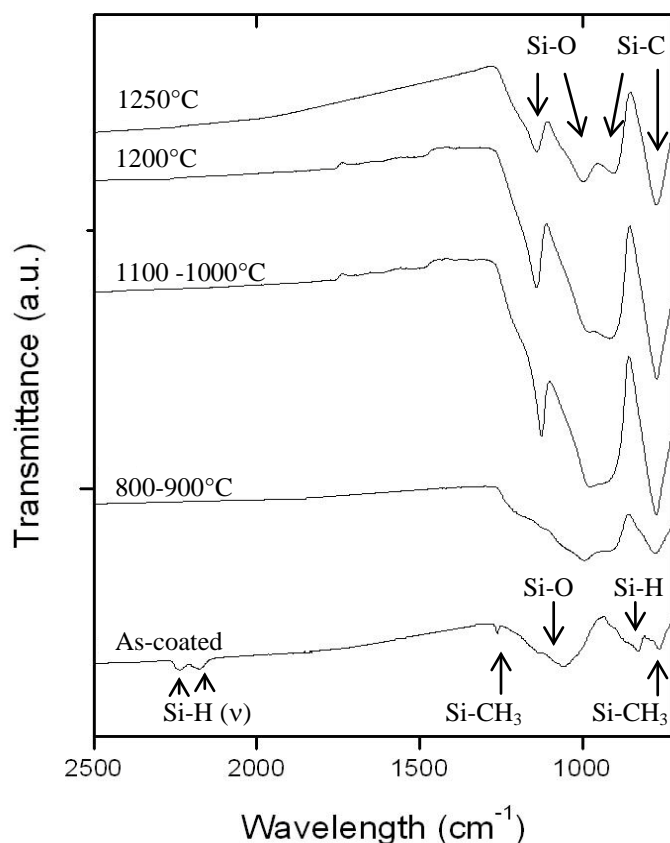


Figure 4.5. FTIR-ATR spectra of as-coated, and pyrolyzed SiOC thin films at different temperatures 800- 1250 °C.

At 800-900°C the Si-H and Si-CH₃ related bands at 2200-2150 and 760 cm^{-1} respectively are absent suggesting that the polymer to ceramic transformation is complete. At the same time a complex and broad absorption band is observed in the range 1300-900 cm^{-1} with a local peak at 1000 cm^{-1} assigned to the vibration of Si-O bonds. It is assumed that this broad band includes contribution of Si-O and Si-C bonds. The presence of inorganic Si-C bonds similar to those of silicon carbide, is also suggested by the formation of a new peak at 780 cm^{-1} .

At higher pyrolysis temperatures (1000-1100°C) the broad peak around the Si-O vibration becomes more defined suggesting that an organization process of the SiOC

network is active in this temperature range. In particular a peak appears at 1140 cm⁻¹ which is assigned to Si-O vibration, the main absorption around 1000 cm⁻¹ reveals a shoulder at 920 cm⁻¹ related to Si-C vibrations and finally the Si-C absorption at 780 cm⁻¹ becomes more intense suggesting the formation of new Si-C bonds. Above 1100°C the FTIR investigations do not show any major evolution: only the shoulder at 920 cm⁻¹ grows as an individual peak, indicating a further increase the number of Si-C bonds or ordering of amorphous network [J.Y. Fan, 2006; A. Karakuscu, 2008]. As a result in ATR-FTIR, films pyrolysed at higher temperatures (≥1200°C) could be analysed. Moreover, the existence of Si-C vibrations is verified for the films on SiO₂ substrate.

Wettability is an important property of solid surfaces and is governed by both the chemical composition and the surface topography. Since the surface chemistry of the films changes with the pyrolysis from polymer to ceramic, they give different hydrophobicity behaviour through the pyrolysis. Moreover, contact angle analysis is useful to measure surface energies of the films.

A variety of different methods have been used to study the wetting of solid surfaces by liquids. They involve measuring the contact angle θ formed by the liquid at the solid–liquid–vapor triple line. The contact angle is related to the solid–liquid interfacial tension, γ_{SL} , solid surface free energy, γ_{SV} , and liquid surface tension, γ_L , through Young's equation [Young, 1805]:

$$\cos\theta = \frac{\gamma_{SL} - \gamma_{SV}}{\gamma_L} \quad \text{Eq. 4.1}$$

The study of wetting under dynamic conditions was performed using the Wilhelmy plate method, in which dynamic contact angles (DCA) are measured by recording the force acting on the solid as it moves through the liquid/air interface at constant speed. Dynamic contact angle and contact angle hysteresis measurements are usable method to measure hydrophobicity of the surface. Although in literature several models exists in literature, Wilhelmy plate technique is used as an indirect method of contact angle measurement due to being the most accurate method for measuring dynamic contact angles. This method measures the advancing contact angle (θ_{adv}) during immersion of the solid plate, and the receding one (θ_{rev}) during the emersion process. The difference

between the two angles is defined as the contact angle hysteresis and it is reported to be related to many different factors such as surface roughness, changes in the organization of molecules on the solid surface, surface heterogeneity, etc [H. Chen, 2009].

The results of Dynamic Contact Angle (DCA) analysis are reported in **Table 4.1** where advancing and receding contact angles obtained in three different liquids are compared. Water, ethylene glycol ($C_2H_6O_2$) and Bromonaphtalene ($\alpha Br-C_{10}H_7$) is used to compare the contact angles. The advancing angle is taken as the largest possible angle and the receding is the smallest possible contact angle. Both were measured at thermodynamic equilibrium. Polymer to ceramic transformation can be easily followed from the contact angle results. Pyrolysed thin film has lower θ values corresponding to an increase in the surface energy. As coated film showed strong hydrophobic behaviour whereas pyrolysed film showed hydrophilic behaviour (**Figure 4.6**).

Table 4.1. Contact angles versus pyrolysis status

Sample	θ_{adv}	θ_{rev}	θ_{adv}	θ_{rev}	θ_{adv}	θ_{rev}
	(H_2O)	(H_2O)	($C_2H_6O_2$)	($C_2H_6O_2$)	($\alpha Br-C_{10}H_7$)	($\alpha Br-C_{10}H_7$)
As-coated	100	98.3	63.6	60.1	56	49.7
1200 °C	40.4	-	12.4	-	12.1	-

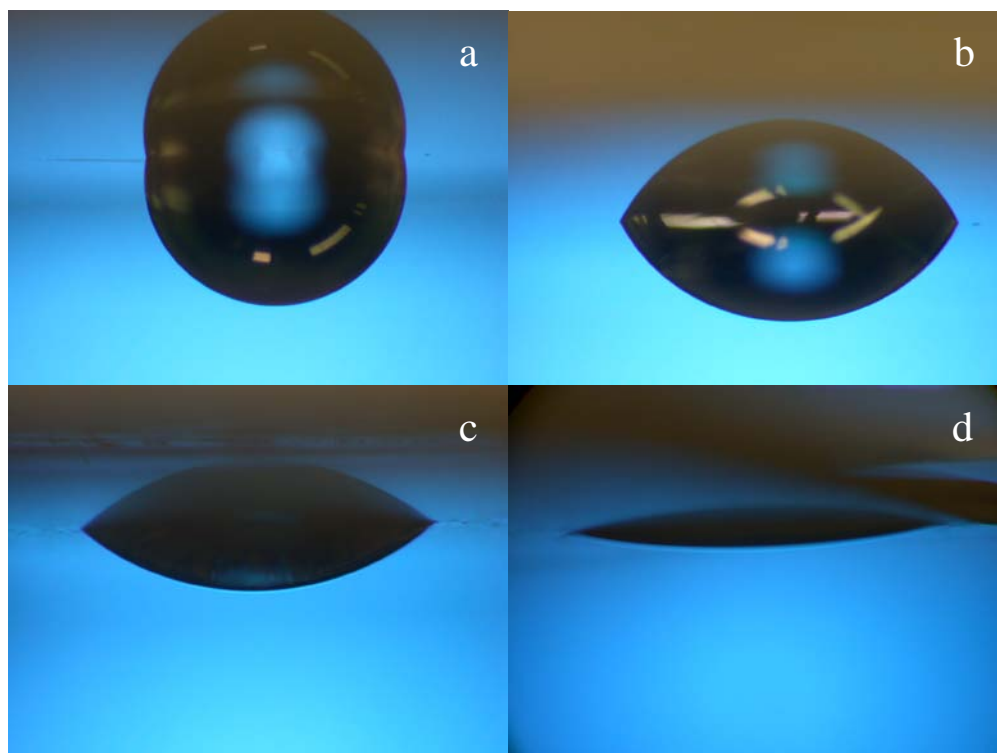


Figure 4.6. The photograph of the surfaces of the “as coated” stoichiometric SiOC film wetted with different liquids to measure advancing and receding contact angles: **(a)** Water droplet **(b)** ethylene glycol ($C_2H_6O_2$) droplet and **(c)** Bromonaphtalene ($\alpha Br-C_{10}H_7$) droplet. The film pyrolysed at $1200^\circ C$ showed high hydrophilicity, therefore only **(d)** water droplet could be used to measure the surface kinetics.

The specific surface energy of a solid were calculated from contact angle measurements using liquids which exhibit different and known polar and disperse components. Corresponding to FTIR results, hydrophobic behaviour of the non pyrolysed thin film is caused by the presence of Si-CH₃ and Si-H groups and with pyrolysis these bonds replace by Si-C bonds. Therefore, the hydrophilicity is suddenly decreasing, while the surface energy of the ceramic film increases. Surface energies of thin films before and after pyrolysis step is calculated according to SURFTEN 4.0 and found as 29 mJ/m^2 and 49 mJ/m^2 , respectively. These results are comparable with the methyl-modified silica films [C. Della Volpe, 1997; J. Yang, 2009].

In order to see the chemical homogeneity through the cross section of the film SIMS measurements were performed. Carbon and hydrogen depth profiles measured by SIMS

analysis of the as-coated and pyrolysed films are given in **Figure 4.7**. For this analysis, a gold 20 nm thick capping layer was deposited on the sample surfaces in order to have a conductive capping layer. This layer is indicated in the figure and affected the first few nanometers of the measurements. A homogeneous carbon distribution is observed in the cross section of each film (**Figure 4.7-a**). Furthermore, H depth profiles of the films did not show any hydrogen after 1000°C indicating that the pyrolysis is complete at that temperature (**Figure 4.7-b**). Indeed, film pyrolysed at 1200°C showed the same H content as the reference SiO₂ substrate - shown in **Figure 4.7-b** as the straight black line – which also corresponds to the detection limit of the equipment.

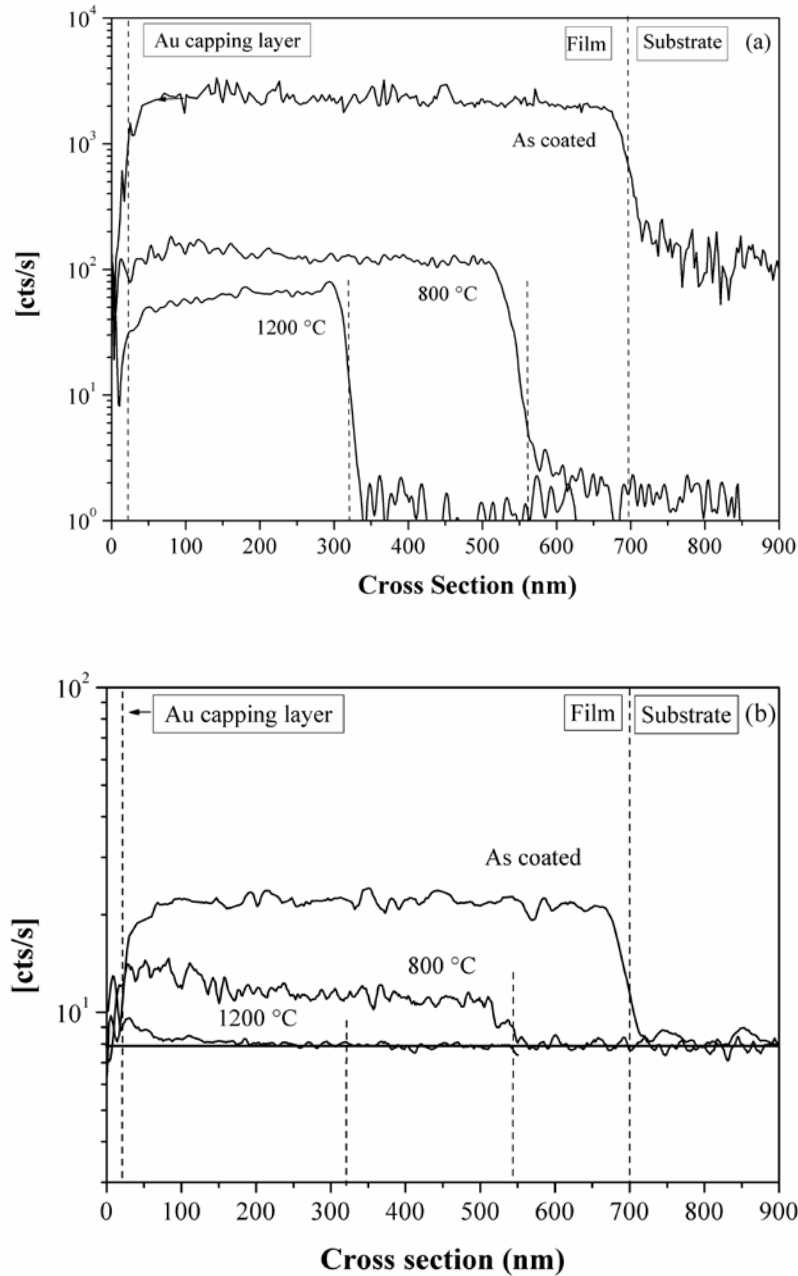


Figure 4.7. (a) Cs^{12}C and (b) Cs^1H SIMS depth profiles on $\text{T}^{\text{H}}\text{D}^{\text{H}2}$ films as-coated, pyrolysed at 800°C and 1200°C . Capping layer, film and substrate are shown with dashed line.

Thickness measurements by profilometer are consistent with the SIMS results. According to profilometer results, films showed a sharp linear shrinkage, namely around 30%, from the as-coated stage up to 900°C . From that temperature, the shrinkage slowed down and after 1100°C , films showed no more shrinkage, which indicates the stabilization of the films. These findings are in good agreement with the

TGA (Thermo-Gravimetric Analysis) performed on the corresponding gels which indicate that the pyrolytic transformation is complete at 1000°C (**Figure 3.5**). Thickness values of the films are given in **Table 4.2**. The slight differences between the SIMS and profilometer values are ascribed to the sample to sample variation in the thickness of the starting film. However, shrinkage results were found similar, showing the coherence of the measurements.

Table 4.2. Thickness values for different temperatures (as-coated, 800 °C and 1200 °C) and calculated linear shrinkage values.

Films	Thickness			Linear Shrinkage
	As-coated	800°C	1200°C	1200°C
T ^H /D ^H 1	800 nm	540 nm	480 nm	40% ±1
T ^H /D ^H 2	910 μm	630 nm	490 nm	45% ±3
T ^H	1.210 μm	810 nm	640 nm	47% ±2

The elemental compositions of SiOC films pyrolysed at 1200°C, deduced by XPS measurements, are given in **Table 4.3**. T^HD^H2 film pyrolysed at 1200°C has a chemical composition close to the expected one with negligible amount of graphitic sp² C present [H. Bréquel, 2004]. On the other hand, T^H films showed an un-expected presence of carbon, since the precursor has no Si-C bonds and theoretically it should lead to films comprising only Si and O. Nevertheless, a similar behaviour was also observed in XRD (X-ray Diffraction) analysis of the powder samples of the same precursor and crystallization of SiC was detected at high pyrolysis temperatures (≥1400°C) (discussed in details **Chapter 3**). The presence of C in the pyrolyzed material from T^H precursor has to be related to residual alkoxy groups left behind by the hydrolysis step. Indeed, it is known that the degree of condensation of gels prepared from mixtures of T^H and D^H precursors decreases by increasing the amount of trifunctional units [G. D. Sorarù, 1995(c)] and that the un-condensed terminal groups consist of residual hydroxyl as well as alkoxy groups. During pyrolysis the alkoxy groups transform into free carbon which is retained in the silica-based structure. At high pyrolysis temperatures this carbon can react with free silicon in the T^H system and gives SiC. In this work T^H system has been chosen to give Si rich SiOC system. On the other hand, T^HD^H1 is a well known system to produce C rich SiOCs [H. Bréquel, 2004].

Table 4.3. XPS elemental composition of the investigated SiOC glasses pyrolysed at 1200 °C.

Films	Si (at. %)	C (at. %)	O (at. %)	Empirical formula	Theoretical Composition ^[4]
T ^H /D ^H 2	38.3	13.3	48.5	SiC _{0.35} O _{1.27}	SiC _{0.33} O _{1.33}
T ^H	36.8	8.0	55.2	SiC _{0.22} O _{1.50}	SiO _{1.5}

XPS measurements gave valuable information about bonding structure as well as chemical composition of the films. C1s and Si2p core line analysis by XPS revealed the bonding structures of the films, which are coherent with FTIR and XPS elemental analysis. By increasing the pyrolysis temperature both core line analyses showed significant shift, towards the Si-C bonding peak region. In **Figure 4.8a**, Si2p XPS analyses of T^HD^H2 films were given for pyrolysis temperatures 800 °C and 1200 °C in order to reveal this peak shift. At 800 °C, the film showed a narrow peak centred at 103.5 eV which was assigned to a Si-O bonding such as those typically observed in silica. Increasing the temperature, the peak shifted toward lower binding energies typical of silicon atoms bonded to carbon atoms such as in SiC. At 1200°C the Si2p peak shifted to 102.7 eV and broadened asymmetrically. The peak fitting of the T^HD^H2 film pyrolysed at 1200 °C is given in **Figure 4.8b** in order to illustrate the corresponding components. Features have been assigned to the presence of mixed silicon oxycarbide units such as CSiO₃ and C₂SiO₂, based on published reference data [G. D. Sorarù, 1996(b); R.J.E Corriu, 1997].

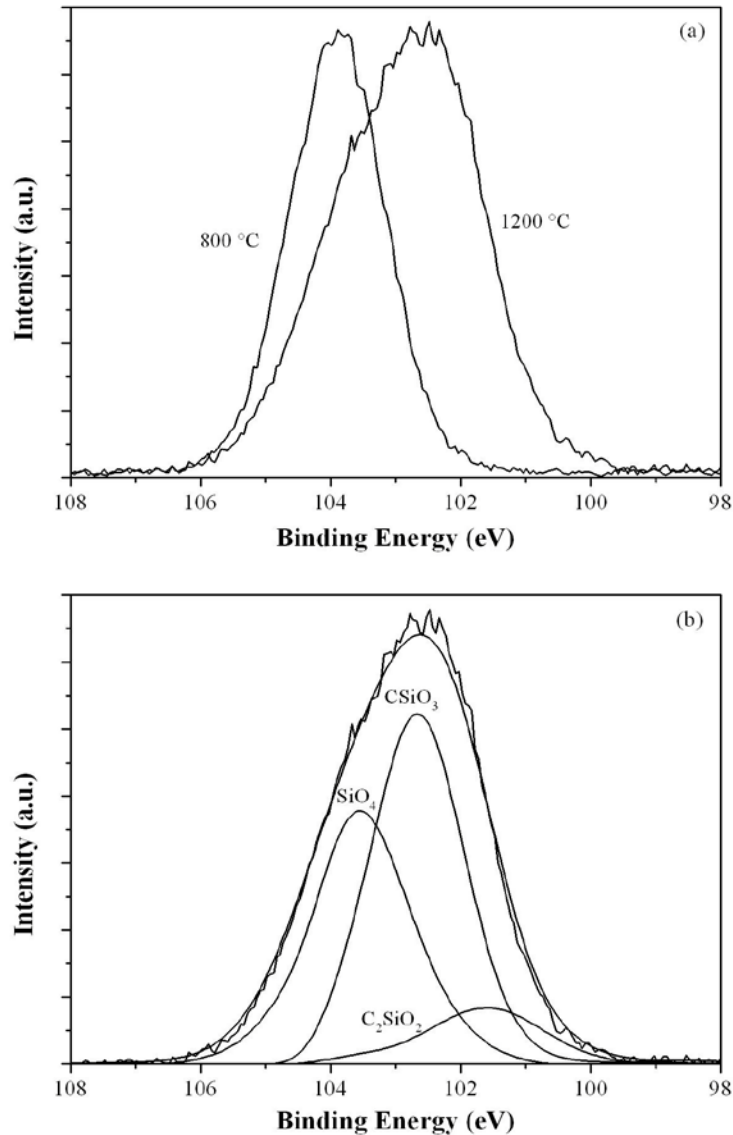


Figure 4.8. Si2p core line XPS analysis of T^HD^H2 films (a) pyrolysed at 800°C and 1200°C, (b) peak fitting of film pyrolysed at 1200°C.

C1s core line analysis of T^HD^H2 films pyrolysed at different temperatures and related peak fitting for the film pyrolysed at 1200°C are given in **Figures 4.9-a and 4.9-b**, respectively. C1s XPS survey showed not a shift but a broadening towards 283.5 eV which is the binding energy of C-Si bonds [R.J.E Corriu, 1997]. C1s and Si2p analysis of the T^HD^H2 films at 1200°C clearly showed the presence of silicon oxycarbide network in which Si-C bonds are present in mixed silicon oxycarbide units; parallel to the studies on SiOCs known to lead SiC phase separation at high temperatures [H. Bréquel, 2004].

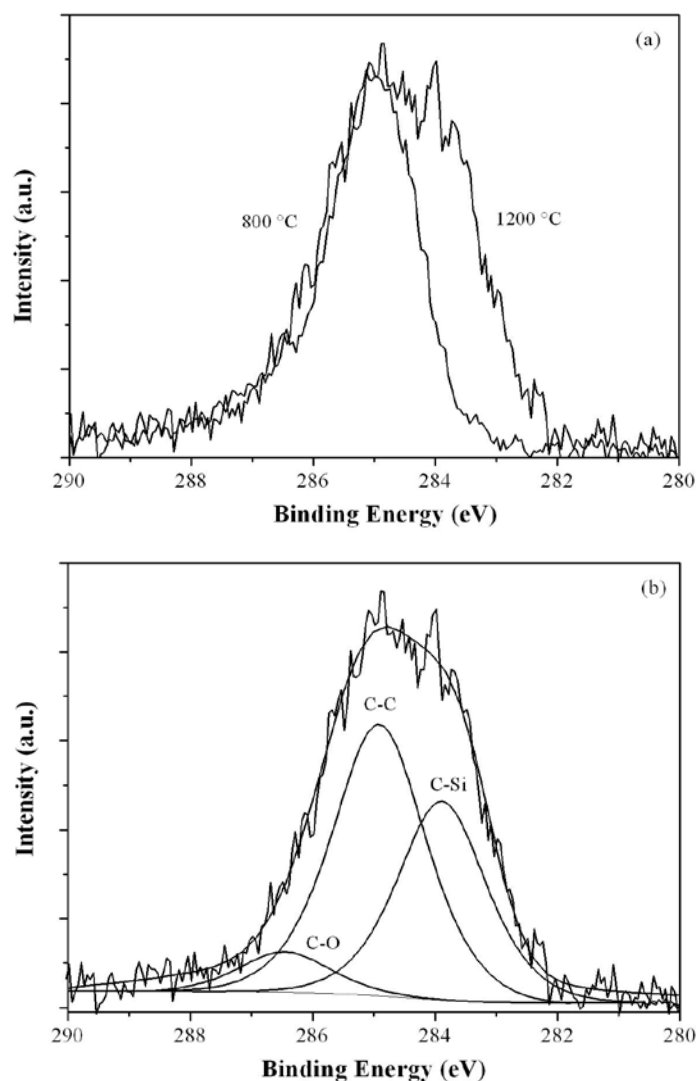


Figure 4.9. C1s core line XPS analysis of T^HD^H2 films (a) pyrolysed at 800°C and 1200°C, (b) peak fitting of film pyrolysed at 1200°C.

The evolution with the pyrolysis temperature of the Si2p peak of T^H films (**Figure 4.10a**) showed only a slight shift from 103.6 to 103.4 eV suggesting possible formation of Si-C bonds belonging to mixed SiOC units. As it can be seen in **Figure 4.10-b**, the Si2p peak of the T^H film pyrolysed at 1200°C could not be convoluted by only one peak; instead another component appeared at 102.8 eV which was assigned to CSiO₃ units. Excess Si could not be observed by Si2p analysis due to the fact that T^H films contained very low amount of Si and/or Si amount was close to detection limit of the

XPS equipment. Additionally, no peak shift or broadening was observed in the C1s XPS analysis.

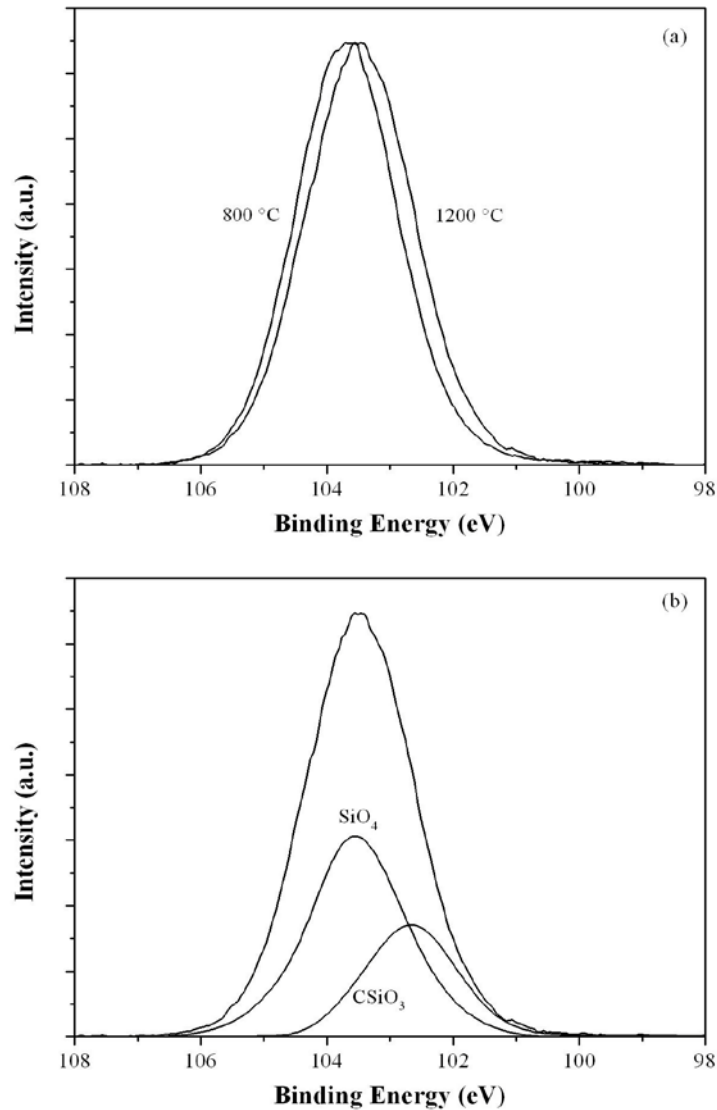


Figure 4.10. Si2p core line XPS analysis of T^H films (a) pyrolysed at 800°C and 1200°C, (b) peak fitting of film pyrolysed at 1200°C.

T^HD^H9 films, which have relatively high C content with respect to T^H, showed very similar Si2p core analysis and shown in **Figure 4.11**. The shift towards the Si-C bonding increase in pyrolysis temperature is evident in Si2p XPS analysis. The convolutions of the peaks for samples pyrolysed at 1250°C are given in insets. With temperature increases, more mixed Si-O-C bonding is formed due to phase separation. However, the expected carbon amount is definitely less that T^HD^H2 films and should be

more than T^H films, which caused in Si2p peak the shifting more noticeable than T^H films but less detectable than $T^H D^{H2}$ films[G. D. Sorarù, 1995(c)].

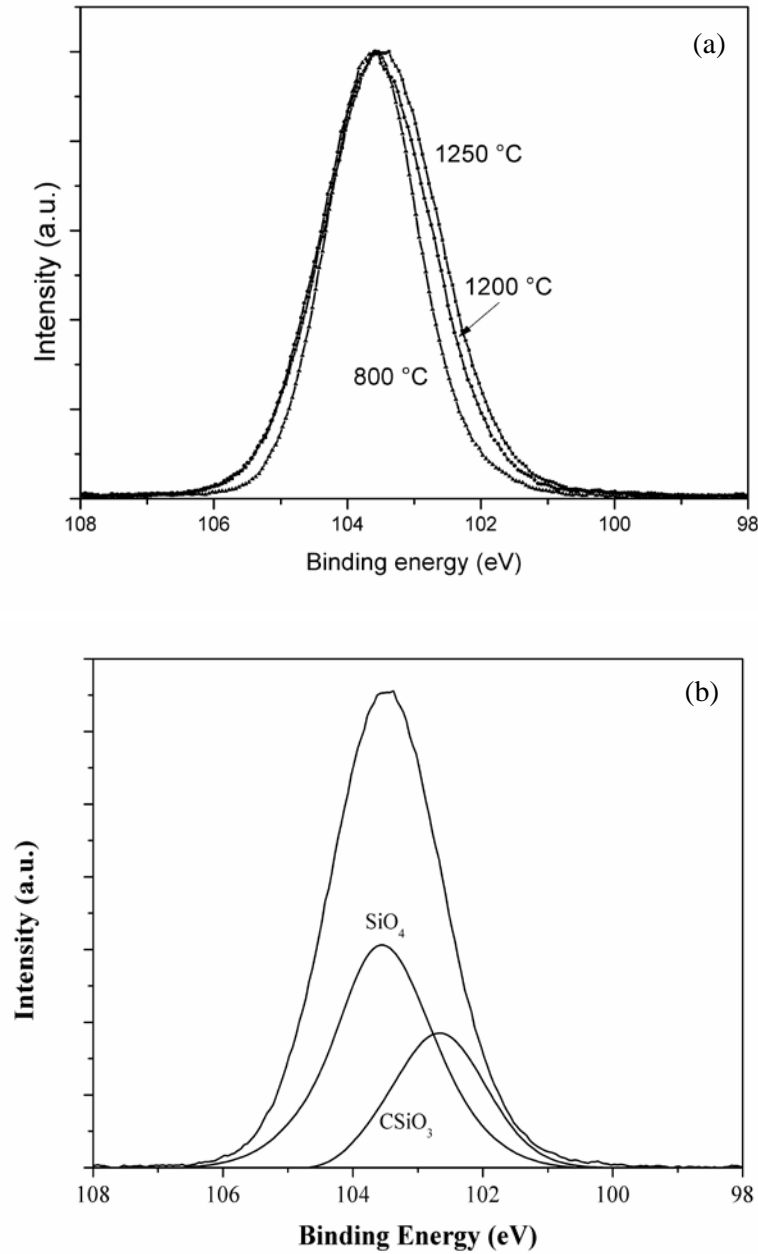


Figure 4.11. Si2p core line XPS analysis of $T^H D^{H9}$ films (a) pyrolysed at 800°C, 1200°C and 1250°C, (b) Peak fitting of film pyrolysed at 1250°C.

In all SiOC films, the same evolution in PL was observed with increasing pyrolysis temperature. At low temperatures, the amorphous state, which is rich in defects, gave rise to an intense UV-blue band detected at about 410 nm. Since the pump light wavelength was close to this band, only the tail of the emission was observed. The

increase of the pyrolysis temperature led to the disappearance of this band and the appearance of another band in the green-yellow range at 560 nm, in parallel with XPS analysis showing the formation of the Si-C bonds at higher temperatures. PL behaviour suggests that when the pyrolysis temperature is raised from “low” degrees (800-1000°C) to “high” degrees (1100-1250°C), phase separation of SiC inside SiOC takes place, whereas this system is totally amorphous at low temperatures. Thus, the PL spectra will be discussed in the following at low temperatures and high temperatures, separately.

Photoluminescence spectra of the SiOC films at low pyrolysis temperatures (800°C) are shown in **Figure 4.12-a**. All peak intensities in PL spectra were normalized to the luminescence of a representative Si nanocrystals sample. At 800°C, T^H films showed the highest emission intensity and with increasing carbon content PL peak intensity decreased which is the case in T^HD^H1 films, the lowest emission observed in SiOC films. .

PL intensity evolution versus pyrolysis temperature is shown in **Figure 4.12-b**. In the figure, peak intensities were normalized by the T^H PL peak intensity for the easiness of comparison. The PL intensities diminished with respect to temperature, vanishing for temperatures higher than 1000°C in all SiOC films.

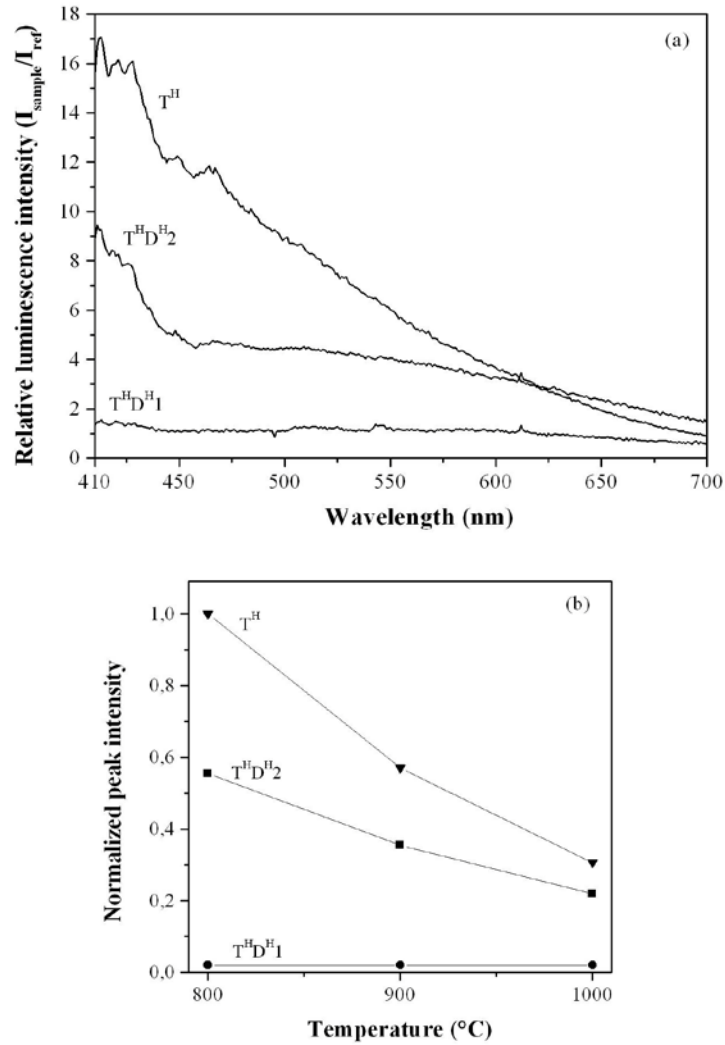


Figure 4.12. (a) Photoluminescence spectra of films pyrolysed at 800°C; (b) change in PL peak intensity versus temperature. PL peak intensities are normalized by the PL peak intensity of the T^H film pyrolysed at 800°C.

In order to illustrate the evolution of the photoluminescence spectra in the low temperature range (800°C - 1000°C) the PL spectra of the $T^H D^{H2}$ and T^H films are given in **Figure 4.13**. The disappearance at elevated temperatures of the UV-blue peak can be explained by the fact that at low temperature (800-1000°C) the amorphous network of the SiOC ceramics is rich in defects, such as dangling bonds, whereas the high temperature annealing (1100-1200°C) allows the reorganization of the structure and leads to a reduction of such defects [R.J.E Corriu, 1997].

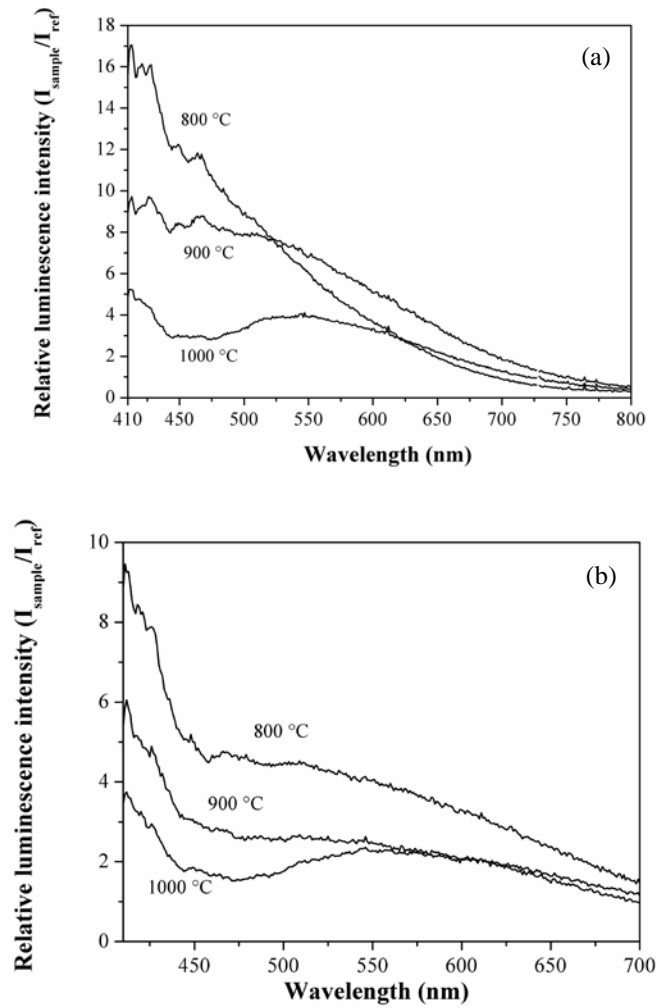


Figure 4.13.(a) Photoluminescence spectra of the $T^H D^H 2$ and (b) T^H films pyrolysed at low temperatures (800 - 1000°C).

The PL spectra of the SiOC films at 1200°C are shown in **Figure 4.14a** with the normalized peak intensities as a function of temperature shown in the **Figure 4.14b**. PL intensity of T^H and $T^H D^H 2$ films strongly increased with the temperature, reached a maximum at 1200°C and then drastically reduced at 1250°C. Conversely, the weak PL intensity of C-rich SiOC ($T^H D^H 1$) films did not show any increase with the temperature. The low photoluminescence intensity of the $T^H D^H 1$ sample is certainly related to the presence of a high excess of free carbon which absorbs the emitted light.

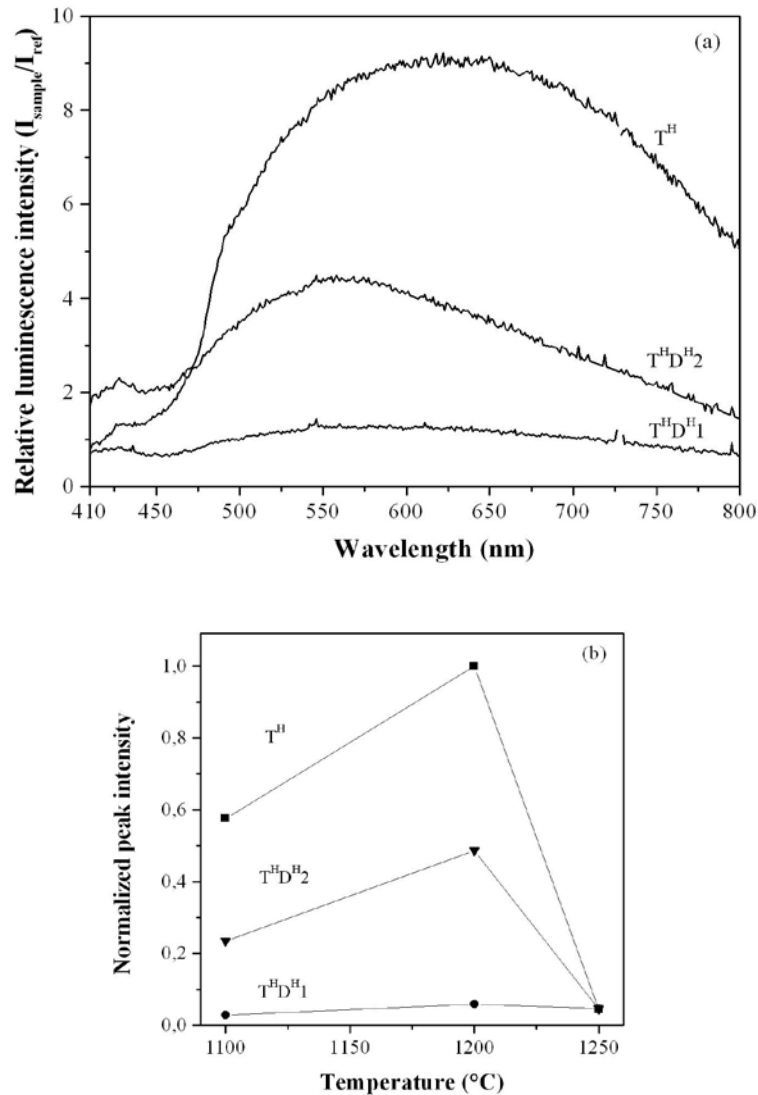


Figure 4.14. (a) Photoluminescence (PL) spectra of films pyrolysed at 1200°C; (b) change in the PL peak intensity of the films versus temperature. PL peak intensities are normalized by the PL peak intensity of the T^H films pyrolysed at 1200°C.

From 1000°C and up to 1200°C, the green-yellow band did not move spectrally in $T^H D^H2$ (stoichiometric SiOC) films and stayed at 560 nm. This band could be assigned to the formation of SiC phase which is known to emit in the green range (550-570 nm) (**Figure 14(a)** and **15(a)**) [A. Karakuscu, 2008; M. B. Yu, 2000]. Moreover, it is known that for pyrolysis temperature above 1000°C silicon oxycarbide glasses undergo a phase separation process with the formation of β -SiC phase [H. Bréquel, 2004]. Indeed, SiC bond formation was also verified with the XPS analysis at high temperatures (**Figure 4.9, 4.10, 4.11**). Additionally, in the sol-gel derived stoichiometric SiOCs, very small amount of free carbon may remain in the films after pyrolysis and cannot be easily

detected by analysis [C. Turquat, 2001]. These small amounts of free C can give luminescence in the yellow range (580 nm) and can influence the photoluminescence by broadening or causing asymmetric PL bands [J. C. Pivin, 1998]. Therefore, the asymmetric band observed in $T^H D^H_2$ films at 560 nm with a tail in the yellow could not be assigned only to SiC clusters but also to a contribution of a low amount of free C. However, the C amount in the films should be kept very low in order to improve the emission. In fact, C-rich SiOC films showed poor luminescence although their carbon content was very low (≤ 0.075 mol%) [H. Bréquel, 2004].

The PL spectra of $T^H D^H_2$ and T^H films, pyrolysed at high temperatures are given in **Figure 4.15(b)**. Similar to $T^H D^H_2$ films, T^H films showed a green-yellow band at 560 nm up to 1100 °C. The luminescence at 1100°C can therefore be assigned to the same combination of SiC and C clusters as in $T^H D^H_2$. However, at 1200°C Si-rich SiOC (T^H) films showed a sudden broadening with an increase in intensity. In previous study [G. D. Soraru, 2003], a very wide luminescence peak centred at 600 nm was reported at 1050°C in polymer derived silica based ceramics. Peak emission was explained by very small Si nanocrystal formation or by silicon-oxide related defect. Si_{ncs} formation was shown at higher pyrolysis temperature and caused a narrowing of the PL peak and red shift [G. D. Soraru, 2003]. Accordingly, in T^H films, the sudden widening at 1200°C of the luminescence can be explained by a phase separation of Si inside silicon oxycarbide network. Moreover, the presence SiC and C clusters in the system as well as the size distribution of the emitting sites could contribute to further widen the range of optical emission thus explaining the very unusual width of the measured PL band which extends beyond the visible range (430 nm-900 nm).

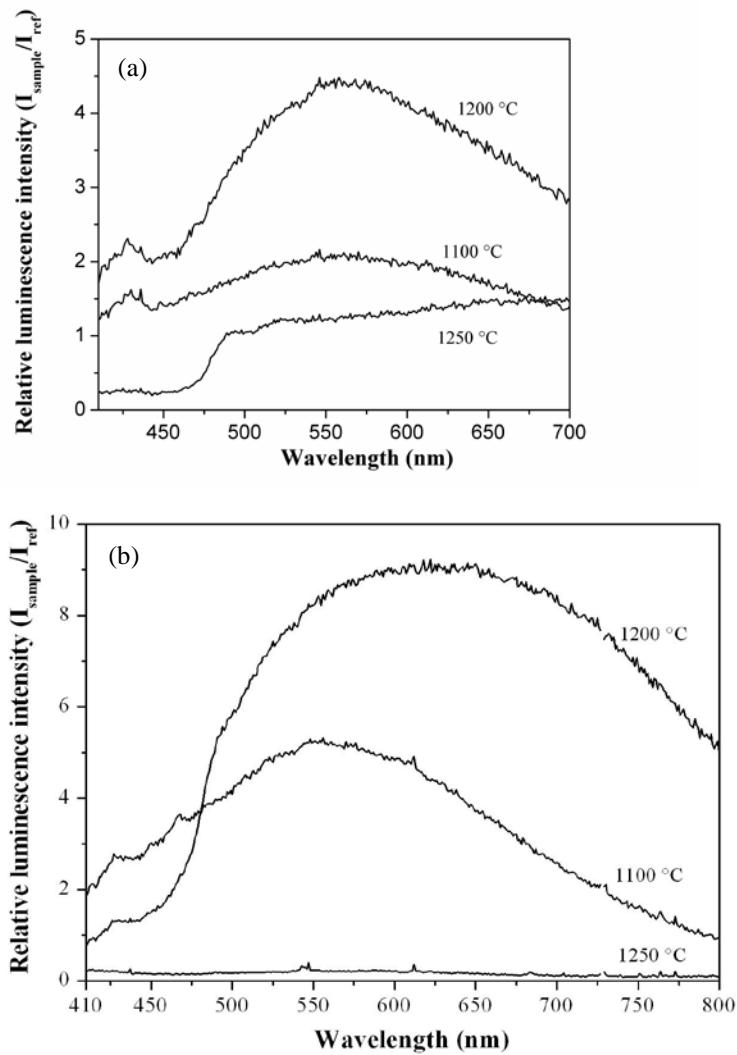


Figure 4.15. Photoluminescence spectra of (a) $T^H D^H 2$ and (b) T^H films pyrolyzed at high temperatures (1100-1250 °C) (Please note the scale differences) .

Photographs of the T^H films pyrolyzed at different temperatures from 800°C to 1250°C under blue light excitation are shown in **Figure 4.16**. The strong emission from the edges of the samples is caused by waveguide effects of the quartz substrate. The colours of the visible photoluminescence range from UV-violet for 800°C to blue at 1000°C and yellow-orange for 1250°C. At 1250°C the substrate starts to show an opaque appearance which could be indicative of thermal stability-related problems and can be the reason of the sudden PL intensity decrease at this temperature.

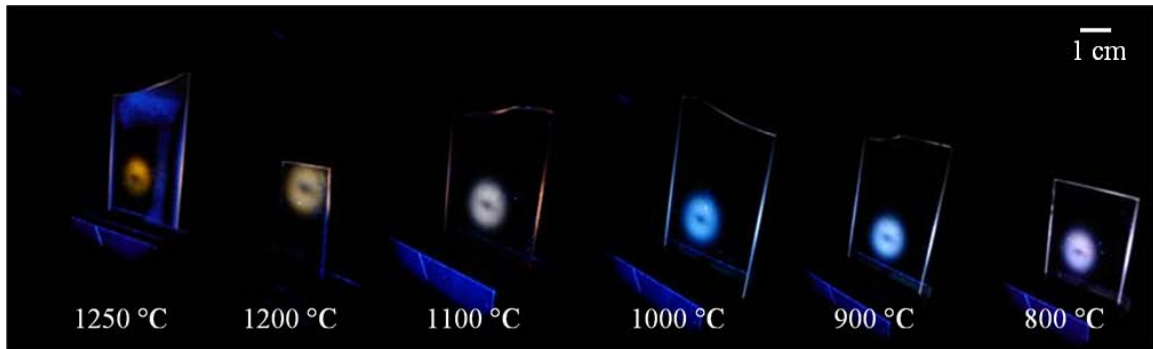


Figure 4.16. Photograph of the T^H films pyrolysed from 800°C to 1250°C under UV laser excitation. The exposure line differs for each photograph.

The unusual broadness of the PL peak of Si rich SiOC thin film at 1200°C, drive us to study another system, between T^{HD^2} and T^H composition. Therefore, T^{HD^9} system having more carbon and less Si compared to T^H is studied optically.

The luminescence behaviour of the film is given in **Figure 4.17** for low and high temperatures. At low temperatures, films showed similar behaviour with other SiOC films. However, the intensity at 900°C gave higher PL luminescence than other systems. Since the wavelength of the laser is very close to the emission peak, it was not possible to define the peak position at lower temperatures. However, from the photo of the films under UV lamp, very intense emission coming from film at 900°C can be seen, given in **Figure 4.18**. The origin of the emission at low temperatures suggested to be caused by defect states present in amorphous structure at these temperatures (800-1000°C). This peak shifted to 570 nm and fixed for the films pyrolysed at high temperatures. This peak is suggested to be originated by SiC clusters with contribution of C due to asymmetric band. Correspondingly, T^{HD^9} film showed a large second peak centred around 650 nm at 1200°C. The peak shape is an indication of contribution of two different emitting centers. Having known that Si clusters start giving luminescence in the red range (~ 650 nm), this large peak can be proposed as a results of Si clusters with the contribution of SiC and C as discussed previously [A. Karakuscu, 2009]. With an increasing Si amount the intensity increase radically and gave a very broad emission peak as in T^H film at 1200°C. Thus, the optimized Si contents in T^H film made it to be the largest and most intense luminescence obtained in SiOC system.

At 1250°C, the emission in green-yellow range decreased and the Si related red emission could not be observed. It can be due to either the red shift caused the peak be outside the detection range or we lost the emission due to the substrate effect, which discussed before.

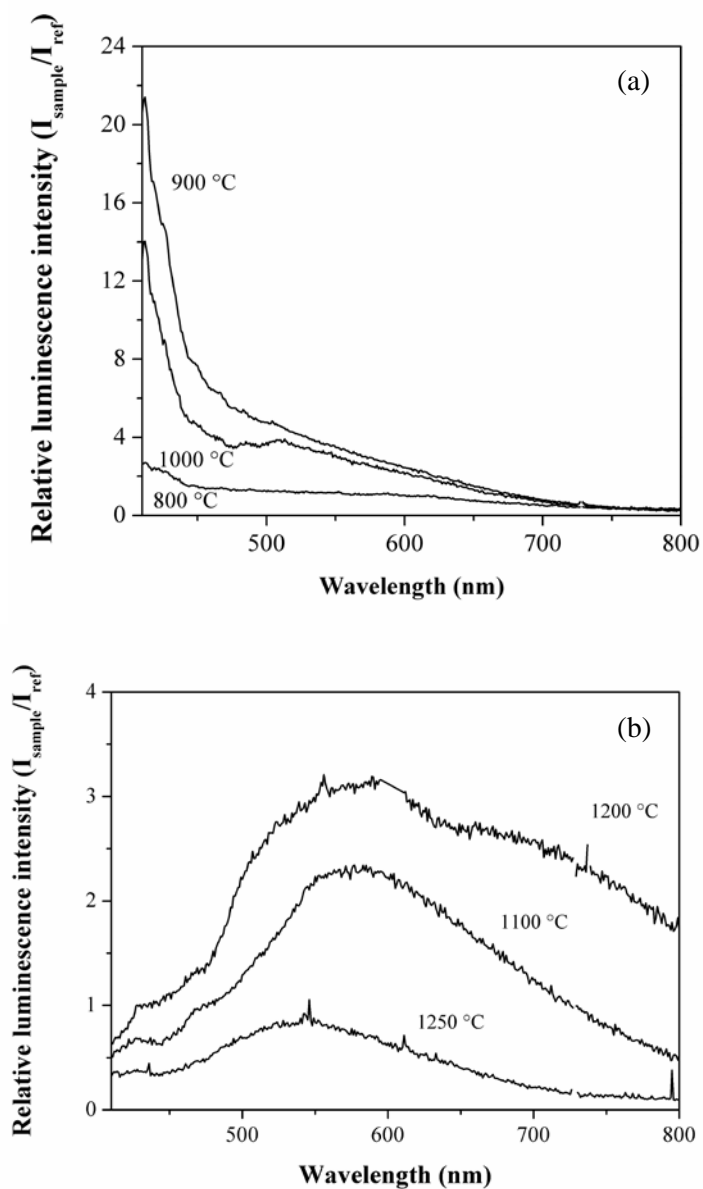


Figure 4.17. Photoluminescence spectra of the $T^H D^H 9$ films pyrolysed (a) at low temperatures (800 -1000°C) and (b) at high temperatures (1100 -1250°C).

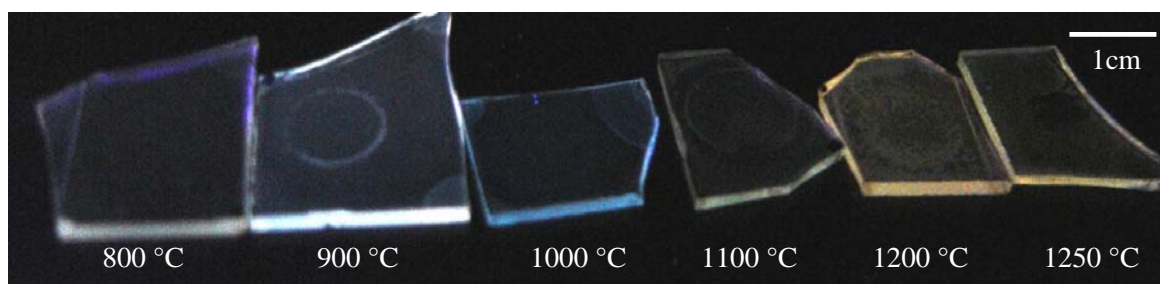


Figure 4.18. Photograph of the $T^H D^H 9$ films, pyrolysed from 800°C to 1250°C, under UV laser excitation.

Finally, in order to evaluate the potential of our films, we measured their external quantum efficiency (EQE). The EQE is defined as the ratio of the number of photons emitted by the film to the number of photoexcited electron-hole pairs. To measure the photon flux emitted from our samples, we calibrated the collection system (collecting lenses, monochromator, photomultiplier, photon counting unit) with a red LED whose response is known. By using this calibration, we measured the spectrally integrated luminescence intensity emitted by our films under photo-excitation and converted it into an emitted photon flux. The so-evaluated photon flux was corrected by the numerical aperture of the collecting system by assuming that the film is a lambertian point source. We considered that the total absorbed power by the active thin film is equal to the total laser power incident on the sample less the power transmitted by the sample, the power reflected by the sample and the power absorbed by the quartz substrate. We measured all these values with a power-meter calibrated at 365nm. Knowing the wavelength of the laser, we deduced the absorbed photon flux. The ratio between the emitted and the absorbed photon fluxes yields the external quantum efficiency of the film. We found the external quantum efficiency of the T^H films pyrolysed at 1200°C was 11.5 %; whereas, $T^H D^H 2$ and $T^H D^H 9$ films showed 5% efficiency. Since $T^H D^H 1$ films did not show noticeable luminescence, they had relatively low quantum efficiency. The EQE values are encouraging as it compares to the best results reported in the literature about Si nanomaterials so far, which is around 1% [L.B. Ma, 2006, D. Jurbergs, 2006].

Lifetime measurements were done on $T^H D^H 2$ films pyrolysed at 800°C and 1200°C. Results showed similar lifetime values for both of the sample as 13.9 ns for film pyrolysed at 800 °C and 16.2 ns for the film pyrolysed at 1200°C. The small increase in

the lifetime may be caused by phase separation of the SiC at 1200°C. However, the lifetime of the SiC as well as defect states are very short (few nanoseconds). Therefore the comparison between these two systems (defects and SiC) and consequently the films pyrolysed at low and high temperatures (800°C and 1200°C) is very difficult (see **Appendix II**).

Experimental absorption data with the corresponding Tauc band fittings for TH/DH2 films are given in **Figure 4.19**. In the high energy region of absorption edge, $\alpha(h\nu)^2$ versus $h\nu$ plot was taken as an evidence for direct band gap. The intercept of the straight line on the $h\nu$ axis gives the optical bands gaps which are shown in **Figure 4.19-b** with the emission band gaps as a function of pyrolysis temperature. The absorption energy decreased from 800°C to 1100°C and then slightly increased. However, the change from 800°C to 1250°C is quite low (less than 0.2 eV) and can be considered stable around 4.4 eV. On the other hand, the emission gap changed radically from low temperatures (800-900°C) to high temperatures (1000-1200°C) but as it is discussed before, the emission did not change the position in these ranges. It should be noted that the exact PL peak positions could not be detected for the samples pyrolysed at low temperatures and for the sample pyrolysed at 1250°C. Whereas for the sake of the discussion, emission gaps for the films pyrolysed at 800°C and 900°C are taken as 3 eV. The fact that no noticeable absorption or emission band changes are observed in T^HD^H2 films can be considered as stability of the emission.

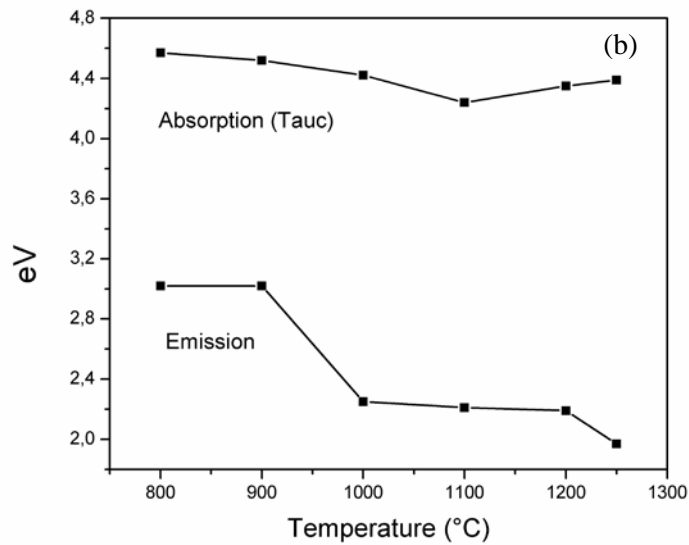
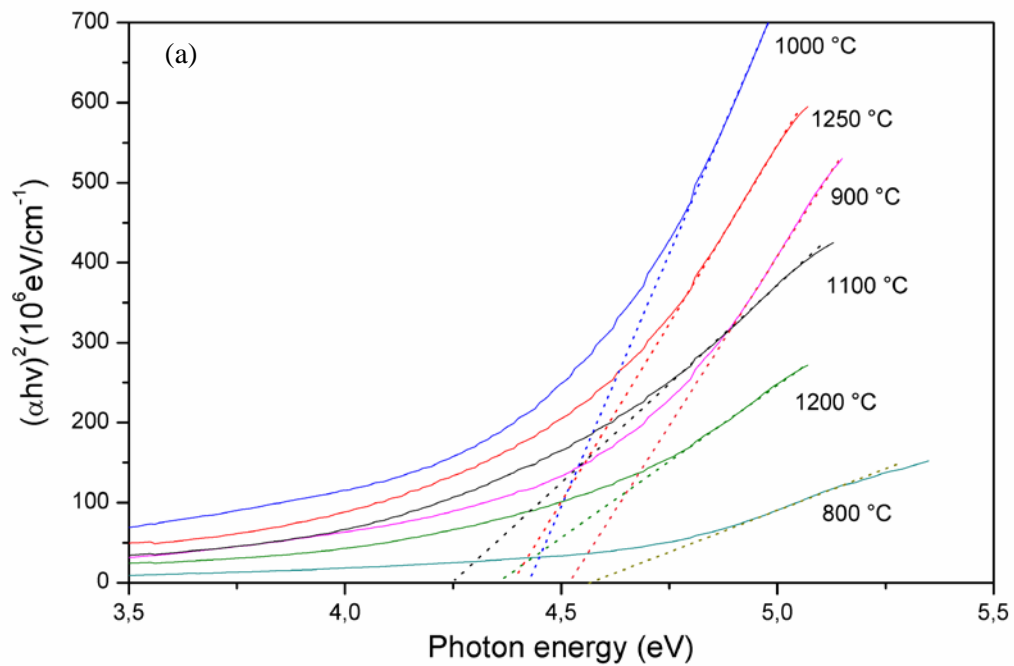


Figure 4.19. (a) Plot of $\alpha(h\nu)^2$ versus photon energy of $\text{SiOC}_{\text{stoichiometric}} (\text{T}^{\text{H}}\text{D}^{\text{H}2})$ thin film annealed at the indicated temperatures. The dashed lines are fittings by using equation (UV-Vis) (b) emission and absorption band-gap energies as a function of the pyrolysis temperature.

T^{H} films showed higher absorption band gap, 5.7-5.2 eV, than the optical band gap of $\text{T}^{\text{H}}\text{D}^{\text{H}2}$ films, 4.6-4.2 eV, up to 1100°C (**Figure 4.20**). This can be due to the fact that

T^H film contains less C, which is considered to be the absorption centre [L. Ferraioli, 2008] and higher amount of SiO₂ ($E_{\text{gap}}= 8 \text{ eV}$) compared to T^HD^H2 films (**Table 4.3**). At 1200°C, Tauc band-gap decreases rapidly to 4.2 eV and at the same time, the emission energy showed a gradual red shifting towards 1.9 eV (640 nm). Both trends can be associated to the absorption effect of free C presents in the system, which is more detectable at high temperatures due to the phase separation; or to the formation of Si, which has a low optical band gap ($E_{\text{gap}}=1.0\text{-}1.1 \text{ eV}$).

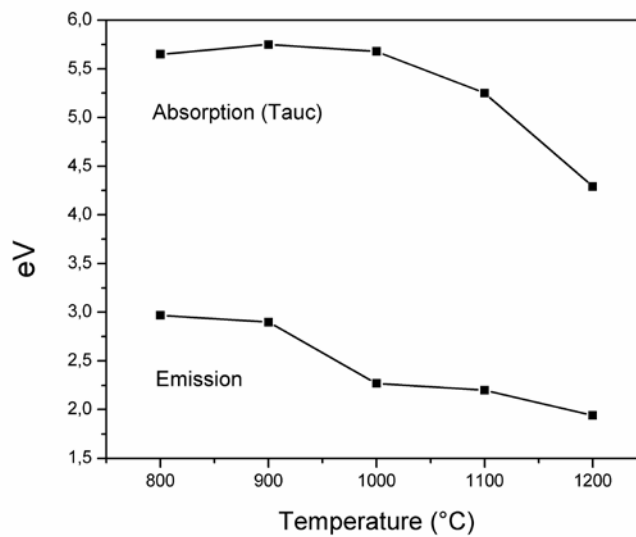


Figure 4.20. Emission and absorption band-gap energies as a function of the pyrolysis temperature.

4.4. Substrate Effect

SiOC films on SiO₂ substrate did not show any reaction between film and substrate even at high temperatures ($\geq 1250^\circ\text{C}$), (see **Figure 4.21-a**). Therefore, all the results reported until now are on SiO₂ substrate. Similarly, no reaction was observed in SiOC films on Si substrate up to 1100°C (**Figure 4.21-b**).

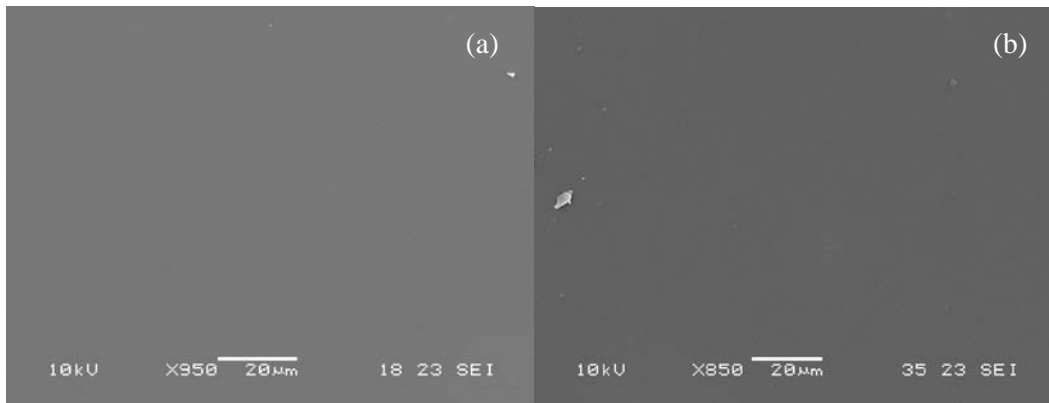


Figure 4.21. SEM images of Si-rich SiOC film (T^H) **(a)** on SiO_2 substrate pyrolysed at 1200°C and **(b)** on Si substrate pyrolysed at 1100°C .

However, after 1100°C , surface defects were detectable even with naked eye for films deposited on Si substrate. For more detailed study FEG-SEM is used to detect the reaction between film and Si substrate. The reacted areas can be seen clearly with porous appearance in **Figure 4.22**. The reaction starts from a defect centre and grows in interface direction. Some voids are visible in cross section and they appear as dark squared sites in backscattering images given in **Figure 4.23**. These voids are explained by Si depletion in literature [K. C. Kim, 2001].

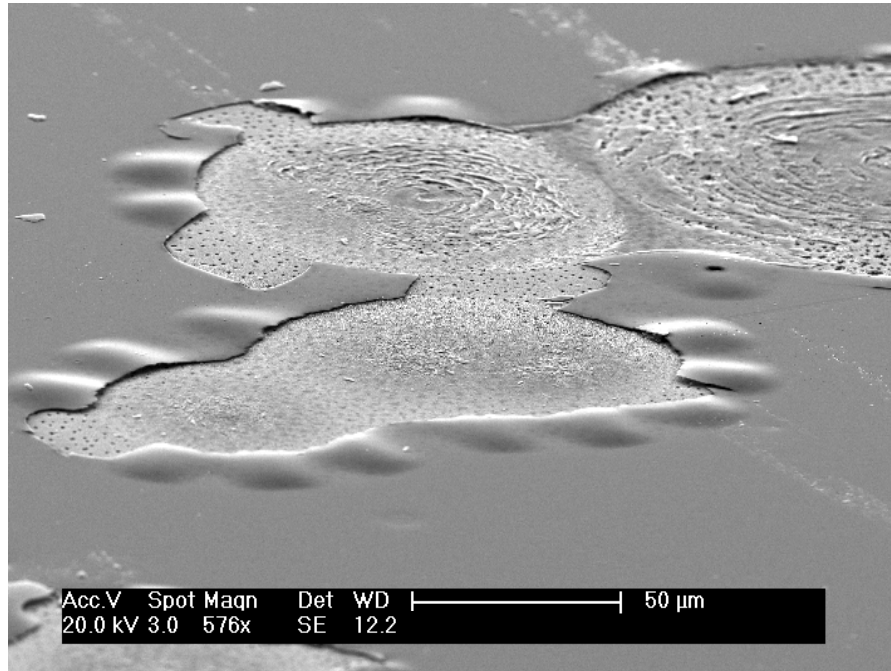


Figure 4.22. FEG-SEM images of Si-rich SiOC film (T^H) on Si substrate. (Pyrolysed at 1200°C)

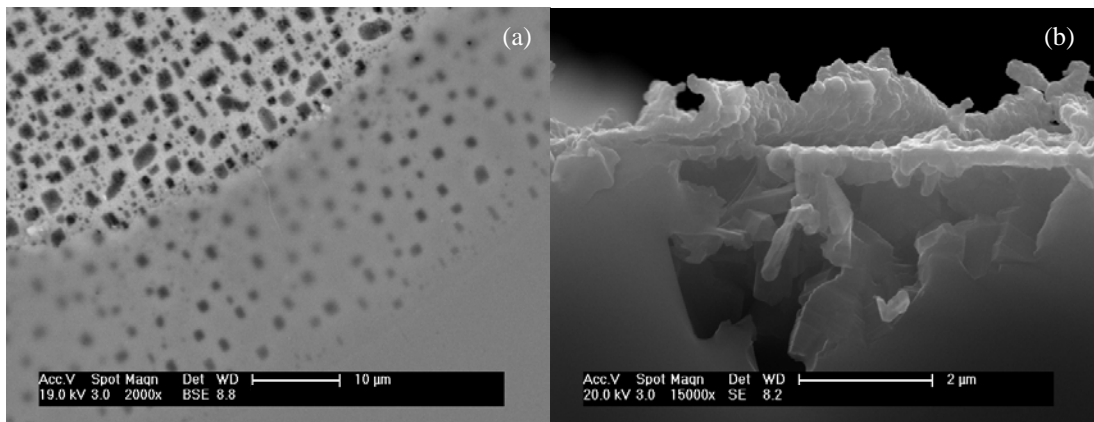


Figure 4.23. (a) Backscattering and (b) cross sectional FEG-SEM images of Si-rich SiOC film (T^H) on Si substrate. (Pyrolysed at 1200°C)

Another mechanism may take place during the SiC formation and cause bubble formation, which can be seen on the edge of the non-reacted films in **Figure 4.22**. Due to the nature of the SiOC system, higher temperature leads the phase separation. During phase separation SiO_2 , SiC and C rich areas can be formed and meanwhile CO and SiO release is reported [K. C. Kim, 2001]. In literature SiO_2 layer is also used as a sacrificial layer on Si substrate and reacted with the C instead of silicon substrate at high

temperatures (>1000°C). The possible reactions are given as followings [R. Sharma, 2008]:



Glancing angle XRD is used for the analysis of films since this method gives the possibility to get more information coming from the film rather than substrate. To understand the effect of the substrate, films coated on SiO₂ and Si substrates were analysed. Parallel to SEM results, film coated on SiO₂ substrate did not show any crystallization even pyrolysed at 1200°C (**Figure 4.24**). Whereas, XRD spectrum of the film on Si substrate gave Si and SiC crystallization at the same temperature given in **Figure 4.25**. In this figure, the same film pyrolysed at 1100°C is given in order to show that crystallization starts at 1200°C, since film pyrolysed at 1100°C is totally amorphous.

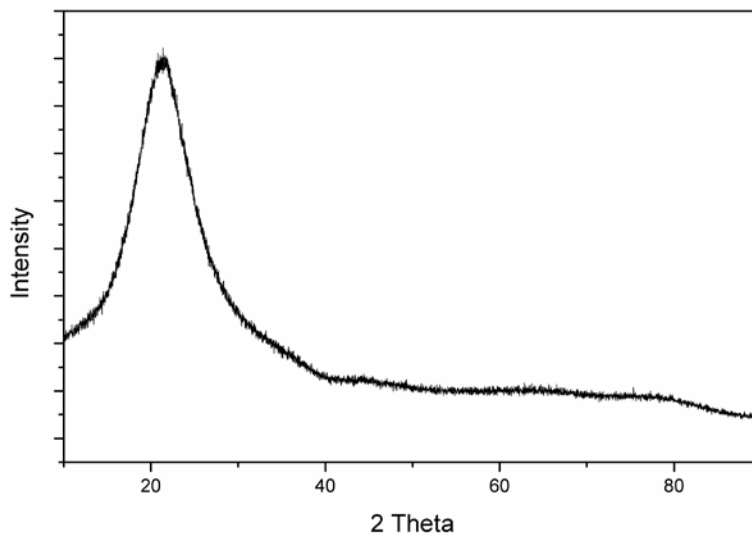


Figure 4.24. XRD spectrum of the Si rich SiOC film (T^H) on SiO₂ substrate pyrolysed at 1200 °C.

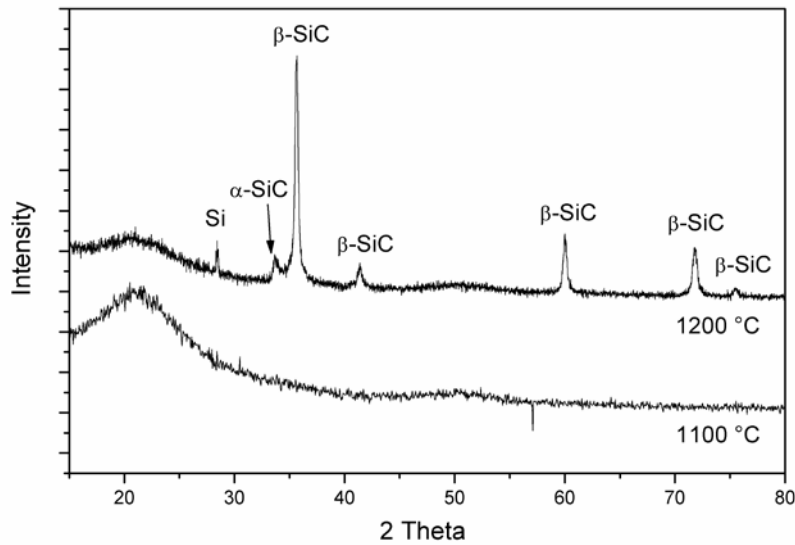


Figure 4.25. XRD spectra of the Si rich SiOC film (T^H) on Si substrate pyrolysed at 1100°C and 1200°C.

The reaction between Si substrate and film is found as the limiting factor to use the films on Si substrate at temperatures higher than 1100°C. However, the reaction can be slowed down or overcome by applying a passive etching by HNO_3 on Si substrate. However, the PhD study is more focused on optical properties of the films therefore this reaction is studied to understand the origin of the photoluminescence.

The PL spectra of the T^H films on Si substrate are given in **Figure 4.26** for films pyrolysed at low temperatures (**Figure 4.26-a**) and high temperatures (**Figure 4.26-b**). PL spectra showed the same luminescence tendency as it is on SiO_2 substrate (**Figures 4.13 and 4.15**). The emission in the UV-blue range is totally disappeared at 1000°C and the yellow green peak rise with the further increasing temperature. Although some minor differences exist between films on SiO_2 and Si substrate, the radical difference is detected for the films at 1200°C, at which the crystallization of SiC is detected by XRD. To visualize the difference in PL, two PL peaks of the films on Si and SiO_2 substrate are shown in **Figure 4.27**.

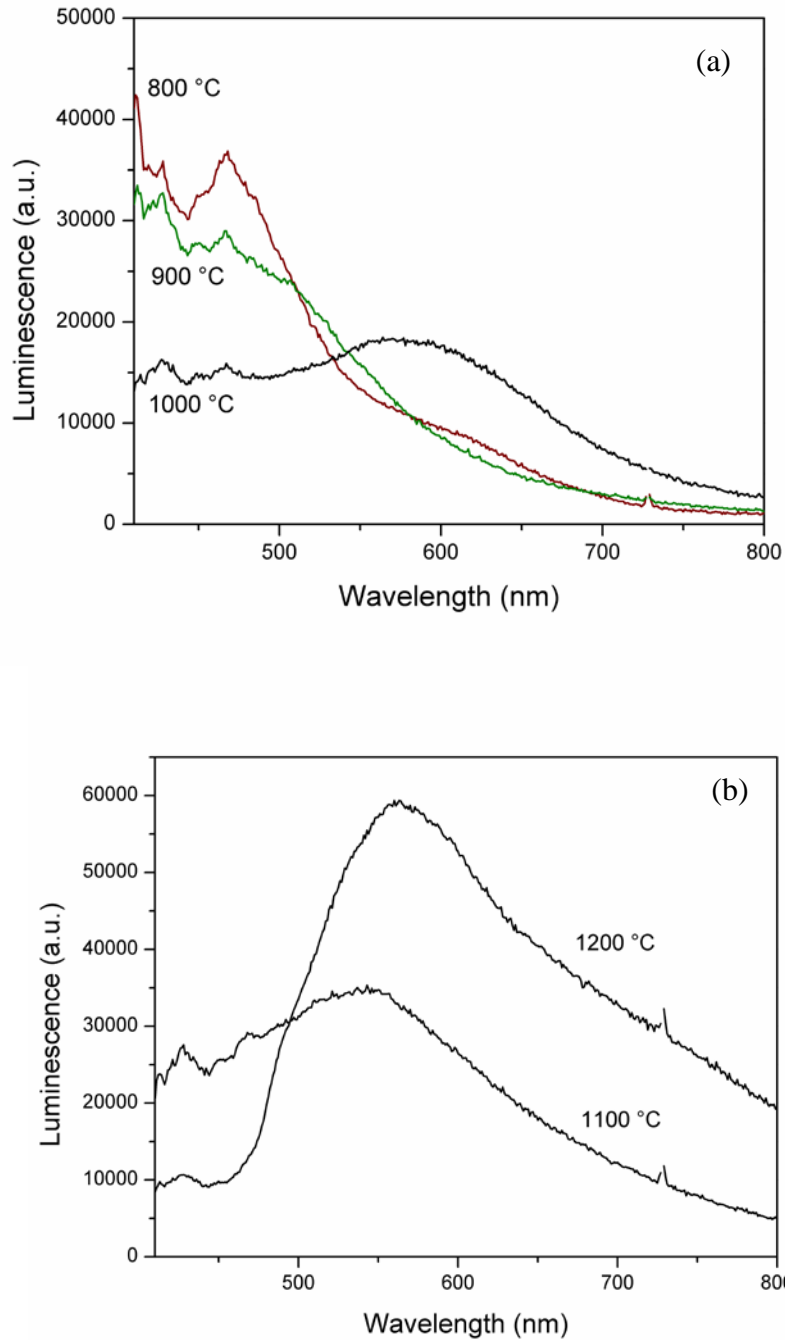


Figure 4.26. Photoluminescence spectra of T^H films on Si substrate pyrolysed at **(a)** low temperatures (800-1000°C) and **(b)** high temperatures (1100-1200°C)

Very broad luminescence covering almost all visible range is suggested to be originated from SiC clusters in films coated on SiO_2 film. Similar broad band is also observed in film on Si substrate. However, the very intense peak between 500 and 650 nm changed

the symmetry of the PL peak. The peak centred at 550 nm like in stoichiometric SiOC films (**Figure 4.15**) giving us the idea that this peak can be originated from SiC clusters.

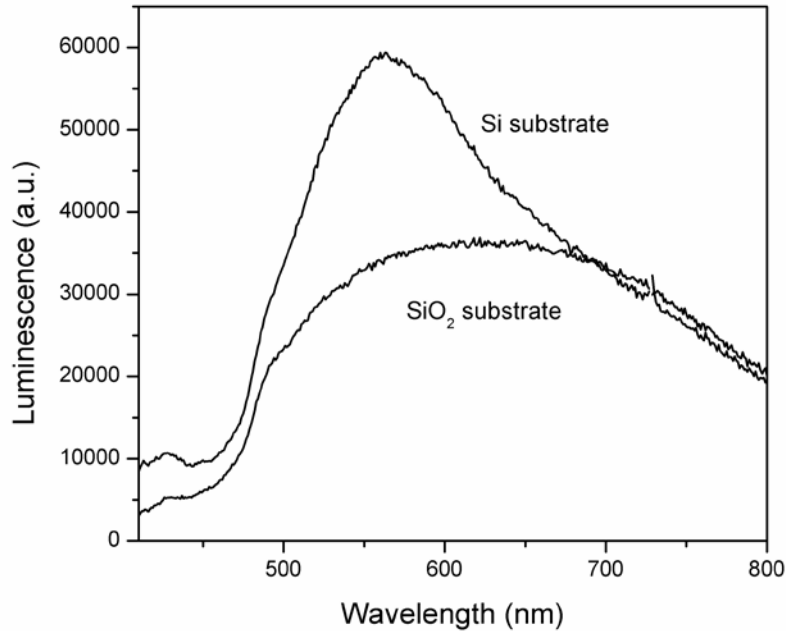


Figure 4.27. Photoluminescence spectra of Si rich SiOC films (T^H) on SiO_2 and Si substrates, pyrolysed at 1200°C .

To get further into the luminescence origin, we used the advantage of Ar laser, which gave us the possibility to get information from very small areas due to its low dimension ($\sim 100 \mu\text{m}$). Therefore the PL measurements can be performed on the areas where the reaction between film and Si substrate took place and on the non-reacted film. PL spectra are shown with FEG-SEM image in **Figure 4.28**. Non-reacted film showed the same PL spectrum as film on SiO_2 . Therefore, it can be suggested that the crystallization, which is detected by XRD, occurring only on reacted areas, where SiC crystallization gave rise to the peak centred 550 nm.

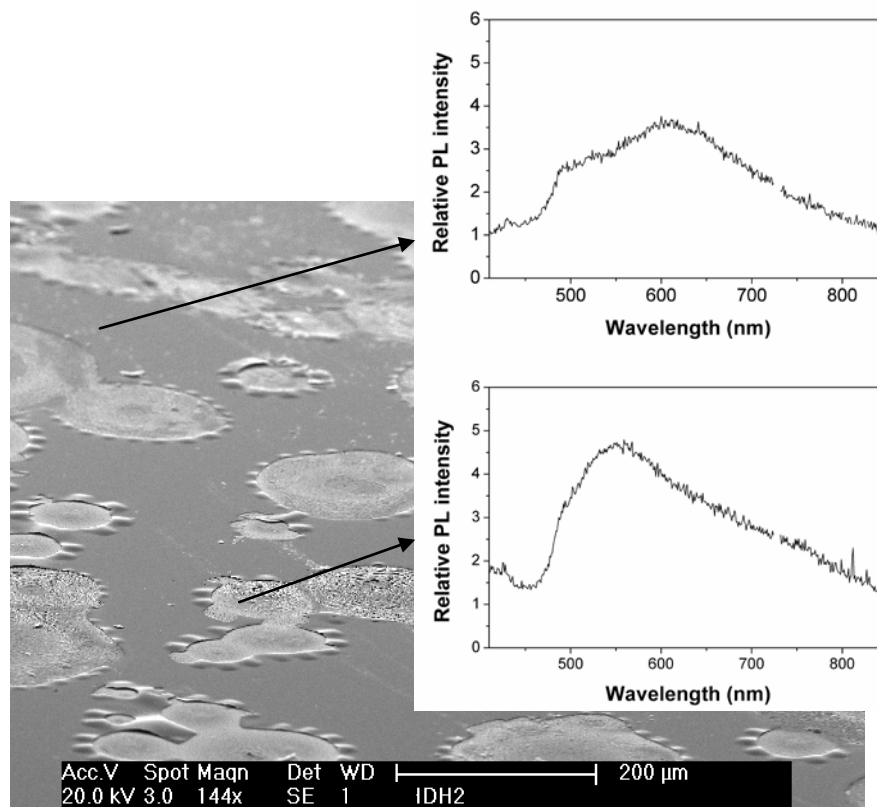


Figure 4.28. Photoluminescence spectra and relevant FEG-SEM image of Si rich SiOC films (T^H) on Si substrates, pyrolysed at 1200°C.

4.5. Stability Measurements/ Weathering Resistance

Luminescent thin-films are of great interest since they may offer high performance in flat panel displays. Thus, many studies have been conducted for the purpose of developing LED devices using various phosphors in order to get white emission. However, luminescence levels of the phosphorous-based LED devices are still not high enough for practical purposes. The low luminescence levels are suspected to be due to their chemical instability and hygroscopic nature [C. W. Wang, 1998]. Therefore, the performance of materials, which are proposed for LED applications, needs to be examined in light of their environmental stability. Environmental instability is essentially attributed to interaction with oxygen and water vapour. In this study, SiOC films were exposed to moisture/stability test in order to confirm the performance and applicability of the products. The experimental procedure has been suggested by Siemens Corporate Technology, Munich. The department working in Siemens is specialized on development of LEDs and they strongly advise us to check the

environmental stability of our films in order to evaluate a possible use of SiOC thin film in commercial field [Liepold, 2008]. These kinds of stability tests in literature are reported also as weathering resistance tests and most of them are suggested by companies as an indication of stability or applicability of the product [H. Lee, 2009].

The stability test under moisture and temperature (80°C, 80% humidity) were carried out by placing samples on a self-made climate chamber consisting on a desiccator with some water as it is shown in **Figure 4.29** placed into an oven at 80°C for 10 days.

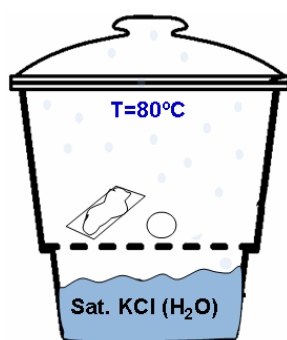


Figure 4.29. Self-made system used in the moisture/temperature stability tests

The stoichiometric films showed no change in the luminescence intensity. The PL spectra of the stoichiometric SiOC films ($T^H D^H 2$) after the moisture/stability test are given in **Figure 4.30**. SiOC films showed very high luminescence even after staying 10 days in a high humid atmosphere. We verify the stability of the SiOC films pyrolysed either at low temperature or high temperature. Therefore, SiOC is a good candidate for a possible commercial LED application.

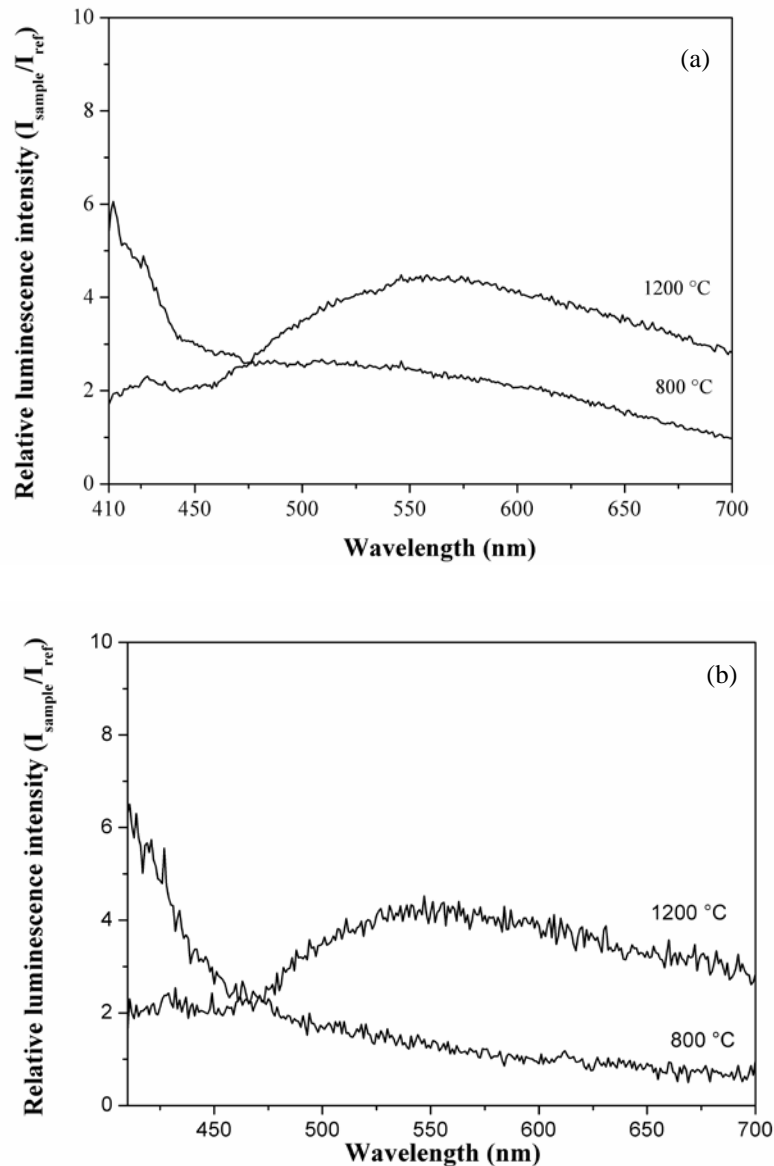


Figure 4.30 (a) Photoluminescence spectra of the $T^{\text{HD}}\text{H}_2$ films pyrolysed at 800°C and 1200°C before and **(b)** after the moisture/stability test.

4.6. Shrinkage behaviour of SiOC films and powders

4.6.1. Background information

Polymer derived ceramics (PDC) have been known for more than 3 decades and are an active field of research due to their unique properties such as high temperature stability [T. Ishikawa, 1998], multifunctionalities [L. G. Zhang, 2008; G. D. Sorarù, 2005; L. A. Liew, 2003] and exceptional shaping flexibility [Colombo, 2008]. According to this

route, during the pyrolysis process in inert atmosphere, the PDCs are formed step by step from the molecular precursor through solid state reactions [D. Bahloul-Hourlier, 2005]. So far, many ceramic systems have been synthesized; however, due to the commercial availability of rather cheap precursors, SiCO and SiCN are the most studied [R. Raj, 2001].

During the polymer-to-ceramic transformation stage, molecular species produced by the solid state reactions are released in the gas phase and account for the weight loss, which can vary between few percent, for the ultrahigh ceramic yield precursors [G. D. Sorarù, 1997], up to 50-60 %wt [R. Riedel, 2006]. Related to the gas evolution and the corresponding volume shrinkage is the difficulty to produce dense bulk components. The only bulk samples reported in the literature are either rods or thin plates having the smallest dimension below $\approx 1-1.5$ mm [T. Rouxel, 2001; S. R. Shah, 2002]. Accordingly, the structural characterization and measurement of physical properties of PDC are usually performed either on millimetre-sized bulk samples or on 10-100 μm sized powders. Moreover, since the pyrolysis gases have to diffuse from the sample through the structure to the surface it is generally accepted that the diffusion distance can play a role in controlling the ceramic yield and consequently the composition and properties of the final ceramics [T. Rouxel, 2001].

PDC thin films, with thickness below 1 μm have been reported in the literature [A. Karakuscu, 2009]. For these ultra thin components the question if their pyrolytic transformation - and consequently their composition and properties- can be estimated through experiments performed on larger scale samples is still open. For example, Colombo et al. [P. Colombo, 1994] have shown that processing thin SiC films from polycarbosilane with standard grade Ar gas results in the complete oxidation of the coating to SiO₂ and SiC films can be obtained only using ultra pure gases or ultra-high vacuum atmosphere. At the same time, polycarbosilane-derived SiC powders, fibers, or bulk components have been reported in the literature using standard grade Ar or He atmosphere [G. D. Sorarù, 2000]. Obviously, in these cases, the higher dimension of the powders, fibers or bulk samples prevents the complete oxidation and allows the formation of the expected SiC material.

In this study we compare the pyrolytic behaviour of 3-D bulk samples and thin films of

sol-gel-derived hybrid siloxane, precursors for SiCO glasses, by studying their shrinkage during pyrolysis from room temperature up to 1200°C. The chosen system has been extensively investigated and allows producing small millimeter sized PDC components as well as thin films [T. Rouxel, 2001; A. Karakuscu, 2009]. The film shrinkage has been investigated using in-situ thermal ellipsometry while bulk samples were studied by classical dilatometry.

4.6.2. Experimental

Stoichiometric SiOC composition has been chosen for this study. Thin films and bulk samples production has been explained previously. Xerogels were obtained after drying the gel by increasing the temperature slowly up to 110°C for 20 days. By this way, crack formation due to fast release of solvent was prevented and xerogel rods 7-8 mm in diameter with length of 3-4 cm were obtained.

Dilatometric experiments were performed in order to evaluate the thermal expansion of the gel and total shrinkage during pyrolysis up to 1400°C. Disc sample having approximately 1.5 mm thickness and 7.7 mm diameter was obtained by cutting and polishing a xerogel rod. Sample was loaded into a Netzsch 402/E dilatometer and the expansion and contraction of the sample along its diameter was recorded as a function of temperature. Experiment was performed under Ar (100 ml/min) with a heating rate of 5°C/min. The samples survived the dilatometric test without breaking -or even developing cracks- allowing for the measurement of their dimensions ex-post at room temperature. Measuring the shrinkage along the disc diameter and thickness provided a means to assess if the volume contraction is isotropic.

Shrinkage of the films during pyrolysis was followed up to 800°C by in-situ thermal ellipsometric analysis. Ellipsometry measurements were performed on a UV-vis variable-angle spectroscopic ellipsometer and data analysis was performed with the WVase32 software. For in-situ ellipsometric analysis, the ellipsometer was fitted with a home-built covered heating unit connected to a programmable temperature regulator. The pyrolysis environment was adjusted by flowing between 1 and 5 l/min of Ar gas through the sample stage at.

For pyrolysis temperature above 800°C the film shrinkage was followed by ex-post measurements by standard ellipsometry. Accordingly, the gel films were pyrolyzed in a C-furnace under Ar flow (100 ml/min) with a heating rate of 5°C/min at different temperatures, in the range 800-1200°C with 1 hour holding time at the maximum temperature. It has been already known that, the C furnace keeps the P_{O2} low enough to allow for the retention of C in the pyrolyzed SiOC film [P. Sajgalik, 1992] and prevents oxidation to SiO₂.

Weight loss of the powdered sample (sieved down to 80 µm) was followed by Thermogravimetric analysis (TGA) in a STA 409 Netzsch apparatus. The experiment was performed under Ar flow of 100 ml/min with a heating rate of 10°C/min.

In order to compare the shrinkage of 3-D bulk samples and thin films we need to remind that the shrinkage of 3-D samples is isotropic (see after for the results proving this behaviour) while the volume shrinkage of the film is accommodated only in the z direction being the shrinkage in the plane constrained by the bonding with the substrate. Accordingly, the raw data, i.e. the linear shrinkage measured by dilatometer and the linear shrinkage measured by ellipsometry cannot be directly compared. It is the volume shrinkage that contains important information in order to evaluate the pyrolysis behaviour of the two types of samples (film vs bulk). Bearing in mind that the film shrinks only in the thickness, h , its volumetric change is equal to:

$$\left(\frac{\Delta V}{V_0}\right)_{films} = \frac{\Delta h}{h_0} \quad \text{Eq. 4.4}$$

while for the isotropic bulk samples the volumetric shrinkage can be easily calculated from the linear shrinkage as:

$$\left(\frac{\Delta V}{V_0}\right)_{bulk} = 3\frac{\Delta l}{l_0} - 3\left(\frac{\Delta l}{l_0}\right)^2 + \left(\frac{\Delta l}{l_0}\right)^3 \quad \text{Eq. 4.5}$$

4.6.3. Results and Discussion

The dimensional changes of the bulk sample after the dilatometric measurement is reported in **Table 4.4**. It can be seen that the linear shrinkage is isotropic and reaches 22% from RT up to 1400°C while the volume shrinkage is 52.7%.

Table 4.4. Dimensional and weight changes of bulk sample after dilatometric test.

Sample	Dimensions (mm)		Volume (mm ³)	Weight (mg)	Density (g/cc)
	Thickness	Diameter			
gel	1.53	7.69	71.06	89.70	1.26
1400°C	1.19	5.99	33.53	84.80	2.53
Change (%)					
gel to 1400°C	22	22	53	5.5	100

The organic-to-inorganic transformation was followed by TGA and is reported in **Figure 4.31**. The precursor gel shows a small weight loss up to 350°C (1.2 wt%) due to the removal of residual OH and/or OEt groups, a 4.3 wt% loss between 350 and 550°C associated to the evolution of silanes formed through redistribution reactions between Si-H, Si-O and Si-C bonds and a final ceramization step (1.4 wt%) with evolution of CH₄ and H₂ [R. Camprostrini, 1996]. Above 800°C the weight of the sample is stable.

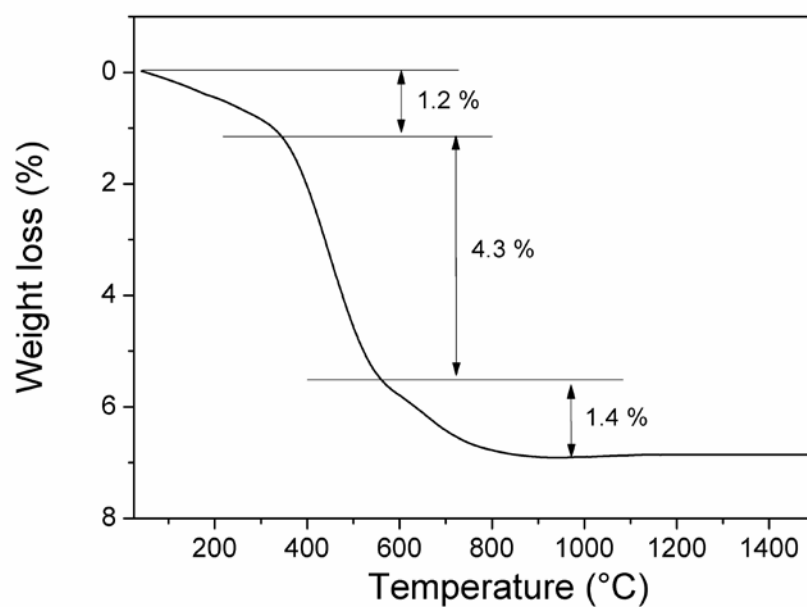


Figure 4.31. TGA curve of the gel sample with corresponding weight losses indicated by arrows.

The volumetric changes of the film and bulk sample are compared in **Figure 4.32**. The shrinkage of the film is measured up to 800°C with in-situ ellipsometry and above that temperature, at 1000 and 1200°C, the thickness is measured after the pyrolysis with standard technique.

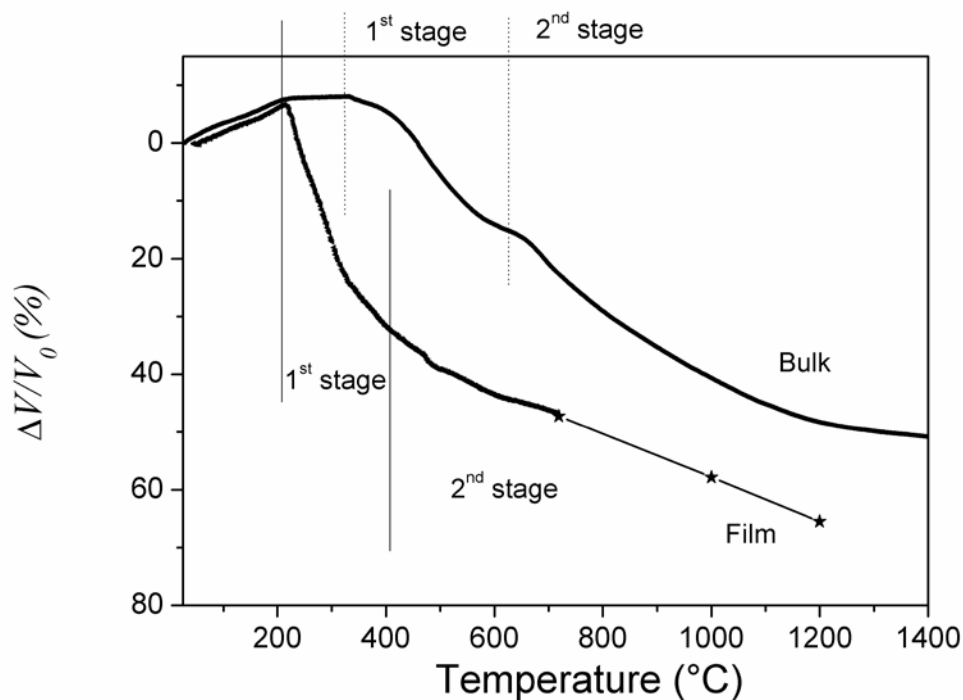


Figure 4.32. Volumetric changes of bulk sample, calculated from dilatometer (-●-) and film measured by in situ ellipsometer (-◄-) and standard ellipsometer (☆)

Both bulk and film samples show an initial volume expansion, reach a maximum and then start to shrink. For bulk samples the inversion is gradual and spans over a temperature range of 100-150°C. The maximum temperature can be estimated at around 300-350°C in good agreement with previous data [P. Sajgalik, 1992]. Above 350°C the 3D sample shows a first shrinkage step up to 600°C and a second step (less steep) up to 1200-1300°C. This dilatometric behaviour of the 3-D sample can be compared with the corresponding TGA curve recorded on micron sized powders (see **Figure 4.31**) and the following information can be obtained: (i) the temperature at which the sample starts to shrink corresponds to the temperature at which the gel starts to decompose; (ii) the main weight loss step, from 350 to 600°C, is associated to the first shrinkage step up to 550-600°C, (iii) the last weight loss step leads to an extended continuous shrinkage from 600 up to 1200-1300°C, well beyond the temperature at which the pyrolysis can be considered complete from the TGA curve (ca 800-900°C). This behaviour could be related either to the escape of very low amount of H₂, below the resolution of the TG instrument or to a structural rearrangement occurring without any compositional changes.

The comparison between the film and bulk volume shrinkage is reported in **Figure 4.32**. Interestingly, the film also shows an expansion stage exactly as the bulk sample; however, the film abruptly inverts his trend and, above 200°C, begins to shrink. The volume shrinkage of the film can also be divided into two stages: a rapid shrinkage from 200°C up to 400-450°C and a second stage, from 500°C up to 1200°C, in which the shrinkage rate is constant (and lower than the first stage). Above 1200°C we do not have and data points since the film becomes unstable and starts to react with the substrate.

These results clearly show that the thin film transforms easier and to a larger extent compared to the bulk: indeed, the maximum temperature above which the film starts to shrink is around 100–150°C lower than the bulk and also the volumetric shrinkage is between 10 to 15% vol. higher for the film compared to the bulk sample. The higher shrinkage of the film is probably due to larger evolution of gaseous species, mainly in the low temperature regime (from 200°C up to 400°C). In this temperature range high molecular weight species such as SiH_4 , CH_3SiH_3 are formed [R. Camprotrini, 1996] and for these relatively large molecules the diffusion distance can play an important role in controlling the diffusion rate. On the other side, at higher temperature the shrinkage rate is similar for the two type of sample (see **Figure 4.32** where the shrinkage curves are almost parallel above 500°C) and this results could be explained knowing that, in this temperature range, smaller H_2 and CH_4 molecules are formed and their diffusion rate could be less dependent from the diffusion distance.

The porosity formation in the film, due to the observed decomposition processes are investigated by in situ ellipsometer, measuring the refractive index which is given in **Figure 4.33** and the standard ellipsometer measurements are also shown for higher temperatures (>800°C). Up to 250°C, a sharp decrease in refractive index is observed as a result of pore creation in the film. Then pores are closing and this leads an increase in refractive index. At this stage, film showed a constant shrinkage (**Figure 4.32**) which indicates that the pore formation and collapse is continuous. In the second stage, refractive index decreased once again till 550°C and followed by a densification step, which cause final refractive index to reach to 1.57.

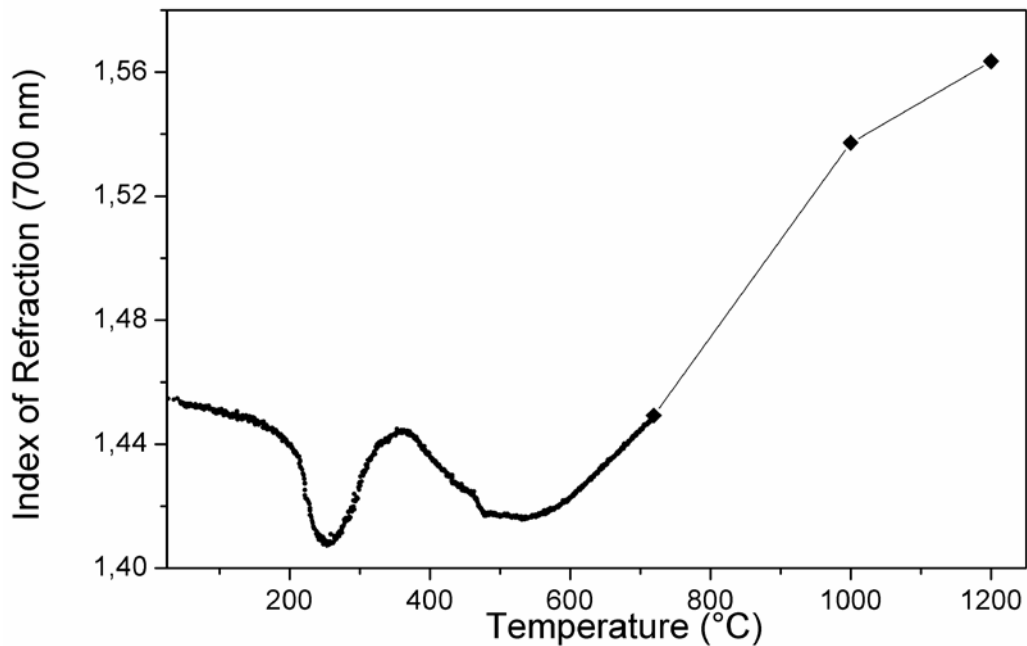


Figure 4.33. Index of refraction of the film measured by in situ ellipsometer (-●-) and standard ellipsometer (◆)

4.7. Conclusions

Homogeneous and crack free SiOC films with different compositions were produced via polymer pyrolysis of sol-gel derived films. Three compositions were chosen to study the effect of Si and C in the SiOC films; C rich SiOC, stoichiometric SiOC and Si rich SiOC (mentioned as $T^H D^H 1$, $T^H D^H 2$ and T^H ; respectively). Films showed different luminescence behaviour at low temperatures (800-1000°C) and high temperatures (1100-1250°C). In the amorphous state (800-1000°C), all SiOC films showed UV-blue luminescence peaking at about 410 nm, which is attributed to defect states present in the matrix such as dangling bonds. The increase of the pyrolysis temperature ($\geq 1100^\circ\text{C}$) led to the partition of SiOC and formation of SiC, C and Si phases. The intense green-yellow luminescence observed in stoichiometric SiOC films caused by the presence of SiC and very low amount of free C. On the other hand, Si rich SiOC film (T^H) showed a very broad and extremely intense white luminescence peak centred at 620 nm covering almost all visible range (430-900 nm) at 1200°C. This behaviour is explained by the

simultaneous presence of SiC, C and Si in the film. External quantum efficiency measurements yielded 11.5% and 5% efficiencies in T^H and T^HD^H2 films, respectively, pyrolysed at 1200°C. On the other hand, C rich SiOC films did not show any noticeable improvement in PL, indicating that C excess in the SiOC system is detrimental for the luminescence behaviour.

The reaction between film and Si substrate at high pyrolysis temperatures ($\geq 1200^\circ\text{C}$) is verified by FEG-SEM, SEM and XRD analyses. The reaction is supposed to occur between C rich areas and Si substrate. The bubble formation can be also originated by reaction between SiO₂ rich areas and C rich areas present in the film due to the phase separation of SiOC, which is known to be taken place at high temperatures. Whereas, no reaction between film and Si substrate is observed at temperatures lower than 1200°C. This is also verified by the similar PL spectra of the films on SiO₂ and Si substrate. PL measurements were done on reacted areas in order to suggest the origin of the luminescence. Due to the peak intensity which is centred at 550 nm increased in reacted areas similar to the stoichiometric SiOC films; this peak is assigned to be caused by SiC crystals.

Finally, a study on volumetric shrinkage of films and powders has been done. The results showed that the shrinkage in films starts almost 200°C lower than powder samples. The shrinkage related to the evolution of silanes is higher in the film compared to bulk and this result can be explained by the very short diffusion distance that the large silane molecules gave to overcome to reach the free surface of the sample compared to bulk system. The difference in the silane release may also cause a difference in final composition. Indeed, SiC cluster formation in a sol-gel derived SiOC films was suggested to start at low temperatures (1000°C) compared to the corresponding bulk [A. Karakuscu, 2009]. Therefore, as it is suggested many times, the powders and films should be considered as two separate systems to study on.

Chapter V. Other systems studied

Study on optical properties of Si based materials is attracting the attention for many years due to their abundance. However, the emission centers in the Si based materials are very hard to define because in most of the cases the emission is obtained from clusters (>1 nm) other than crystals. The detection of this emission centers as we have discussed **Chapter 4** is quite difficult. However, by changing the composition, some comparison can be made between the systems, which can give another perspective for understanding the origin of the emission. Therefore, in this part two other systems have been studied to understand the effect of boron and nitrogen: SiBOC and SiOCN.

SiBOC system is known to give several advantages over SiOC system. The crystallization of SiC is found to start earlier than boron-free SiOCs [G. D. Soraru, 1998]. Additionally, crystalline SiO₂ formation is inhibited and larger sp² carbon nanocrystals are formed in SiBOCs, which makes SiBOC a good candidate for Li battery applications [R. Pena-Alonso, 2007]. However, neither films nor optical properties have been explored in literature. Therefore, the study on SiBOCs has been done not only to compare this system with SiOCs but also to investigate deeper the SiBOC system, which is still an open and unexplored field in PDCs.

In the first part of the study, the gels and relevant powders have been characterized thermally and structurally to understand the effect of the boron addition on pyrolytic transformation. SiOC gels with a compositional range from stoichiometric to Si rich SiOC have been used for the boron addition. However, although very few studies could be found in the literature about SiBOCs, most of them were focused on structural characterization of stoichiometric SiOCs. Therefore, this system will not be discussed structurally in the first part in order not to repeat the similar findings.

In the second part of the study, the SiBOC films produced by boron addition in the stoichiometric SiOC solution have been discussed. The study is dedicated to optical properties of the films but several other characterizations have been done to understand the structure of the film better (XPS, profilometer, FTIR, SEM etc.). Photoluminescence properties as well as UV-Vis measurements have been performed and discussed.

Production of SiCNs is extensively reported in literature by polymer pyrolysis method. Nowadays several commercial polysilazanes are in the market and many studies focused on production of ceramic components from these commercial polymers. On the other hand, the production of the pure SiCNs is quite complicated due to high oxidation rate of the polysilazanes. However, by an alternative approach, SiOCNs can be produced easily in open atmosphere with controlled oxidation. Therefore, in our study SiOCN films were synthesized by open atmosphere route. Optical properties of the resultant films were then studied by PL measurements and FTIR analyses have been performed in order to understand the possible relationship between bonding and emission.

5.1. SiBOC Ceramics

SiBOC ceramics are quite new materials; they have been studied only for 10 years and the few studies present in the literature focused on boron added to stoichiometric SiOC system. On the other hand, some compositions like Si rich SiOC ceramics have not been investigated. Therefore, in this work, Si rich SiBOC ceramics are investigated structurally and PL analysis has been performed.

5.1.1. Experimental Details

Two different Si rich SiBOC gels have been prepared from $T^H D^H 9$ and T^H compositions (see **Chapter 3.1**, **Chapter 4.2**). For the seek of clarity, the samples have been labelled with the TEB prefix to indicate the boron addition. TEB- $T^H D^H 9$ solution has been prepared by using triethoxysilane (T^H) and methyldiethoxysilane (D^H) precursors with a ratio of 9. Boron addition has been done by triethylborate (TEB) having a ratio B/Si=0.1. Whereas, TEB- T^H gels has been prepared by T^H with and addition of TEB (B/Si =0.3). Solution preparations, as well as drying step have been done according to the same route to prepare Si rich SiOC ceramics (**Chapter 3.2**). Gels have been pyrolysed in a carbon furnace under Ar flow at temperatures in the range of 800–1400°C. Thermal evolution of gels has been studied by TGA. Crystallization and bonding structure of the powders has been investigated by XRD and FTIR, respectively.

Photoluminescence properties of the films are studied by Photoluminescence (PL) measurement. For the easiness, boron free SiOC powders are given as a benchmark.

5.1.2. Results And Discussion

As it can be seen in **Figure 5.1**, boron addition decreased the weight loss; modify the pyrolytic transformation, with a significant increase of the ceramic yield. The structural transformation of boron free sample has been discussed in details in **Chapter 3.3.2**. To briefly summarize, three step are present in the boron free sample; the sample is stable till 200°C and only H₂O removal is seen, from 200°C to 600°C the organic to inorganic transformation caused high weight loss (3%), and between 600°C and 800°C the weight loss slow down due to H₂ and CH₄ gas formation. After 800°C, samples are stable. Since T^HD^H9 contains more carbonaceous groups in the structure than T^H, the third stage showed higher weight loss due to higher organic release [G. D. Sorarù, 1995].

The introduction of boron in borosilicate gels leads to an increase in low temperature weight loss (up to 350°C) due to evolution of water from B–OH species [G. D. Sorarù, 1997]. This weight loss step, which immediately starts from RT and continues till 350°C, confirms that the presence of boron has a strong influence on the pyrolysis pathway of the precursor gel. Note that the gas formation starts 200°C lower than boron free sample. From 350°C up to 550°C, redistribution reactions leads to the evolution of low molecular weight siloxane species. After this temperature the weight loss rate decreased and only formation of H₂ and CH₄ is expected [G. Trimmel, 2003; L. Pederiva, 2002]. Boron added samples showed the same tendency and slightly the same weight losses. TEB-T^H showed only 1.7% whereas TEB-T^HD^H9 gave 1.9% final weight loss at 800°C. It needs to be noted that boron addition in T^HD^H9 system improved the ceramic yield more drastically (from 9% to 2%) than in T^H system, in which ceramic yield is increased from 3% to 1.5% by boron addition.

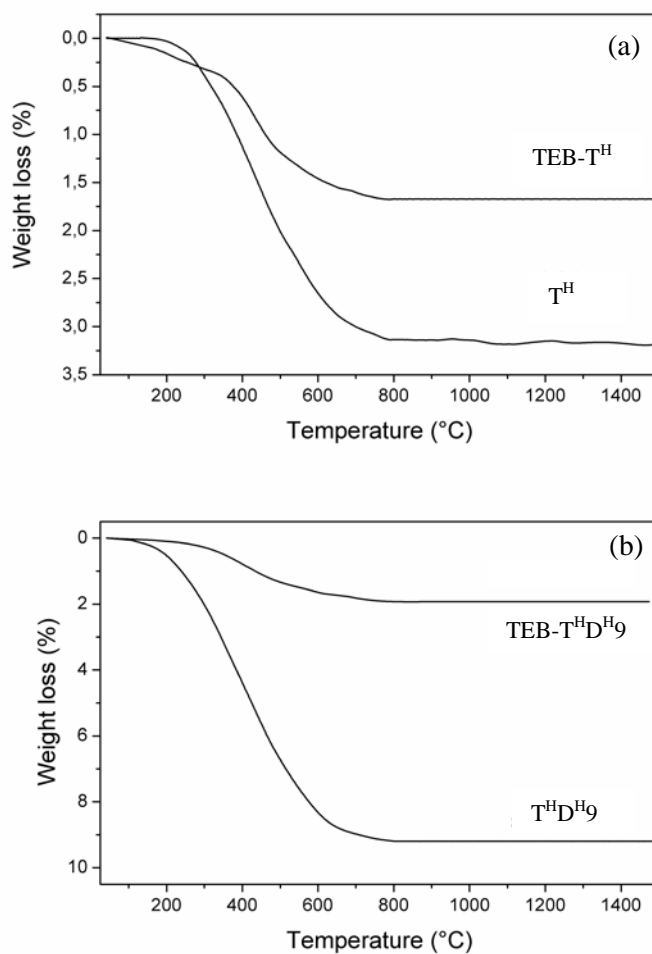


Figure 5.1. TGA measurements of SiOC and SiBOC gel samples.

The bonding structure of boron added powders are investigated by FTIR and given in **Figure 5.2** and **5.3**. The bands related to boron addition are shown with an asterisk. Boron added gel sample showed B-OH and B-O stretching bonding at 3200 cm^{-1} and 1400 cm^{-1} , respectively. Additionally, B-O stretching peak at 1400 cm^{-1} is an indication of boron oxide formation at high temperatures. The pyrolysis leads the Si-O-B bonding, which gave rise the peak at 910 cm^{-1} [M. A. Villegas, 1988]. This peak could not be distinguished in TEB-T^HD^{H9} sample pyrolysed at 1400°C since Si-C bonding gave a very broad band in this range also in T^HD^{H9} sample. This wide peak covers in range of 950 cm^{-1} and 650 cm^{-1} , where Si-C, Si-O-B and Si-O-C bands are present. This peak seems to be the only difference between T^H and T^HD^{H9} glasses, pyrolysed at 1400°C . It can be due to the higher carbon presence in T^HD^{H9} system causing mixed bonds. Other than boron related peaks, SiBOC showed similar features with SiOC samples.

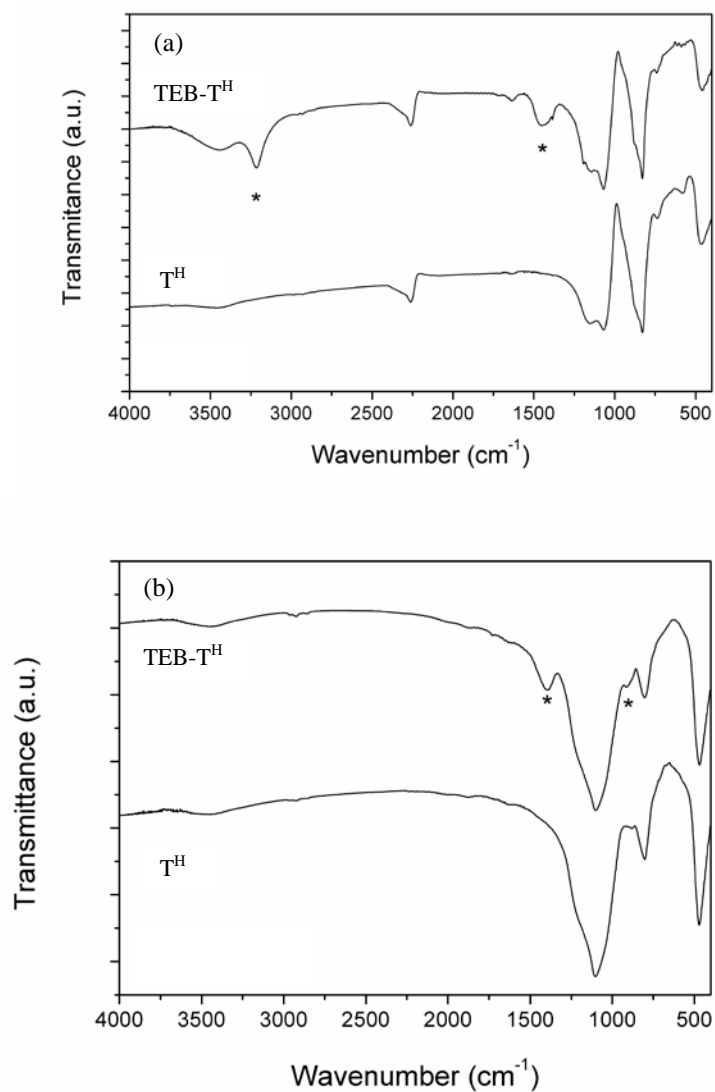


Figure 5.2. FTIR spectra of (a) gel and (b) pyrolysed TEB-T^H and T^H powders. Asterisk is given to indicate boron related bands.

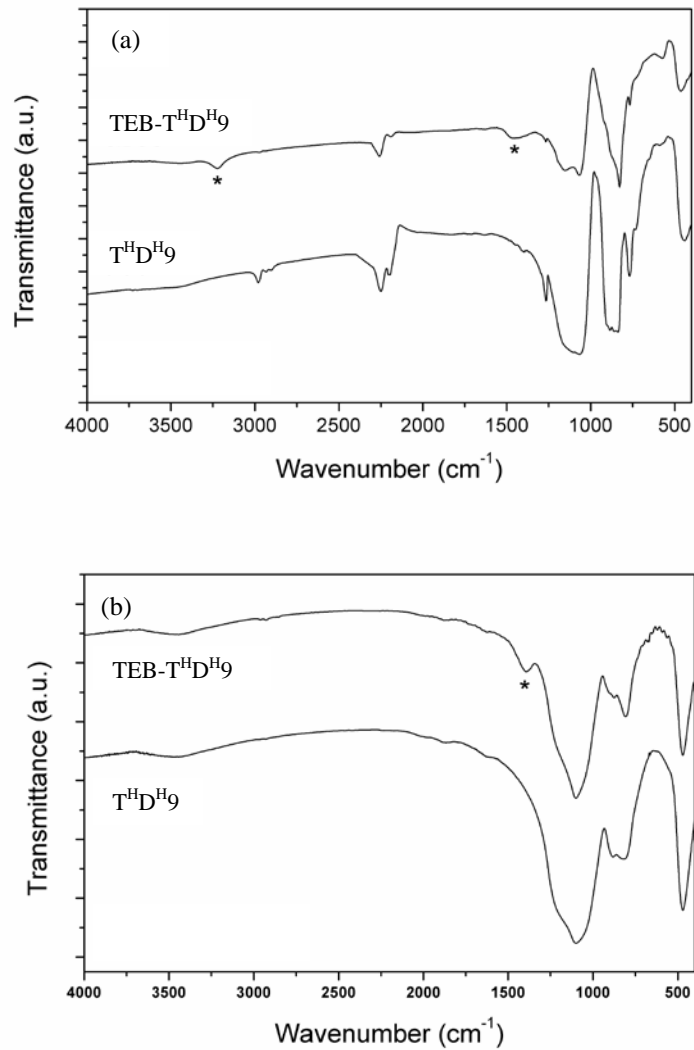


Figure 5.3. FTIR spectra of (a) gel and (b) pyrolysed TEB- $T^H D^H9$ and $T^H D^H9$. Asterisk is given to indicate boron related bandings.

In TEB- T^H system, Si crystallization is started at 1200°C and gave a broadening in x-ray spectrum, shown in **Figure 5.4-a**. The asymmetric peak appeared at 1000°C is clearly an indication of Si crystallization, whereas the size of the Si nanocrystals is too low to be detected. The crystallization of SiC and Si started spontaneously at 1200°C , unlike boron free sample (**Figure 3.10, Table 3.5**). The particle sizes of crystalline phases are estimated in the **Table 5.1**. Clearly, boron addition enhanced crystallization of both phases and lowers the crystallization more than 200°C .

Crystallization of Si is detected at 1000°C in TEB- T^HD^H9 system, earlier than TEB-T^H system. However, the crystallization rate is rather low and the Si crystal size reached to 15 nm at 1400°C instead in TEB-T^H system it reached estimated up to 0.2 μm. This trend is not the same for SiC crystallization. Higher carbon presence in the system led larger SiC crystals at 1400°C in TEB- T^HD^H9 (Table 5.1).

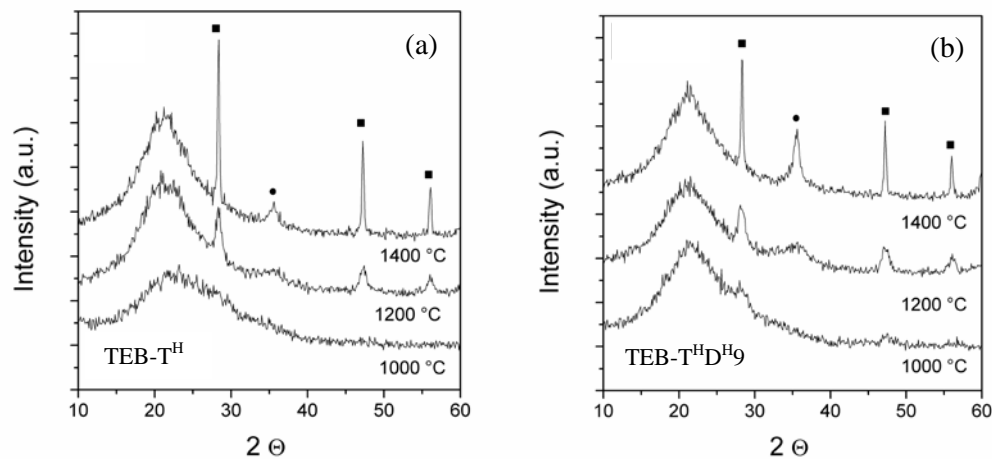


Figure 5.4. X-ray spectra of SiBOC samples pyrolysed at different temperatures (1000-1400°C). Crystalline phases have been indicated above the spectra (■ Si and ●SiC).

Table 5.1. Estimated particle sizes of phases present in the boron added SiOC samples by using Scherer formula

Sample	Particle size (nm)			
	T ^H		T ^H D ^H 9	
	Si [111]	SiC [111]	Si [111]	SiC [111]
1000°C	-	-	1.3	-
1200°C	3.8	0.9	3.4	0.9
1400°C	210.9	2.8	15.3	4.4

In conclusion, boron added Si rich SiOC glasses showed interesting features. Crystallization of SiC and Si phases started 200°C lower than boron free sample. The modification in pyrolytic transformation is detected by TGA and boronsilicate

occurrence is detected by FTIR. With the help of boron, the system forced to give faster crystallization starting from lower temperatures.

5.2. SiBOC films

SiC_n embed in SiO₂ are of great interest to produce Light-Emitting Diode (LED) due to the high emission of SiC nanocrystals. However, with a conventional processing route it is very difficult to obtain SiC_n/SiO₂ composite. To overcome this problem the use of the Polymer Pyrolysis Route has been proposed in **Chapter 3** and **4**. According to this process, SiC nanocrystals can be grown in situ in the silica matrix from a silicon oxycarbide glass (SiOC) obtained from suitable precursors. However, the SiC crystallization temperature from SiOC is usually above 1200°C and this temperature can be too high to avoid film/substrate reactions. Therefore, by introducing boron into the SiOC, it is aimed to decrease the crystallization temperature and allow the synthesis of the aimed SiC_n/SiO₂ films at $T \leq 1250^\circ\text{C}$. Accordingly, the aim of this study is to produce SiBOC thin films and to investigate their optical properties.

5.2.1. Experimental Details

SiBOC thin films are produced by sol-gel method using a mixture of triethoxysilane (T^H) and methyldiethoxysilane (D^H) with a T^H/D^H molar ratio of 2 to obtain silicon oxycarbide glass with a negligible amount of free C. Triethylborate, B(OCH₂CH₃)₃, with B/Si ratio of 0.1 is used as a source of boron and added to the solution after adding proper amount of ethanol and water [G. D. Sorarù, 1997]. Thin films, which will be called as TEB-T^HD^H2 for the easiness, are deposited on Si and SiO₂ substrate by spin coating and pyrolysed in a carbon furnace under Ar flow at temperatures in the range of 800–1250°C. Surface properties of the SiBOC films are investigated by SEM. Thicknesses of the films are investigated by profilometer measurements. The bonding characteristics and photoluminescence properties of the films are studied by Fourier-Transform Infrared Spectroscopy (FTIR) and Photoluminescence (PL) Measurement, respectively. UV-Vis measurement has been done to measure the optical band gaps of the films.

5.2.2. Results And Discussion

For simplicity, results have been compared with $T^H D^H_2$ films prepared by the same composition without triethylborate addition. The homogeneity of the films has been verified by SEM. Cross-section of the TEB- $T^H D^H_2$ film, given in **Figure 5.5**, showed a continuous uniform crack free behaviour. In order to follow the thickness evolution with respect to pyrolysis temperature, the thickness measurement done by profilometer is shown in **Figure 5.6**. The values of the shrinkage measured at 1250°C are also given in the inset. In agreement with the literature on SiBOC glasses, shrinkage of TEB- $T^H D^H_2$ thin films showed lower shrinkage than $T^H D^H_2$ thin films [P. Colombo, 1994]. Therefore, even the starting thicknesses were similar; the resultant pyrolysed $T^H D^H_2$ films were thinner than TEB- $T^H D^H_2$ films. As it is reported in index the SiBOC films have not been studied in the literature and the other reference with asterisk is taken from polycarbosilane film, shrinkage of which is the only reported PDC film in literature [P. Colombo, 1994].

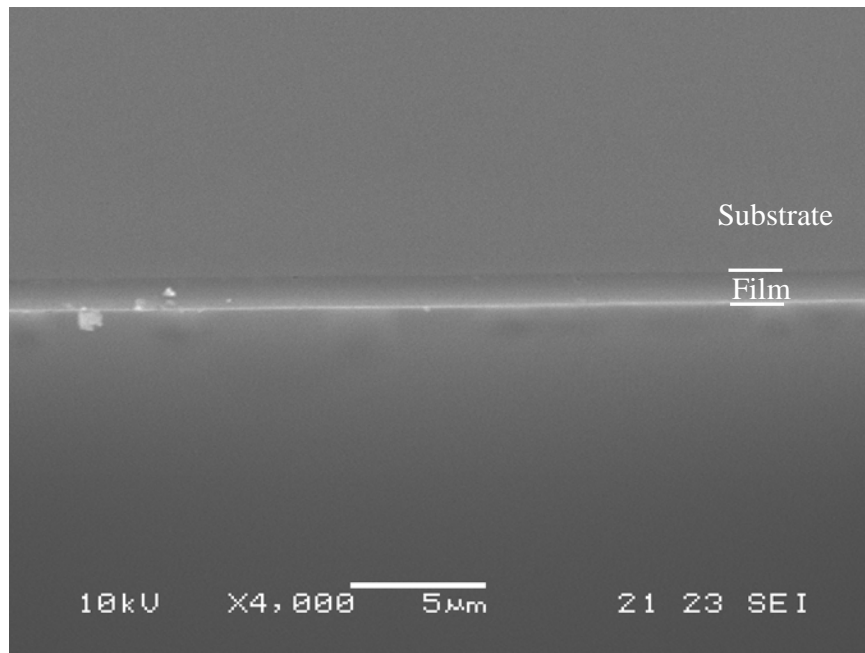


Figure 5.5. SEM micrograph of as-coated TEB- $T^H D^H_2$ thin film in cross section.

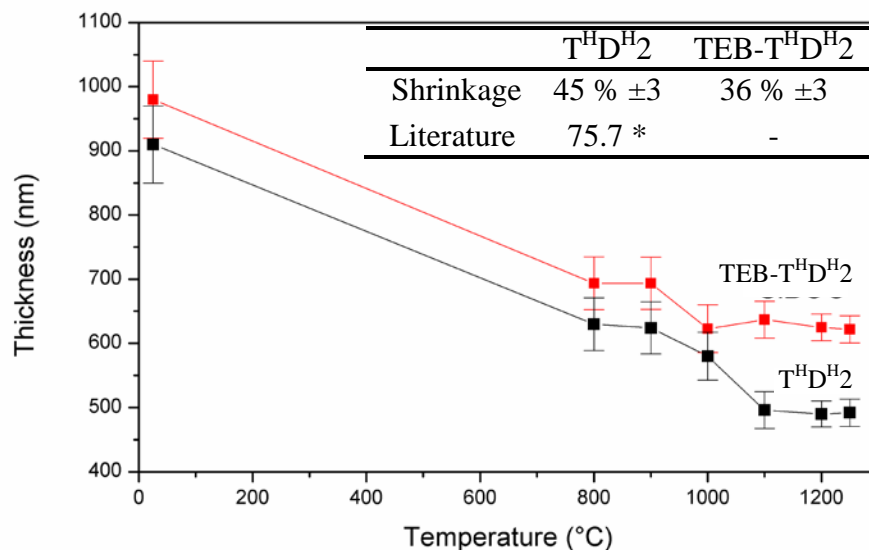


Figure 5.6. Thicknesses of the TEB- $T^H D^H 2$ and $T^H D^H 2$ thin films pyrolysed at different temperatures. **Inset.** Shrinkage values of the films pyrolysed at 1200°C.

The bonding structure of the as coated films is investigated by FTIR (**Figure 5.7**). B-O stretching bond at around 1400 cm^{-1} in as coated films is an indication of boron existence in the structure [M. A. Villegas, 1988]. Two peaks at 1100 cm^{-1} and 1060 cm^{-1} are assigned to Si-O-Si vibrations in SiOC. However, the total assignment of the wide peak from 1250 cm^{-1} to 1000 cm^{-1} is not easy because it is a complex combination of many peaks, namely Si-O and Si-O-C (as it is discussed in SiOC films). The peak assigned as an indication of SiOC network formation at centred at 1100 cm^{-1} , is more evident in TEB- $T^H D^H 2$ [G. Das, 2007]. This can be attributed to a more ordered structure in TEB- $T^H D^H 2$ films. Finally, Si-H bending peak at 830 cm^{-1} is less evident in TEB- $T^H D^H 2$ films, most probably because of the hydrolysis of Si-H bonds induced by the presence of triethylborate in the sol-gel solution.

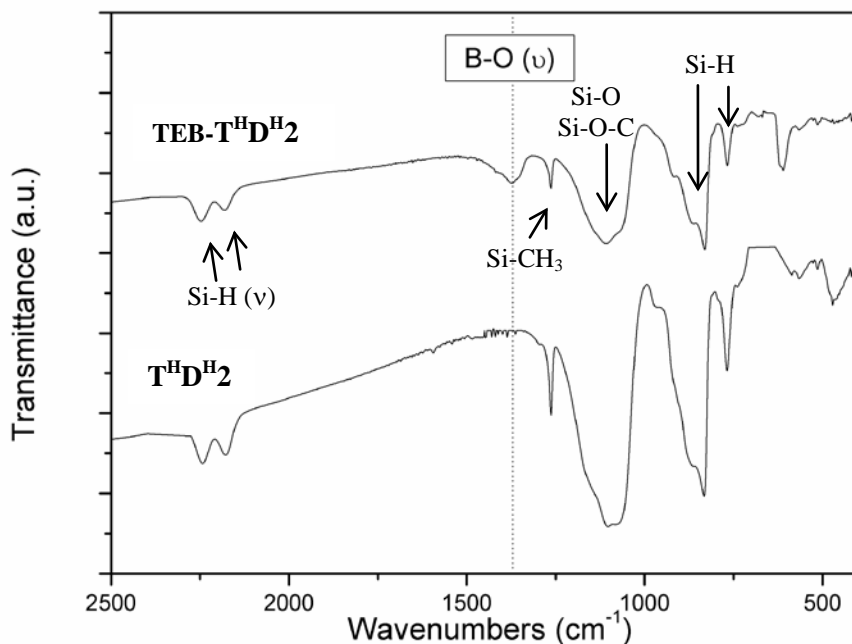


Figure 5.7. FTIR spectra of as-coated TEB-T^HD^H2 and T^HD^H2 films. Corresponding band is indicated.

With the pyrolysis, the boron related peaks became more noticeable as shown in **Figure 5.8**. B-O stretching vibration is still visible at 1400 cm⁻¹, B-O-Si bond formation gave rise a peak at 915 cm⁻¹ and peak at 545 cm⁻¹ corresponds to O-B-O bending bond [C. Gervais, 2001]. In TEB-T^HD^H2 film, the intensity of Si-C bonding at 800 cm⁻¹ is higher and narrower than in T^HD^H2 film, which is an indication of ordered structure. TEB-T^HD^H2 film showed very intense Si-C bonding at around 610 cm⁻¹, which is less evident in T^HD^H2 film.

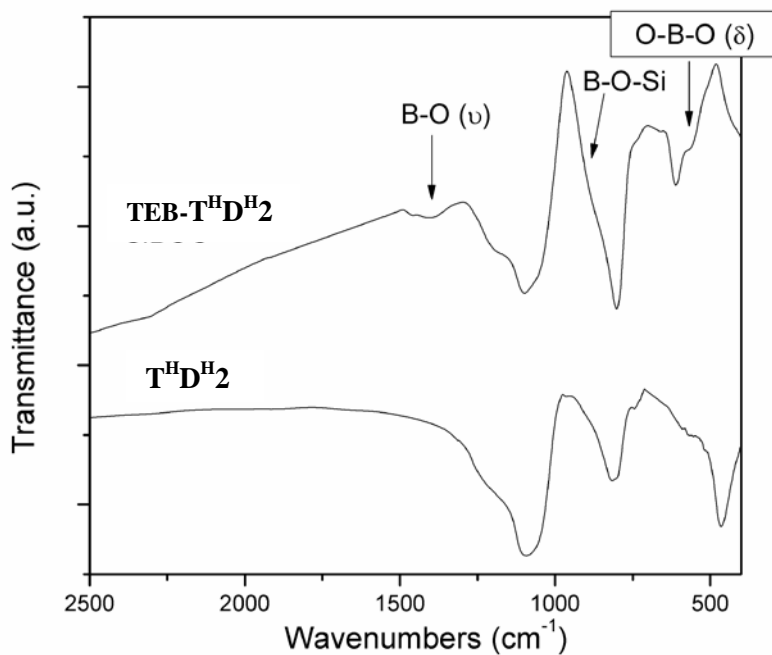


Figure 5.8. FTIR spectra of TEB-T^HD^H2 and T^HD^H2 films pyrolysed at 1100 °C. Corresponding bands are indicated.

XPS is used to measure the bonding evolution of the resultant TEB-T^HD^H2 films and Si2p XPS analysis showed in **Figure 5.9**. The films showed a significant shifting towards the Si-C bonding region with increasing pyrolysis temperature. This is suggested to be the result of phase separation process happening at 1200°C. The peak deconvolution for the Si2p peak at 1200°C is also given to demonstrate the development of the bonding structure of the film.

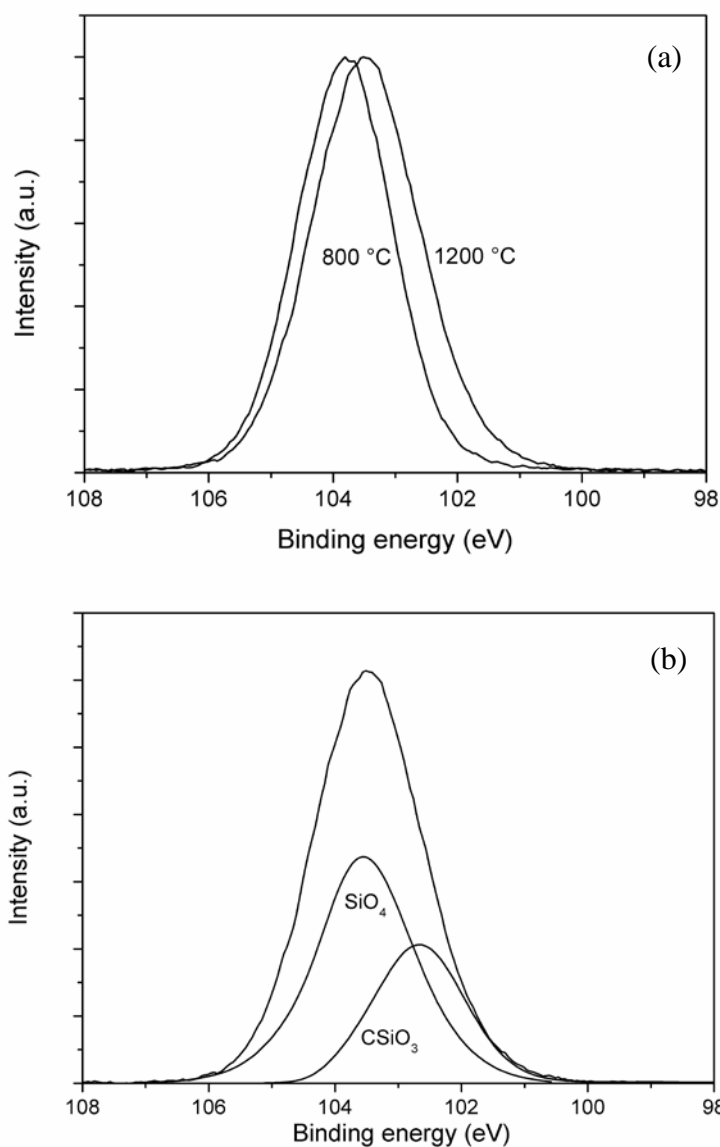


Figure 5.9. Si_{2p} core line XPS analysis of TEB-T^HD^H2 films (a) pyrolysed at 800°C and 1200°C, (b) peak fitting of film pyrolysed at 1200°C. Possible components used for the fitting are shown in **Figure 5.9-b**.

Optical properties of the TEB-T^HD^H2 films are examined by PL and UV-Vis measurements (**Figure 5.10**). PL emission band showed a strong red-shift from 400 nm to 700 nm by shifting through all visible color range. The films pyrolysed at 800°C showed a very broad emission centred around 420 nm in UV-blue range. However, the excitation wavelength is very close to the emission band, therefore the real shape and emission centre could not be defined certainly. Similar to 800°C, film pyrolysed at 900°C had a very broad emission band covered all visible range with a centre at 600

nm. Therefore, the film appeared as very light yellow-green in photo under UV- lamp (**Figure 5.11**). Without narrowing the PL peak, emission shifted slightly towards yellow-orange to red with the pyrolysis from 1000°C to 1100°C. Pyrolysis at 1200°C should have caused phase separation and free carbon formation in the film. Correspondingly, it is well known that boron enhances the growth of segregated sp²-carbon nanocrystals, which caused high absorption. Therefore, films pyrolysed at $\geq 1200^\circ\text{C}$ were not discussed here.

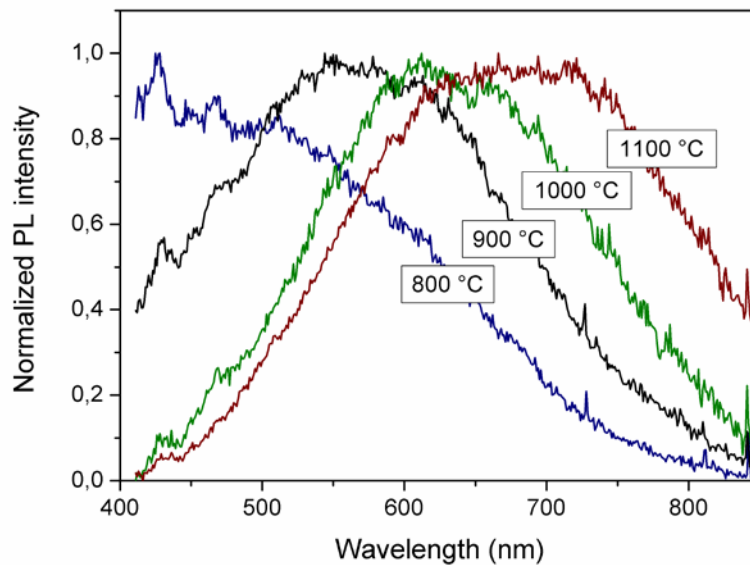


Figure 5.10. Photoluminescence spectra of the TEB-T^HD^H2 thin films pyrolysed at temperatures in the range of 800-1100°C.

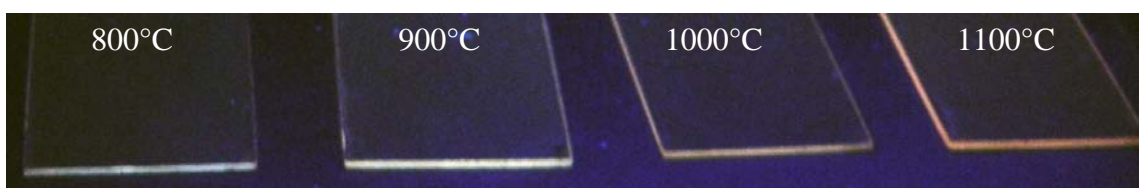


Figure 5.11. Photograph of the SiBOC thin films pyrolysed from 800°C to 1100°C under UV laser excitation.

In order to understand the absorption behaviour of the TEB-T^HD^H2 films, UV- Vis measurements were done and the transmittance spectra are shown in **Figure 5.12**. The transmittance of the films is decreasing with increasing the pyrolysis temperature. Film pyrolysed at 800°C is almost totally transparent for almost all visible colours (≥ 420 nm). Increasing pyrolysis temperature led red shift as well as a decrease in transparency.

Optical absorption edge is below than 200 nm for all the films. The oscillation in the graphs observed in films pyrolysed at 800°C and 900°C is due to the interference of the reflected lights from the substrate. This phenomenon is less evident at higher temperatures ($\geq 1000^\circ\text{C}$) due to high shrinkage after 900 °C (see **Figure 5.6**).

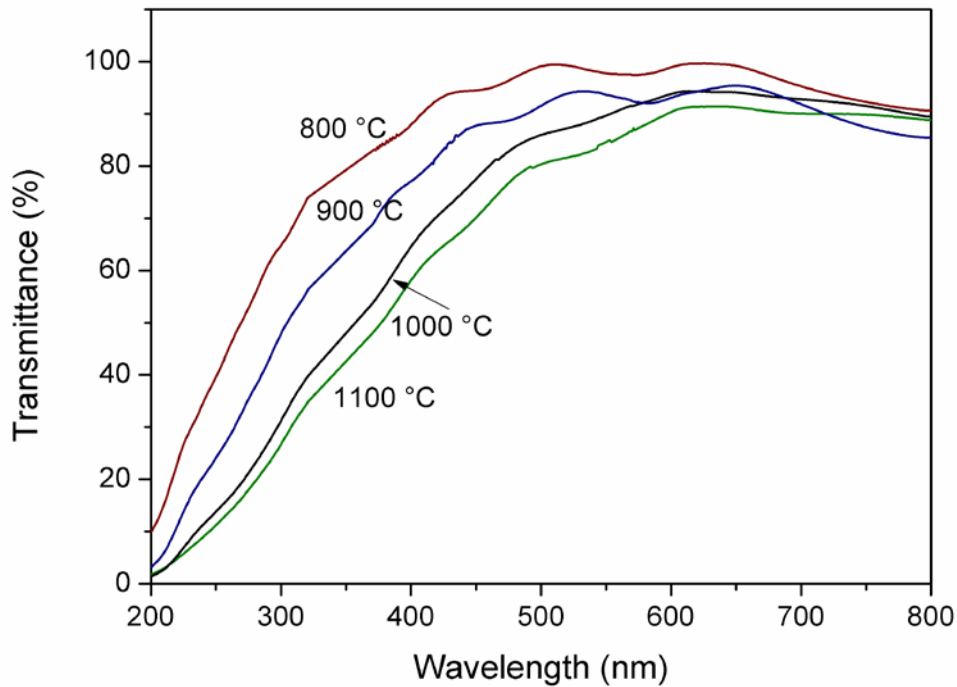


Figure 5.12. UV-visible spectra of TEB- T^HD^H2 thin films pyrolysed at 800–1100°C

The absorption band gap and emission values are reported in **Figure 5.13** as a function of pyrolysis temperature. Absorption values are higher than SiOC films however they followed the same trend (**Chapter 3, Figure 3.13**). Decrease in absorption and emission wavelengths are an indication of phase separation as well as free carbon formation.

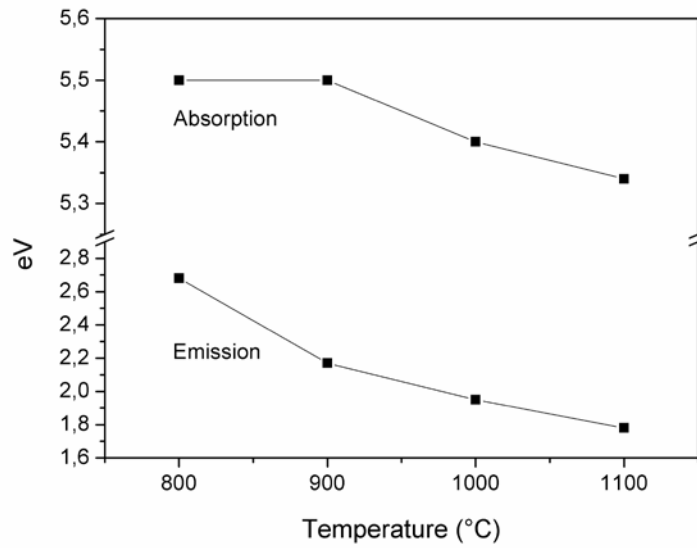


Figure 5.13. Band-gap energy changes of the TEb-T^HD^H2 films as a function of the pyrolysis temperature.

TEb-T^HD^H2 thin films showed very interesting PL features with external quantum efficiency as 4%, which is comparable to T^HD^H2 films. They showed quantum confinement which has not been reported till recently in literature for SiC system [J.Y. Fan, 2006]. One of the main reasons, why quantum confinement is not easily achieved in SiC, is supposed that luminescence dominated by many surface or defect states. Correspondingly, boron is well known to have a reducing effect on defects [R. Pena-Alonso, 2007]. Therefore, by adding very small amount of boron, quantum confinement can be achieved in SiOC system, which can give us the possibility to tune the emission through the all visible color range. It should be noted that the emission band gap at all temperature showed very broad band gap by covering also all the spectrum. Parallel to emission, transparency of the films are quite high till 1000°C (~ 90%), and after this temperature because of phase separation, free carbon caused a decrease in absorption band gap.

In conclusion, the TEb-T^HD^H2 films were studied structurally and optically and their properties are compared with T^HD^H2 films for the clarity. TEb-T^HD^H2 films showed lower shrinkage parallel to the SiBOC ceramics reported in literature. In addition, the B-O-Si bonding is verified with FTIR. The boron addition caused phase separation process

earlier than SiOC system, which gives us the possibility to observe quantum confinement (red shift) in the PL spectra. Therefore, the films are good candidate to be used for LED applications in the visible range from UV-blue to red. Moreover, the emission band found to be very broad, covering larger than visible spectrum, at every pyrolysis temperature. Finally, the external quantum efficiency is found to be close to $T^H D^H 2$ films, namely 4%. A slight decrease in PL intensity can be explained by the effect of carbon, which is segregated with the boron addition.

5.3. SiOCN Films

Silicon oxycarbonitride (SiOCN) ceramics are promising materials for microelectronics and optoelectronics, owing to high-temperature oxidation resistance, tunable band gap characteristics, adjustable transparency in the visible and IR regions, and high-temperature thermal stability [R. Riedel, 1995; T.J. Cross, 2006]. SiOCN films can be deposited by various techniques, including CVD [A. Bendeddouche, 1997] and pulsed laser deposition [T. Tharigen, 1999]. In this work polymer-derived ceramic (PDC) route has been applied to produce SiOCN films by direct pyrolysis of commercially available polysilazane precursor and their photoluminescence (PL) properties have been studied [K. B. Sundaram, 2000].

The structural evolution occurring during the pyrolysis process of the polymer derived films was investigated by using FT-IR absorption spectroscopy. PL of the resultant films pyrolyzed at different temperatures showed wide and intense luminescence. Tunable emission is observed by PL measurements changing from UV range (300 nm) to yellow-orange (600 nm). Finally, energy band gap of the films are used to understand the origin of the luminescence.

5.3.1. Experimental Details

Commercially available polysilazane, known as CerasetTM (KiON Corp., Clariant, USA), was used as precursor. As a curing agent 0.5% of dicumyl peroxide is added at 80°C and total curing at room temperature took place in couple of days. Films on Si and SiO₂ substrates have been prepared by spin coating at 300 rpm for 1 min. The stabilization of the films has been done at 110°C for 24 hours. Cross-linking is supposed

to start at this temperature and is expected to end around 400°C. Accordingly, the as-spun films have been kept at this temperature and then annealed in Ar or N₂ up to 400°C with an holding time of 1 hour. These procedure lead to the synthesis of crack-free polymeric films, suitable for the subsequent pyrolysis process at higher temperatures.

Further pyrolysis has been done at 500-800°C to see the effect of temperature on structural and optical properties. The heating rate in all the process has been kept at 5°C/min. Bonding structure of the films has been analyzed by FTIR and the fittings of the possible components were done by dmfit program [D.Massiot, 2002]. In order to use this fitting program, different from other previous results, FTIR spectra are reported in absorption instead of transmittance. Whereas, optical properties were examined by PL and UV-Vis analyses. PL measurements were recorded in air on Cary Eclipse, Varian Spectrophotometer using a Xenon lamp as the excitation source, sensitive across the whole wavelength range. Several different excitation wavelengths have been used, whereas samples pyrolysed at 400°C and 600°C showed strong emission in the range of 250 nm excitation lamp. However, the film pyrolysed at 800°C gave an emission well beyond the range of 250 nm excitation lamp therefore Ar laser excitation (365 nm) is used to excite this sample.

5.3.2. Results And Discussion

Stability of the SiOCN films is one of the most critical problems in production. The SiCN precursors have high oxidation rate and therefore, they are always studied under glove box. However, in order to increase the commercialization, the handling conditions need to be improved. Therefore the basic aim of this study is to produce a reproducible SiOCN films by controlling oxidation with experimental details. By optimizing pyrolysis conditions, films aimed to be produced stable by avoiding the continuous oxidation and preventing the structural changes in the film knowing that very small structural changes may affect the optical properties drastically.

Both data sheet of commercial precursor (CerasetTM) and some studies on SiCNs in the literature indicated that 400°C is a critical temperature for cross-linking to be accomplished. Therefore, films kept at this temperature for 30 min for further pyrolysis

process. Moreover, the bonding structure of the film, pyrolysed at 400°C for 1 hour, was studied by FTIR and measurements are repeated after 1 and 6 months. The spectra showed that there is a radical change in bonding structure from initial stage to the measurement done month later (**Figure 5.14**). However, stored samples (1 month and 6 month later) showed same features, which can be an indication of stabilization of the films after 1 month.

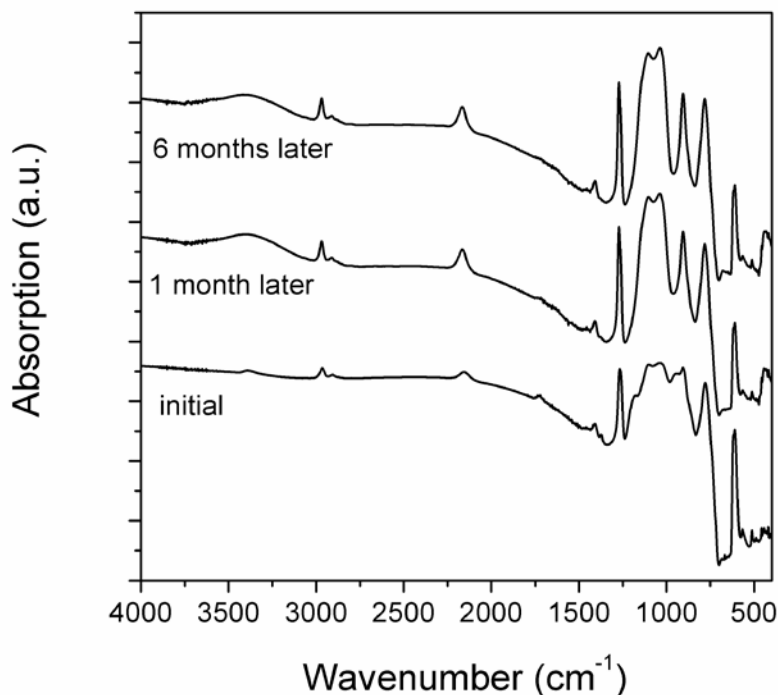


Figure 5.14. FTIR spectra of SiOCN films pyrolysed at 400°C for 1 hour. The experiment is repeated after 1 month.

The water absorption gave rise a broad peak appeared between 3600 cm⁻¹ and 3000 cm⁻¹. However, this bond centred at 3380 cm⁻¹ is also considered as N-H vibration, which is more visible in initial film [S. R. Shah, 2002]. Similarly, small peak at 1720 cm⁻¹ belonging to C=O vibration is seen only in spectrum of the initial film and it is not clearly detectable in film examined stored films (1 month later and 6 months later) [T.J. Cross, 2006]. More dramatic changes are observed in the complex system at 1240-835 cm⁻¹. Thus, these regions are examined by the fitting program separately for samples measured initially and examined after 1 month. The spectra are shown in **Figure 5.15** with possible peak fittings.

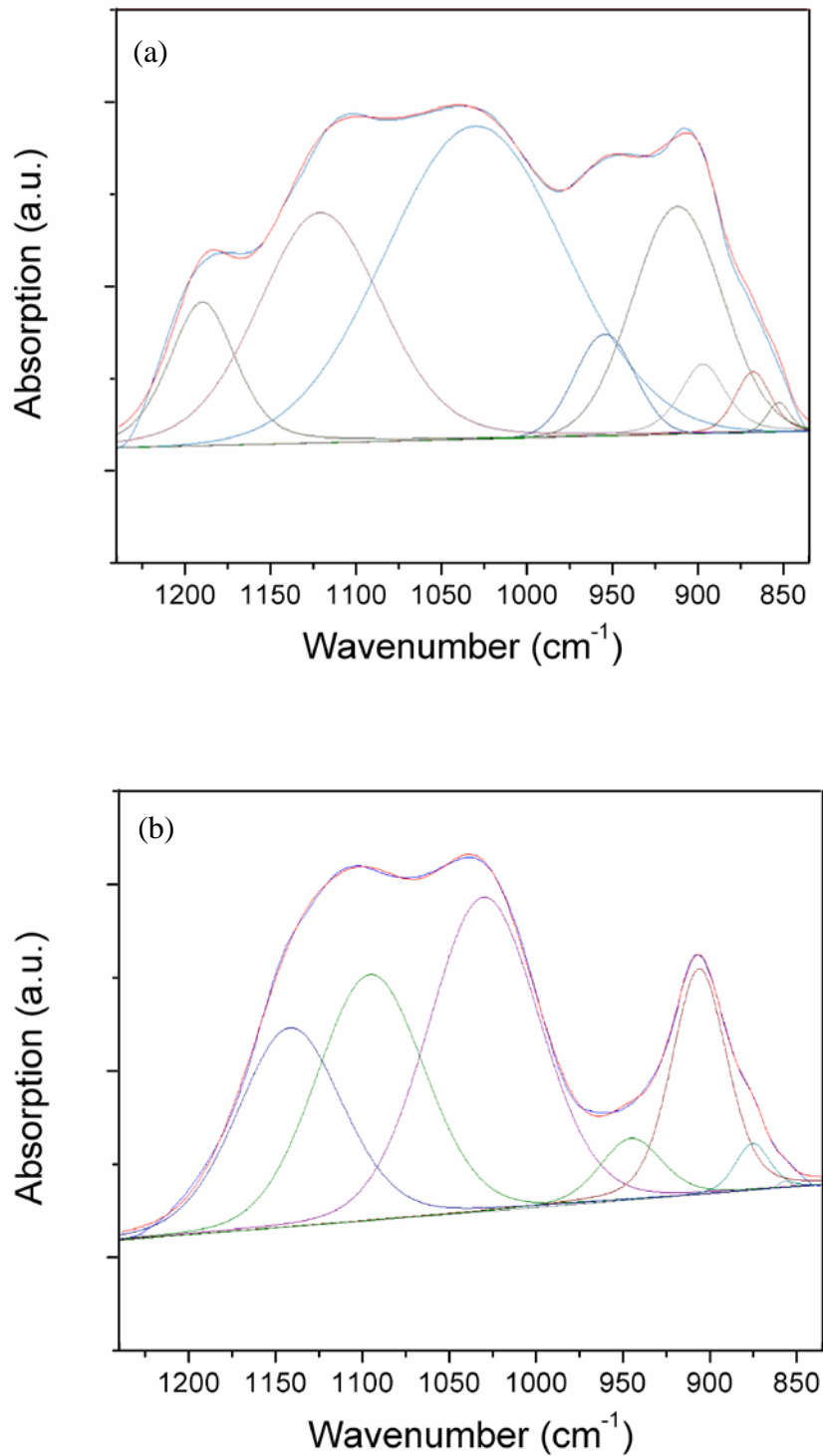


Figure 5.15. FTIR spectra (1240-835 cm⁻¹) of SiOCN films pyrolysed at 400°C for 1 hour. (b) The experiment is repeated after 1 month.

The active oxidation mechanism caused a drastic change in the bonding structure of the film. The produced film (initial) showed Si₂-NH vibration at 1190 cm⁻¹ as well as

intense peak at 1120 cm^{-1} belonging to Si-N vibration [T.J. Cross, 2006]. These two peaks replaced by Si-O bonding at 1141 cm^{-1} and mixed Si-O-C bonding at 1094 cm^{-1} [G. Das, 2007]. It is a clear indication of instability of the film at 400°C . Moreover, there is a decrease in Si-N bond appeared at 954 and 905 cm^{-1} due to oxidation but still visible after 1 month of soaking time. For both films, the Si-C peak contribution at 850 cm^{-1} is visible.

The oxidation rate decreased radically after 1 month of storage and there is only slight difference in the Si-N bonding even after 6 months of storage. Therefore, for further optical studies film pyrolysed at 400°C and stored for 6 months are used as a representative of 400°C . Other films pyrolysed at higher temperatures (500 - 800°C) did not show any noticeable structural changes in FTIR during the storage and therefore these samples are investigated further on to understand the optical potential of the SiOCN films. Moreover, the film pyrolysed at 500°C did not show any noticeable structural or optical changes different than 400°C so it is not considered in the discussion.

The FTIR spectra of SiOCN film pyrolysed at different temperatures are shown in **Figure 5.16**. The transmittance spectrum of the dried film showed different features: peak around 3379 cm^{-1} attributed to the N-H bond, peaks between 3051 - 2907 cm^{-1} and at 1407 cm^{-1} related to C-H related vibrations, peak at 1720 cm^{-1} assigned to the C=O bond and a small broad band at 1598 cm^{-1} related to the C=C vibration. The intense band at 2145 cm^{-1} is attributed to Si-H bond. Si-CH₃ stretching gave rise a peak at 1270 cm^{-1} , whereas Si-C bending and Si-O rocking can be seen at 780 cm^{-1} and 440 cm^{-1} , respectively [S. R. Shah, 2002]. The bond structure of the films has changed during pyrolysis (400 - 800°C). Si-H vibration around 2160 cm^{-1} disappeared totally at 600°C . On the other hand, Si-N vibrations at 2970 cm^{-1} and 1410 cm^{-1} could be seen even at 600°C but not visible at 800°C .

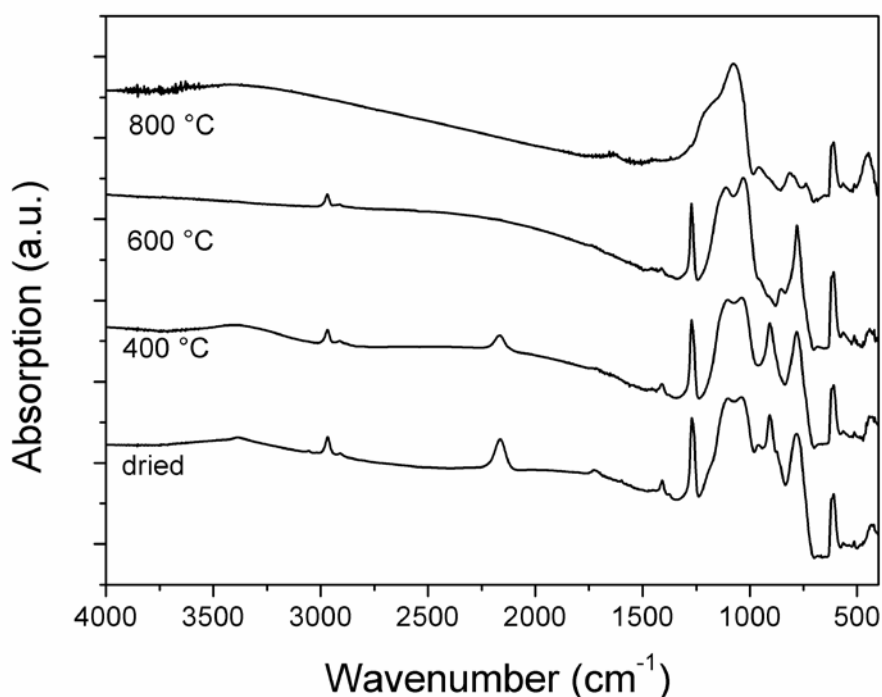


Figure 5.16. FTIR spectrum of SiOCN dried film and pyrolysed films at 400-800°C.

Because of the complexity of the area in the range of 1240-835 cm^{-1} , this range studied separately for the dried film and with the possible convoluted peaks given in **Figure 5.17**. This area is a complex combination of Si-N, Si-C and Si-H bonds. The convolution has been done in order to give a perspective to possible bonds, however, it needs to be mentioned that this area contains many other possible vibrations (Si-O, Si-O-C etc.). Therefore, this study is nothing but a possible suggestion about the bonding. The Si-N vibrations gave rise to peaks at 1112 cm^{-1} , 954 cm^{-1} and 906 cm^{-1} ; whereas Si₂-NH bond caused a peak at 1194 cm^{-1} . Si-O vibration at 1029 cm^{-1} showed that the oxidation process started but system is still containing Si-H vibration, which can be seen at 873 cm^{-1} . Si-C wagging bond is visible at 858 cm^{-1} .

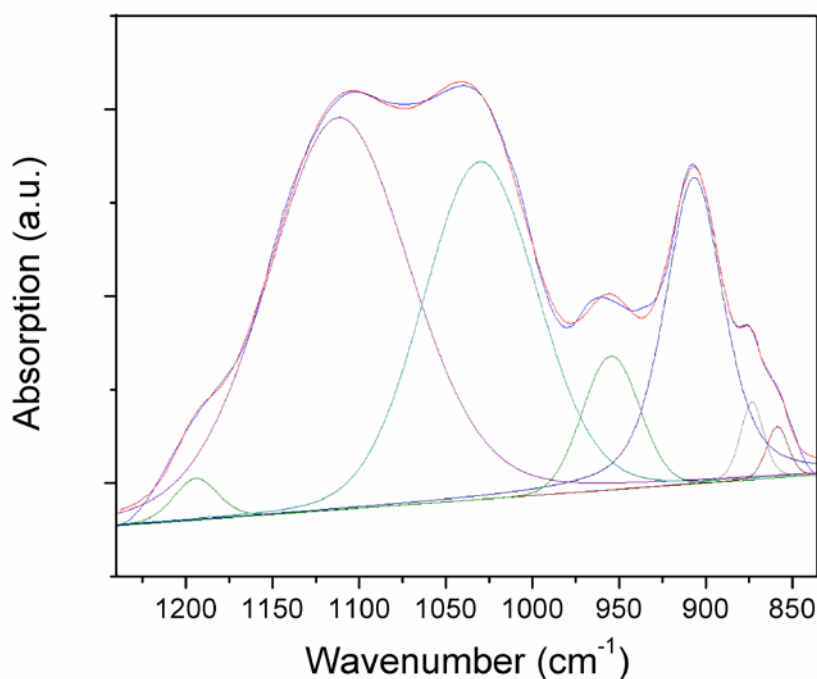


Figure 5.17. FTIR spectrum of dried SiOCN film in the range of 1240-835 cm⁻¹ with possible peak fittings.

For the film pyrolysed at 800°C, the peak range modified to 1350-700 cm⁻¹ in order to not to lose the information coming from new appeared peaks (**Figure 5.18**). During pyrolysis Si₂-NH bond at 1194 cm⁻¹ and Si-H bond at 873 cm⁻¹ disappeared completely indicating that inorganic to organic transformation is accomplished. The Si-O vibrations at 1141 cm⁻¹ and 1029 cm⁻¹ increased their intensity during pyrolysis. On the other hand, the possible Si-O-C bond at around 1095 cm⁻¹ decreased its intensity and totally disappeared at 800°C. The area between 1240 cm⁻¹ and 1000 cm⁻¹ has totally changed its shape at 800°C and gave rise a broad peak centred at 1157 cm⁻¹ and intense peak at 1072 cm⁻¹. The peak at 1157 cm⁻¹ was assigned to Si-O bonding however due to its broadness; it can contain other vibrations like Si-N vibration at around 1112 cm⁻¹. On the other hand, the Si-O peak at 1072 cm⁻¹ was very close to the value in SiO₂ (1060 cm⁻¹). Thus, it can be an indication of starting of phase separation. Similarly, a radical decreased in peak intensity of Si-N wagging vibrations at 950 cm⁻¹ and 905 cm⁻¹ are detected, respectively. However, these components were still visible even at 800°C. The intensity of the peak centred at 780 cm⁻¹ decreased radically after 600°C but Si-C components were still visible in spectrum. All the peaks between 850 cm⁻¹ and 720 cm⁻¹

assigned to Si-C vibrations. Very small component at 1220 cm^{-1} was suggested to be caused by C-C vibrations.

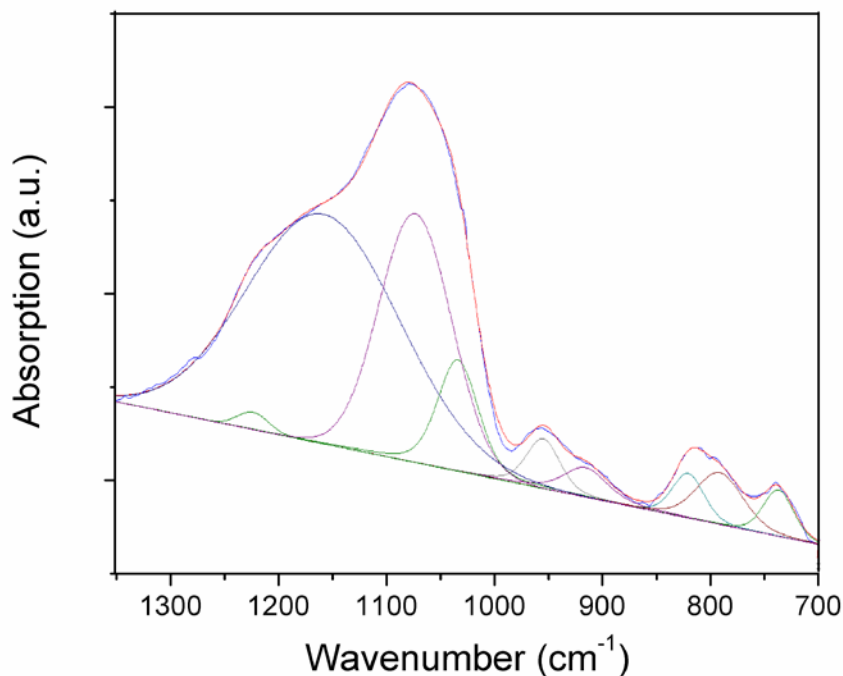


Figure 5.18. FTIR spectrum of SiOCN film pyrolysed at 800°C in the range of $1350\text{-}700\text{ cm}^{-1}$ with possible peak fittings.

FTIR results reveal that the system is still dynamic at 400°C and cross-linking is continuing at this temperature. The change in the bonding structure of the film affected also the luminescence behaviour; which can be seen in **Figure 5.19**. Film pyrolysed at 400°C and measured after production showed an intense UV emission centred at 360 nm with a hump at 320 nm . The peak at 320 nm diminished in PL spectra of the same sample measured after 1 month. Looking at the bonding structure of both sample, the most radical changes appeared to be in $\text{Si}_2\text{-NH}$ and Si-N bonding. The decrease in the intensity of these bonds seems to be caused to a decrease in the PL peak at 320 nm . Relatively, the Si-C and Si-N bond areas ($950\text{-}840\text{ cm}^{-1}$) seems to be separate from Si-O vibration area ($1240\text{-}950\text{ cm}^{-1}$), which is the result of cross-linking. As the cross-linking takes place, the chains rearrange and increase branching. In the literature, the cross-linking is reported to be caused an increase in emission intensities. Indeed, in our sample the intensity of the emission increases by more than 10 times within 1 month of storage. Films after 1 month of storage did not show any difference in PL spectra

(similar to FTIR) indicating that the cross-linking rate is decreased and the samples are stable for storage in air.

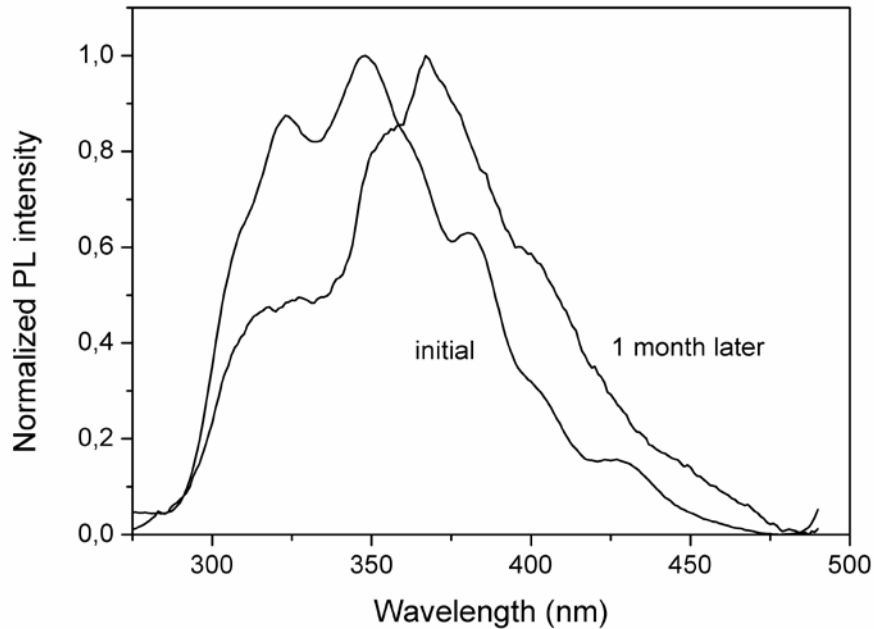


Figure 5.19. Photoluminescence spectra of the SiOCN films pyrolysed at 400°C measured after pyrolysis and 1 month of storage.

PL spectra of films pyrolysed at different temperatures are shown in **Figure 5.20**. Pyrolysis 600°C caused a slight shift towards the visible range but the emission is still in UV range with a peak centered at 380 nm. The decrease in the intensity of the Si-N peak at 927 cm^{-1} in FTIR affected the PL peak at 320 nm and caused a parallel decrease. On the other hand, the emission centered at 360-380 nm (3.4-3.3 eV) is caused by the uncondensed Si-CH₃, C-H and Si-H bonds, which are indicating that inorganic to organic transformation did not completed at 600°C. The slight red shift can be also explained by the continuing of cross-linking process.

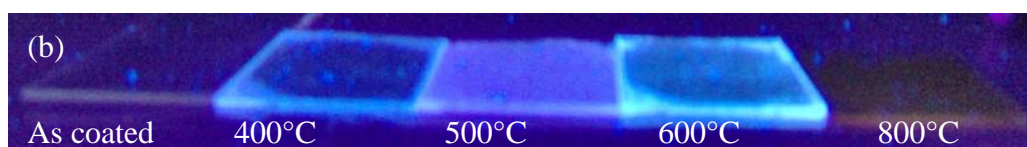
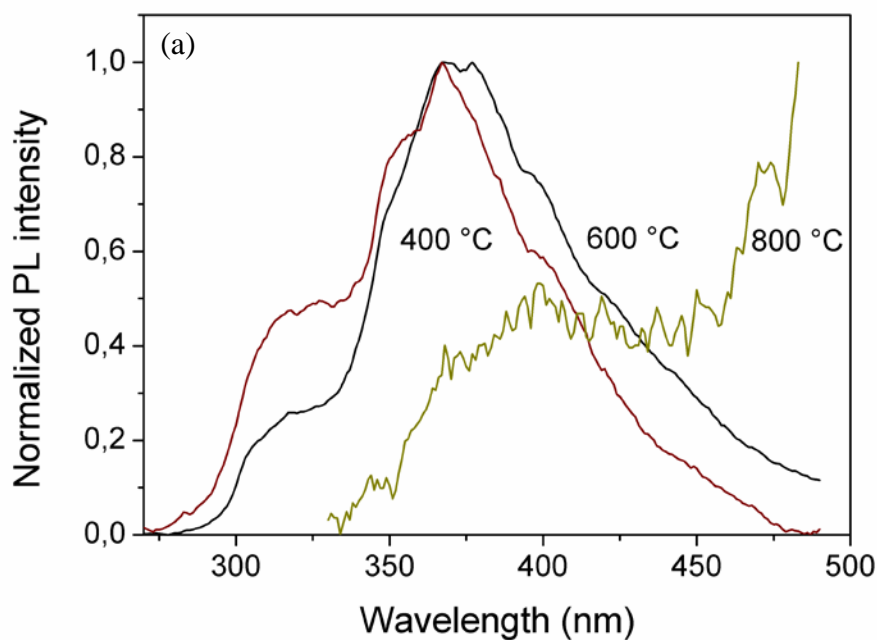


Figure 5.20. (a) Photoluminescence spectra of the SiOCN films pyrolysed at 400-800°C. (b) Photograph of the SiOCN thin films under UV laser excitation.

Further increase in pyrolysis temperature caused radical red shift to visible range, which can be seen also in **Figure 5.20**. The real shape of the emission could be detected by Ar laser (365 nm) and given in **Figure 5.21**. SiOCN films pyrolysed at 800°C showed an emission centered at 650 nm possibly due to the replacement of Si-CH₃ and C-H bonding by Si-C bonds. The organic to inorganic transformation led the separation of the areas of Si-O, Si-N and Si-C bonds, which is visible in FTIR of film pyrolysed at 800°C. In literature, similar red shift is explained by the existence of the C radicals in the system. C dangling bond is suggested to be caused a radical red shift (from 320 nm to 550 nm) starting from low temperatures (200°C) to high temperatures (600°C). Meanwhile, a small C-C bond contribution at 800°C in FTIR is observed and this graphitic carbon can be the cause of the red shift and decrease in PL intensity. PL spectrum of the sample at 600°C is shown in **Figure 5.21-b** to compare the PL intensities of the samples. Even only the tail of the emission can be seen (the emission is

centered at 380 nm, **Figure 5.20**), it gave very high intensity with respect to the Si reference, which is showing that SiOCN film give very intense emission in UV range and they can be good candidates for UV-LED.

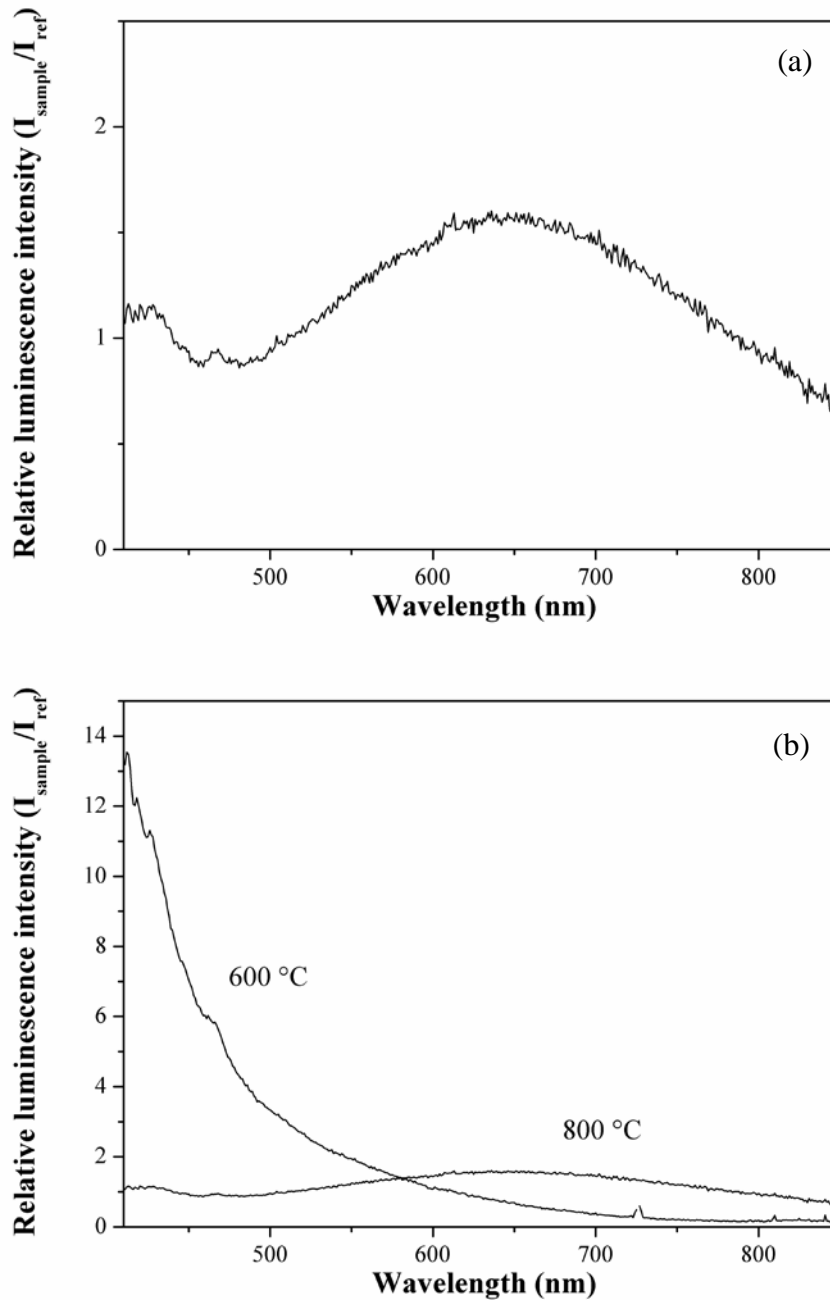


Figure 5.21 (a) Photoluminescence spectrum of the SiOCN film pyrolysed at 800°C and (b) together with 600°C.

Tauc band calculations showed that the E_{gap} is decreasing dramatically pyrolysis at 800°C to 4.5 eV (**Figure 5.22**). The E_{gap} is almost stable at 5.6 eV for the lower

pyrolysis temperatures, which is corresponding to the PL results. It is an indication that the system is stable at temperatures lower than 800°C and the emission is obtained from the same source of the emitting centers. The radical changes observed at 800°C are due to the inorganic to organic change of the structure and it led a radical red shift in the emission.

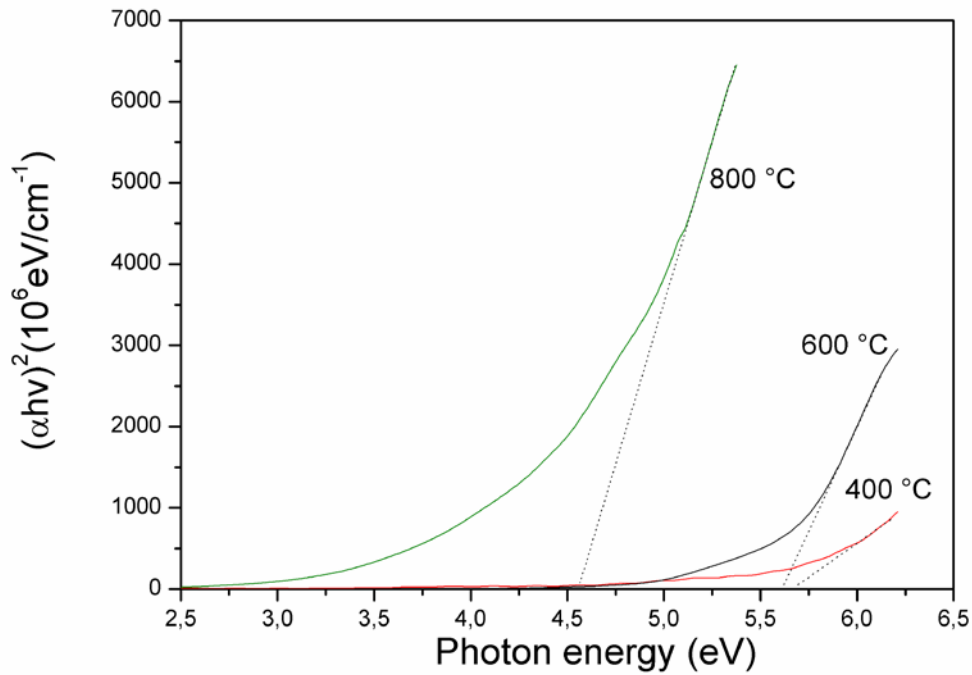


Figure 5.22. Plot of $\alpha(h\nu)^2$ versus photon energy of SiOCN thin films annealed at the indicated temperatures. The dashed lines are fittings by using Eq. 2.4 and 2.5.

5.4. Conclusions

Parallel to previous studies on boron added SiOCs, boron addition increased the crystallization of SiC and enhanced the growth of segregated sp²-carbon nanocrystals C. The effect of these two mechanisms were detected in optical analysis. The quantum confinement, a continuous red shift in emission spectrum due to cluster size increase, is observed with pyrolysis temperature increase. The boron addition did not only decrease the phase separation temperature of the SiC but also decreased defects states, which does not let us see the quantum confinement in SiOC. The emission intensity as well as quantum confinement increased radically by boron addition. However, luminescence intensity decreased radically after 1100°C, and therefore not discussed in the study

which is probably due to higher free C formation. This study showed that, the luminescence quality can be improved extremely by addition of boron. Moreover, the processing temperature can be decreased and very broad emission can be obtained.

The study on boron added Si rich SiOC powders were more focused on structural properties of these systems, since they were not studied in the literature. The structural properties of these powders indicated that starting of crystallization temperature is decreased radically (300°C) and crystallization rate is found to be very high compared to SiOC system. The crystal size of Si in SiBOC found to be more than 10 times bigger than in SiOC at 1400°C. The high crystallization rate led us detect the emission coming from Si at 1000°C although it is not observed in boron free SiOC powders. As the pyrolysis temperature increases, emission coming from Si clusters either red shift to out of spectra or diminished due to high crystalline size and emission only coming from β -SiC can be seen at 1200°C. Finally at 1400°C, the PL peak shift to UV range like in boron free samples due to possible α -SiC formation.

In the last part, we have studied on SiOCN system to understand the possible relationship between bonding of the structure and emitting centers. Study showed that the system is highly dynamic and continue both cross-linking and oxidation if the pyrolysis performs lower than 400°C. After this temperature the emission is stable and gives high UV emission at around 360 nm. The intensity of the emission increases with the cross-linking increases. Moreover, transformation from organic to inorganic stage caused a disappearance of the Si-CH₃, C-H and Si-H bonds, which led emission shift radically towards visible range and gave very high red emission at 650 nm. A possible contribution of free carbon at this temperature may be another reason of the red emission at this temperature.

Conclusion on PhD Study

A new approach to obtain visible luminescence from sol-gel derived SiOC films is proposed in this PhD study. This novel method is based on a simple processing route to produce nanostructured multicomponent ceramics. According to this route, hybrid sol-gel derived precursors are converted to ceramic materials by a pyrolysis process in controlled atmosphere at 800-1000°C. Higher temperatures lead to formation of Si-rich SiOC, C-rich SiOC or stoichiometric SiOC according to the starting composition. The final composition, which is relevant to line emission, can be easily controlled through a number of processing parameters like the composition of the preceramic gel and the heat treatment conditions. Thus, this new processing method seems very well suited for the production of white emitting materials since the Si- and C-based emission can be tuned across the visible spectral range from UV-blue to red by controlling film composition. A further advantage of this method is that the thin films can be formed on Si or quartz wafers and this can serve as starting material to process more complex photonic devices such as waveguides or LEDs.

By optimizing the synthesis conditions, homogeneous, crack free and stable SiOC films have been obtained even at high temperature pyrolysis and demonstrated by surface analyses. Bonding structure of the films during the pyrolysis is investigated by means of several characterization methods (FTIR, XPS and SIMS) and the existence of the mixed Si-O-C bonds is verified at higher temperatures ($\geq 1200^\circ\text{C}$). The change in bonding structure at 1200°C leads us to suggest the starting of the phase separation at this temperature.

Wettability of the films are investigated by contact angle measurements and showed high hydrophobicity in as-coated stage due to existence of Si-CH₃ bonds. On the other hand hydrophilicity increased radically with pyrolysis.

Films showed different luminescence behaviour at low temperatures (800-1000 °C) and high temperatures (1100-1250°C). In the amorphous state (800-100°C), all SiOC films showed UV-blue luminescence peaking at about 410 nm, which is attributed to defect states present in the matrix such as dangling bonds. The increase of the pyrolysis

temperature ($\geq 1100^\circ\text{C}$) led to the partition of SiOC and formation of SiC, C and Si phases. The intense green-yellow luminescence observed in stoichiometric SiOC films caused by the presence of SiC and very low amount of free C. On the other hand, Si rich SiOC film (T^{H}) showed a very broad and extremely intense white luminescence peak centred at 620 nm covering almost all visible range (430 nm-900 nm) at 1200°C . This behaviour is explained by the simultaneous presence of SiC, C and Si in the film. External quantum efficiency measurements yielded 11.5% and 5% efficiencies in T^{H} and $\text{T}^{\text{H}}\text{D}^{\text{H}2}$ films, respectively, pyrolysed at 1200°C . On the other hand, C rich SiOC films did not show any noticeable improvement in PL, indicating that C excess in the SiOC system is detrimental for the luminescence behaviour.

Solutions which used in thin film production have been characterized extensively by means of several characterization properties. Moreover, the related powders and bulks have been characterized for the sake of coherency and widen the study.

Structural study on T^{H} precursor showed many important facts about this precursor. In our study, triethoxysilane has been chosen as precursor for Si-rich SiOC glasses. By FTIR and ^{13}C NMR, residual alkoxy group have been observed in the gel sample due to lack of full condensation. These residual alkoxy groups produced C in the system that can react with excess Si and forms SiC at high temperatures ($\geq 1000^\circ\text{C}$), which has been shown by XRD. Therefore, the resultant ceramic became Si rich SiOC and with an increase in pyrolysis temperature $\text{Si}_{\text{nc}}+\text{SiC}_{\text{nc}}/\text{SiO}_2$ has been achieved.

In addition, a study on volumetric shrinkage of films and powders has been done. The results showed that the shrinkage in films happens almost 200°C earlier than powder and higher amount of siloxane release due to the low dimension, the shrinkage is higher than powders. This can be considered as an indication that the pyrolytic transformation in films occurs earlier than powders. The compositional difference due to high siloxane release may also cause a difference in final composition.

The last part of the study dedicated to two different systems, SiBOCs and SiOCNs, in order to understand the effect of the boron addition on SiOC system and study the optical properties of the SiOCN.

Mainly, the boron addition causes the crystallization of SiC and enhanced the growth of segregated sp²-carbon nanocrystals. They strongly affected the optical properties which were investigated by PL and UV-Vis measurements. The quantum confinement, a continuous red shift in emission spectrum due to cluster size increase, is observed with pyrolysis temperature increase. In other words, tunable (color emission change) SiOC films is obtained with high quantum efficiency by adding very few amount of boron in SiOC. Moreover, the processing temperature is decreased and very broad emission is obtained.

The study on boron added Si rich SiOC powders were more focused on structural properties of these systems, since they were not studied in the literature. The structural properties of these powders indicated that starting of crystallization temperature is decreased radically (300°C) and crystallization rate is found to be very high compared to SiOC system. The crystal size of Si in SiBOC found to be more than 10 times bigger than in SiOC at 1400°C by XRD study.

Finally optical characterization of a SiOCN PDC system showed very promising optical properties. In this case the film is obtained from a commercial polymer precursor. Since this system is rich of free carbon the optical characterization has been limited to samples pyrolyzed at low temperatures, when the graphitic phase is not yet fully developed. Study showed that the system is highly dynamic and continue both cross-linking and oxidation if the pyrolysis performs lower than 400°C. After this temperature the emission is stable and gives high UV emission at around 360 nm. The intensity of the emission increases with the cross-linking increases. Moreover, transformation from organic to inorganic stage caused a disappearance of the Si-CH₃ and C-H bonds, which led emission shift radically towards visible range and gave very high red emission at 650 nm. A possible contribution of free carbon at this temperature may be another reason of the red emission at this temperature. Accordingly, results showed that SiOCN PDC gives very high emission in UV range and they are promising materials for UV-LEDs.

References

- A. Bendeddouche, R. Berjoan, E. Beche, T. Merle-Mejean, S. Schamm, V. Serin, G. Taillades, A. Pradel, R. Hillel.** (1997) "Structural Characterization of Amorphous SiC_xN_y Chemical Vapor Deposited Coatings." *Journal of Applied Physics*, 6147–6154.
- A. Karakuscu, R. Guider, L. Pavesi, G. D. Sorarù.** (2008) "Synthesis and Optical Properties of SiC_n/SiO₂ Nanocomposite Thin Films." In *Materials and Nanotechnology II, Ceramic Engineering and Science Proceedings*, by M. Singh S. Mathur, 85-91. online: American Ceramic Society.
- A. Karakuscu, R. Guider, L. Pavesi, G. D. Sorarù.** (2009) "White luminescence from sol-gel derived SiOC thin films." *Journal of American Ceramic Society*, 2969–2974.
- A. Karakuscu, G. D. Sorarù.** (2009(b)) "Si and SiC nanocrystals by pyrolysis of sol-gel-derived precursors." In *Silicon Nanocrystals*, by R. Turan L. Pavesi. Weinheim: Wiley-VCH.
- A. Kumar, F. Singh, J.C. Pivin, D.K. Avasthi.** (2005) "Photoluminescence studies of carbon clusters formed by irradiation of Si-based polymer." *Radiation Measurements*, 785 – 788.
- A. Perez-Rodriguez, O. Gonzalez-Varona, B. Garrido, P. Pellegrino, J. R. Morante, C. Bonafos, M. Carrada, A. Claverie.** (2003) "White luminescence from Si and C ion-implanted SiO₂ films." *Journal of Applied Physics*, 254-262.
- A. Quaranta, A. Karakuscu and G. D. Soraru.** (2009) "Optical Properties." In *Polymer Derived Ceramics*, by R. Riedel, G.D. Sorarù and A. Kleebe P. Colombo, 253-261. Lancaster, PA: DEStech Publications.
- A. Saha, R. Raj, D. L. Williamson.** (2006) "A Model for the Nanodomains in Polymer-Derived SiCO." *Journal of the American Ceramic Society*, 2188–2195 .
- A. Saha, S. R. Shah, R. Raj, S. E. Russek.** (2003) "Polymer-derived SiCN composites with magnetic properties." *Journal of Materials Research*, 2549-2551.

- A. Stesmans, F. Scheerlinck.** (1994) "Natural intrinsic EX center in thermal SiO₂ on Si: 17O hyperfine interaction." *Physical Review B*, 5204–5212 .
- A. Stesmans, F. Scheerlinck.** (1995) "Electron-spin-resonance analysis of the natural intrinsic EX center in thermal SiO₂ on Si." *Physical Review B*, 4987-97.
- A. Stesmans, K. Clémer, V.V. Afanas'ev.** (2008) "Primary ²⁹Si hyperfine structure of E' centers in nm-sized silica: Probing the microscopic network structure." *Physical Review B*, 094130-1-12.
- C. Della Volpe, S. Dire, E. Pagani.** (1997) "A comparative analysis of surface structure and surface tension of hybrid silica films." *Journal of non-crystalline solids*, 51-60.
- C. Della Volpe, D. Maniglio, S. Siboni, M. Morra.** (2001) "An Experimental Procedure to Obtain the Equilibrium Contact Angle from the Wilhelmy Method." *Oil & Gas Science and Technology*, 9-22.
- C. Gervais, F. Babonneau, N. Dallabonna, G. D. Soraru.** (2001) "Sol–Gel-Derived SiBOC Glasses Containing Mixed Silicon Oxycarbide and Boron Oxycarbide Units." *Journal of the American Ceramic Society*, 2160–64.
- C. P. Lindsey, G. D. Patterson.** (1980) "Detailed comparison of the Williams–Watts and Cole–Davidson functions." *The Journal of the Chemical Physics*, 3348-3357.
- C. Turquat, H.J. Kleebe, G. Gregori, S. Walter, G.D. Sorarù.** (2001) "Transmission Electron Microscopy and Electron Energy-Loss Spectroscopy Study of Nonstoichiometric Silicon-Carbon-Oxygen Glasses." *Journal of the American Ceramic Society*, 2189-96.
- C. W. Wang, R. H. Horng, D. S. Wu, B. C. Huang.** (1998) "Luminescence improvement of SrS:Ce thin films by rapid thermal annealing: Evidence of energy-transfer model for SrS:Ce electroluminescent devices." *Journal of Applied Physics*, 7958-64.
- C.J. Brinker, G.W. Scherer.** (1990) *Sol-Gel Science: The Physics and Chemistry of Sol-Gel Processing*. San Diego: Academic Press.
- Ceraset®, KiON®.** "Polyureasilazane and KiON® Ceraset® Polysilazane 20."

- Colombo, P.** (2008) "Engineering porosity in polymer-derived ceramics." *Journal of the European Ceramic Society*, 1389–1395.
- D. A. Glocker, S.I. Shah.** (1998) *Handbook of Thin Film Process Technology*. Bristol and Philadelphia: Institute of Physics Publishing.
- D. Bahloul-Hourlier, J. Latournerie, P. Dempsey.** (2005) "Reaction pathways during the thermal conversion of polysiloxane precursors into oxycarbide ceramics." *Journal of the European Ceramic Society*, 979–985.
- D. Galusek, S. Reschke, R. Riedel, W. Dressler, P. Sajgalík, Z. Lencés, J. Majling.** (1999) "In-Situ Carbon Content Adjustment in Polysilazane Derived Amorphous SiCN Bulk Ceramics." *Journal of the European Ceramic Society*, 1911-1921.
- D. Jurbergs, L. Mangolini, E. Rogojina, U. Kortshagen.** (2006) "Silicon Nanocrystals with Ensemble Quantum Yields exceeding 60%." *Applied Physics Letters*, 233116-1-3.
- D. Stentz, S. Blair, C. Goater, S. Feller, M. Affatigato.** (2000) "Determination of the mesostructure of lead borate glasses using laser photoionization mass spectroscopy." *Applied Physics Letters*, 61-63.
- D.E. Bornside, C.W. Macosco, L.E. Scriven.** (1987) "On the modeling of spin coating." *Journal of Imaging Technology*, 122-130.
- D.Massiot, F.Fayon, M.Capron, I.King, S.Le Calvé, B.Alonso, J-O.Durand, B.Bujoli, Z.Gan, G.Hoatson.** (2002) "Modelling one- and two-dimensional Solid State NMR spectra." *Magnetic Resonance in Chemistry*, 70-76.
- D'Andrea. G.** (1995) "Vetri SiOC via Sol-Gel" *Tesi di Dottorato di Ricerca in Ingegneria dei Materiali*. Italy: Università di Trento.
- F. Babonneau, L. Coury, J.I. Ivage.** (1990) "Aluminum sec-butoxide modified with ethylacetoacetate: An attractive precursor for the sol-gel synthesis of ceramics ." *Journal of Non-Crystalline Solids*, 153-157.

- F. Giorgis, P. Mandracci, L. Dal Negro, C. Mazzoleni, L. Pavesi.** (2000) "Optical Absorption and Luminescence Properties of Wide-Band Gap Amorphous." *Journal of Non-Crystalline Solids*, 266–269.
- F. Iacona, G. Franzo, C. Spinella.** (2000) "Correlation between luminescence and structural properties of Si nanocrystals." *Journal of Applied Physics*, 1295-13.
- G.D. Sorarù, F. Babonneau, J.D. Mackenzie.** (1990) "Structural Evolution from Polycarbosilane to SiC Ceramics." *Journal of Materials Science*, 3886-93.
- G.D. Soraru, G. D'Andrea, R. Campostrini, F. Babonneau.** (1995) "Characterization of Methyl-substituted Silica Gels with Si-H Functionalities." *Journal of Materials Chemistry*, 1363-1374.
- G. D. Sorarù, G. D'Andrea, R. Campostrini, F. Babonneau, G. Mariotto.** (1995(b)) "Structural Characterization and High-Temperature Behavior of Silicon Oxycarbide Glasses Prepared from Sol-Gel Precursors Containing Si-H Bonds." *Journal of the American Ceramic Society*, 379 - 387.
- G. D. Sorarù, G. D'Andrea, R. Campostrini, F. Babonneau.** (1995(c)) "Si-O-C Glasses from Gels." *Proceedings of the International Symposium on Sol-Gel Science and Technology*. (Sol-Gel Science and Technology): American Ceramic Society. 135-146.
- G.D.Sorarù, E. Dallapiccola, G. D'Andrea.** (1996) "Mechanical Characterization of Sol-Gel-derived Silicon Oxycarbide Glasses." *Journal of the American Ceramic Society*, 2074-80.
- G. D. Sorarù, G. D'Andrea, A. Glisenti.** (1996(b)) "XPS Characterization of Gel-Derived Silicon Oxycarbide Glasses." *Materials Letters*, 1-5.
- G. D. Sorarù, R. Campostrini, S. Maurina, F. Babonneau.** (1997) "Gel-Precursor to Silicon Oxycarbide Glasses with Ultra-High Ceramic Yield." *Journal of the American Ceramic Society*, 999-1004.
- G. D. Soraru, F. Babonneau, S. Maurina, J. Vicens.** (1998) "Sol-gel synthesis of SiBOC glasses ." *Journal of Non-Crystalline Solids*, 173-183 .

- G. D. Sorarù, P. Colombo.** (2000) "Polymer to Ceramic Transformation: Processing of Ceramic Bodies and Thin Films." In *Handbook of Hard Materials, Part I*, by R. Riedel, 410-440. Weinheim: VCH.
- G.D. Soraru, S. Modena, E. Guadagnino, P. Colombo, J. Egan, C. Pantano.** (2002) "Chemical Durability of Silicon-Oxycarbide Glasses." *Journal of the American Ceramic Society*, 1529-36.
- G. D. Soraru, S. Modena, P. Bettotti, G. Das, G. Mariotto, L. Pavesi.** (2003) "Si nanocrystals obtained through polymer pyrolysis." *Applied Physics Letters* , 749-751.
- G. D. Sorarù, Y. Zhang, M. Ferrari, L. Zampedri, R. R. Goncalves.** (2005) "Novel Er-doped SiC/SiO₂ nanocomposites: synthesis via polymer pyrolysis and their optical characterization." *Journal of the European Ceramic Society*, 277-281.
- G.D.Sorarù, H.J. Kleebe R. Ceccato, L. Pederiva.** (2000) "Development of Mullite-SiC Nanocomposites by Pyrolysis of Filled Polymethylsiloxane Gels." *Journal of the European Ceramic Society*, 2509-2517.
- G. Das, P. Bettotti, L. Ferraioli, R. Raj, G. Mariotto, L. Pavesi, G. D. Soraru.** (2007) "Study of the pyrolysis process of an hybrid CH₃SiO_{1.5} gel into a SiCO glass." *Vibrational Spectroscopy*, 61–68.
- G. Das, L. Ferraioli, P. Bettotti, F. De Angelis, G. Mariotto, L. Pavesi, E. Di Fabrizio, G.D. Soraru.** (2008) "Si-nanocrystals/SiO₂ thin films obtained by pyrolysis of sol–gel precursors ." *Thin Solid Films*, 6804-6807.
- G. Gregori, H.-J. Kleebe, Y. Blum, F. Babonneau.** (2006) "Evolution of C-rich SiOC ceramics Part II, Characterization by high lateral resolution techniques: electron energyloss spectroscopy, high-resolution TEM and energy-filtered TEM." *International journal of materials research*, 710-720.
- G. R. Lin, C. J. Lin, C. K. Lin, L. J. Chou, Y. L. Chueh.** (2005) "Oxygen defect and Si nanocrystal dependent white-light and near-infrared electroluminescence of Si-implanted and plasma-enhanced chemical-vapor deposition-grown Si-rich SiO₂ ." *Journal of Applied Physics*, 94306-1–8.

- G. Trimmel, R. Badheka and F. Babonneau, J. Latournerie, P. Dempsey, D. Bahloul-Houlier, J. Parmentier, G. D. Soraru.** (2003) "Solid-State NMR and TG/MS Study on the transformation of Methyl Groups During Pyrolysis of Preceramic Precursors to SiOC Glasses." *Journal of Sol-Gel Science and Technology*, 279–283.
- G. Winter, W. Verbeek, and M. Mansmann.** (1975) "Production of Shaped Articles of Silicon Carbide and Silicon Nitride,". Production of Shaped Articles of Silicon Carbide and Silicon Nitride. U.S. Patent Patent 892, 583.
- Greil, P.** (2000) "Polymer Derived Engineering Ceramics." *Advanced Engineering Materials*, 339-348.
- Guider, R.** (2009) *Novel materials and optical waveguide systems for silicon photonics*. Trento: PhD Thesis, University of Trento.
- H. Bréquel, J. Parmentier, S. Walter, R. Badheka, G. Trimmel, S. Masse, J. Latournerie, P. Dempsey, C. Turquat, A. Desmartin-Chomel, L. Le Neindre-Prum, U.A. Jayasooriya, D. Hourlier, H. J. Kleebe, G. D. Sorarù, S. Enzo, F Babonneau.** (2004) "Systematic structural characterisation of the high temperature behaviour of nearly-stoichiometric silicon oxycarbide glasses." *Chemistry of Materials*,: 2585-2598.
- H. Chen, F. Zhang, T. Chen, S. Xu, D. G. Evans, X. Duan.** (2009) "Comparative analysis of the dynamic contact angles for two types of superhydrophobic layered double hydroxide film surfaces." *Chemical Engineering Science*, 2957-2962.
- H. El Rassy, A.C. Pierre.** (2005) "NMR and IR spectroscopy of silica aerogels with different hydrophobic characteristics." *Journal of Non-Crystalline Solids*, 1603–1610.
- H. Schmidt, G. Borchardt, A. Müller, J. Bill.** (2004) "Formation kinetics of crystalline Si₃N₄/SiC composites from amorphous Si–C–N ceramics." *Journal of Non-Crystalline Solids*, 133-140 .
- H. Sirringhaus, N. Tessler, R. H. Friend.** (1998) "Integrated optoelectronic devices based on conjugated polymers." *Science*, 1741–1744.
- Hagen, W. R.** (2009) *Biomolecular EPR Spectroscopy*. NW: CRC press.

- I. A. Movtchan, W. Marine, R. W. Dreyfus, H. C. Le, M. Sentis, M. Autric.** (1996) "Optical spectroscopy of emission from Si---SiO_x nanoclusters formed by laser ablation." *Applied Surface Science*, 251-260.
- I. D. W. Samuel, B. Crystall, G. Rumbles, P. L. Burn, A. B. Holmes, R. H. Friend.** (1993) "Time-resolved luminescence measurements in poly(p-phenylenevinylene)." *Synthetic Metals*, 281-288 .
- I. Menapace, G. Mera, R. Riedel, E. Erdem, R. Rüdiger, A. Eichel, A. Pauletti, G.A. Appleby.** (2008) "Luminescence of heat-treated silicon-based polymers: promising materials for LED applications." *Journal of Materials Science*, 5790–5796.
- J. B. Wachtman, R. A. Haber.** (1993) *Sol-Gel Derived Ceramic Coatings*. NJ: Noyes Publications.
- J. C. Pivin, M. Sendova-Vassileva.** (1998) "Visible Photoluminescence of Ion Irradiated Polysiloxane Films." *Solid State Communications*, 133–38.
- J. C. Pivin, M. Sendova-Vassileva, P. Colombo, A. Martucci.** (2000) "Photoluminescence of composite ceramics derived from polysiloxanes and polycarbosilanes by ion irradiation." *Materials Science and Engineering B*, 574-577 .
- J. Linnros, N. Lalic, A. Galeckas, V. Grivickas.** (1999) "Analysis of the stretched exponential photoluminescence decay from nanometer-sized silicon crystals in SiO₂." *Journal of Applied Physics*, 6128-6134.
- J. S. Hartman, M. F. Richardson, B. L. Sherriff, B. G. Winsborrow.** (1987) "Magic Angle Spinning NMR Studies of Silicon Carbide: Polytypes, Impurities, and Highly Inefficient Spin-Lattice Relaxation." *Journal of the American Chemical Society*, 6059-67.
- J. Yang, J. Chen, J. Song.** (2009) "Studies of the surface wettability and hydrothermal stability of methyl-modified silica films by FT-IR and Raman spectra." *Vibrational Spectroscopy*, 178-184.
- J.D. Mackenzie, D.R. Ulrich.** (1988) *In Ultrastructure Processing of Advanced Ceramics*. New York: Wiley.

- J.H. Burroughes, D.D.C. Bradley, A.R. Brown, R.N. Marks, K. Mackay, R.H. Friend, P.L. Bum, A.B. Holmes.** (1990) "Light-emitting diodes based on conjugated polymers." *Nature*, 539 - 541.
- J.Y. Fan, X.L. Wu, P. K. Chu.** (2006) "Low-dimensional SiC nanostructures: Fabrication, luminescence, and electrical properties ." *Progress in Materials Science* , 983-1031.
- K. B. Sundaram, J. Alizadeh.** (2000) "Deposition and Optical Studies of Silicon Carbide Nitride Thin Films." *Thin Solid Films*, 151–154.
- K. C. Kim, C. I. Park, J. I. Roh, K. S. Nahm, Y. B. Hahn, Y. S. Lee, K. Y. Lim.** (2001) "Mechanistic Study and Characterization of 3C-SiC(100) Grown on Si(100)." *Journal of The Electrochemical Society*, C383-C389.
- Karakuscu, A.** (2006) " *Characterization of Maghemite Thin Films Prepared by Sol-Gel Processing*" M.S. Thesis. Turkey: Middle East Technical University.
- Kroll, P.** (2005) "Modelling polymer-derived ceramics." *Journal of the European Ceramic Society*, 163–174.
- L.A. Liew, W.G. Zhang, V.M. Bright, L.N. An, M.L. Dunn, R. Raj.** (2001) "Fabrication of SiCN ceramic MEMS using injectable polymer-precursor technique." *Sensors and Actuators A-Physical*, 64-70 .
- L. A. Liew, R. A. Saravanan, V. M. Bright, M. L. Dunn, J. W. Daily, R. Raj.** (2003) "Processing and characterization of silicon carbon-nitride ceramics: application of electrical properties towards MEMS thermal actuators." *Sensors and Actuators A: Physical*, 171-181.
- L. An, R. Riedel, C. Konetschny, H.-J. Kleebe, Rishi Raj.** (1998) "Newtonian Viscosity of Amorphous Silicon Carbonitride at High Temperature." *Journal of the American Ceramic Society*, 1349–52.
- L. Ferraioli, D. Ahn, A. Saha, L. Pavesi, R. Raj.** (2008) "Intensely Photoluminescent Pseudo-Amorphous SiliconOxyCarboNitride Polymer–Ceramic Hybrids." *Journal of the American Ceramic Society*, 2422-2424.

- L. G. Zhang, Y. S. Wang, Y. Wei, W. X. Xu, D. J. Fang, L. Zhai, K. C. Lin, L. N. An.** (2008) "A silicon carbonitride ceramic with anomalously high piezoresistivity." *Journal of the American Ceramic Society*, 1346–1349.
- L. Pavesi, M. Ceschini.** (1994) "Stretched-exponential decay of the luminescence in porous silicon." *Physical Review B*, 17625–17628 .
- L. Pederiva, G.D. Soraru, J. Latourneire, R. Raj .** (2002) "Pyrolysis kinetics for the conversion of a polymer into an amorphous ceramic." *Journal of the American Ceramic Society*, 2181-7.
- L.B. Ma, R. Song, Y.M. Miao, C.R. Li, Y.Q. Wang, Z.X. Cao.** (2006) "Blue-violet photoluminescence from amorphous Si-in-SiN_x thin films with external quantum efficiency in percentages." *Applied Physics Letters*, 093102-1-4.
- Liepold, Dr. Ute.** (2008) *private communication*. Munich: Siemens AG.
- Loner, S.** (2001) *Vetri Ossicarburi Trasparenti, Tesi di Laurea in Ingegneria dei Materiali*. Italy: Università di Trento.
- M. A. Villegas, J. M. Fernández Navarro.** (1988) "Characterization of B₂O₃-SiO₂ glasses prepared via sol-gel." *Journal of Materials Science*, 2464-2478.
- M. B. Yu, Rusli, S. F. Yoon, Z. M. Chen, J. Ahn, Q. Zhang, K. Chew, J. Cui.,** (2000) "Deposition of nanocrystalline cubic silicon carbide films using the hot-filament chemical-vapor-deposition method." *Journal of Applied Physics*, 8155-8158 .
- M. Baran, B. Bulakh, N. Korsunskaya, L. Khomenkova, J. Jedrzejewski.** (2004) "Luminescence and EPR studies of defects in Si-SiO₂ films ." *The European Physical Journal - Applied Physics*, 285-287.
- M. Monthieux, O. Delverdier.** (1996) "Thermal behavior of (organosilicon) polymer-derived ceramics. V: Main facts and trends ." *Journal of the European Ceramic Society*, 721-737 .
- M. Pauthe, J. Phalippou, J. Corriu, D. Leclercq, A. Vioux.** (1989) "Silica xerogels containing a functional group at silicon." *Journal of Non-Crystalline Solids*, 21-30.

- Mehrotra, R.C.** (1990) "Chemistry of alkoxide precursors." *Journal of Non-Crystalline Solids*, 1-6.
- Modena, S.** (2004) *SiOC/C/Si Nanocomposites: a study of the oxidation process and optical properties*. Trento: PhD Thesis; University of Trento.
- Mutin, P. H.** (2002) "Role of Redistribution Reactions in the Polymer Route to Silicon–Carbon–Oxygen Ceramics." *Journal of the American Ceramic Society*, 1185–89.
- N. Daldosso, G. Das, S. Larcheri, G. Mariotto, G. Dalba, L. Pavesi, A. Irrera, F. Priolo, F. Iacona, F. Rocca.** (2007) "Silicon nanocrystal formation in annealed silicon-rich silicon oxide films prepared by plasma enhanced chemical vapor deposition." *Journal of Applied Physics*, 113510-7.
- N. F. Mott, E. A. Davis.** (1971) *Electronic Processes in Non-Crystalline Materials*. Oxford: Clarendon Press.
- N. T. Son, W. M. Chen, J. L. Lindström, B. Monemar, E. Janzén.** (1999) "Carbon-vacancy related defects in 4H- and 6H-SiC ." *Materials Science and Engineering B*, 202-206 .
- P. A. Ramakrishnan, Y. T. Wang, D. Balzar, L. An, C. Haluschka, R. Riedel.** (2001) "Silicoboron-carbonitride ceramics: A class of high-temperature, dopable electronic materials." *Applied Physics Letters*, 3076-3078 .
- P. Colombo, T. E. Paulson, C. G. Pantano.** (1994) "Atmosphere Effects in the Processing of Silicon Carbide and Silicon Oxycarbide Thin Films and Coatings." *Journal of Sol–Gel Science and Technology*, 601–604.
- P. Sajgalik, M. Haviar.** (1992) "Pressureless Sintering Of Si₃N₄ with Y₂O₃ and Al₂O₃ Additives - Compatibility of Powder Beds." *Ceramics International*, 279-283.
- Pankove, J. I.** (1971) *Optical Processes in Semiconductors*. NJ : Englewood Cliffs,.
- Peng, J.** (2002) *Thermochemistry and Constitution of Precursor Derived Si-(B-)C-N Ceramics*. Germany: PhD. Thesis, Universität Stuttgart.
- PerkinElmer.** (2009) *Technical note FTIR-Spectroscopy Attenuated Total Reflectance (ATR)*. USA: PerkinElmer Inc.

- R. Campostrini, G. D'Andrea, G. Carturan, R. Ceccato, G. D. Sorarù.** (1995) "Pyrolysis Study of Methyl-Substituted Si-H Containing Gels as Precursors for Oxycarbide Glasses, by Combined Thermogravimetric, Gas Chromatographic and Mass Spectrometric Analysis." *Journal of the American Ceramic Society*, 379–387.
- R. Campostrini, G. D'Andrea, G. Carturan, R. Ceccato, G. D. Sorarù.** (1996) "Pyrolysis Study of Methyl-Substituted Si-H Containing Gels as Precursors for Oxycarbide Glasses, by Combined Thermogravimetric, Gas Chromatographic and Mass Spectrometric Analysis." *Journal of Materials Chemistry*, 585–94.
- R. Guider, A. Karakuscu, G. D. Soraru, L. Pavesi.** (2009) "Optical Characterization of SiOC Thin Films Prepared by Pyrolysis of Sol Gel Precursors." *submitted to Thin Solid Films*.
- R. Pena-Alonso, G. Mariotto, C. Gervais, F. Babonneau, G.D. Sorarù.** (2007) "New insights on the high-temperature nanostructure evolution of SiOC and B-doped SiBOC polymer-derived glasses." *Chemistry of Materials*, 5694–5702.
- R. Raj, R. Riedel, G. D. Soraru.** (2001) "Introduction to the special topical issue on Ultrahigh-Temperature Polymer-derived Ceramics." *Journal of American Ceramic Society*, 2158-59.
- R. Riedel, H. J. Kleebe, H. Schonfelder, F. Aldinger.** (1995) "A Covalent Micro/Nano-Composite Resistant to High-Temperature Oxidation." *Nature*, 526–528.
- R. Riedel, M. Seher, J. Mayer, D.V. Szabo.** (1995(b)) "Polymer-Derived Si-Based Bulk Ceramics, Part I: Preparation, Processing and Properties." *Journal of the European Ceramic Society*, 703-715.
- R. Riedel, G. Mera, R. Hauser, A. Klönczynski.** (2006) "Silicon-based polymer-derived ceramics: Synthesis properties and applications - A review." *Journal of the Ceramic Society of Japan*, 425-444.
- R. Sharma, D.V. Sridhara Rao, V.D. Vankar.** (2008) "Growth of nanocrystalline β -silicon carbide and nanocrystalline silicon oxide nanoparticles by sol gel technique." *Materials Letters*,: 3174–3177.

- R.J.E Corriu, D. Leclercq, P.H. Mutin, A. Vioux.** (1997) "Preparation and Structure of Silicon Oxycarbide Glasses Derived from Polysiloxane Precursors." *Journal of Sol-Gel Science and Technology*, 327-330.
- R.W. Siegel, E.H. Hu, M.C. Roco.** (1997) "WTEC panel report on R&D status and trends in nanoparticles." *Proceedings of the Nanostructured Materials and Nanodevices Workshop*. London: Kluwer academic publisher, 197-200.
- S. Dirè, M. Oliver, G.D. Sorarù.** (1999) "Effect of Polymer Architecture on the Formation of Si-O-C Glasses." In *Advanced Synthesis and Processing of Composites and Advanced Ceramics II*, by Z. Munir, R. M. Spriggs K. V. Logan, 251-61. Ceramic Transactions.
- S. I. Andronenko, I. Stiharu, S. K. Misra.** (2006) "Synthesis and characterization of polyureasilazane derived SiCN ceramics." *Journal of Applied Physics*, 113907-1-5.
- S. J. Xu, M. B. Yu, Rusli, S. F. Yoon, C. M. Che.** (2000) "Time-resolved photoluminescence spectra of strong visible light-emitting SiC nanocrystalline films on Si deposited by electron-cyclotron-resonance chemical vapor." *Applied Physics Letters*, 2550-2552.
- S. Modena, G. D. Soraru, Y. Blum, R. Raj.** (2005) "Passive Oxidation of an Effluent System: the case of a Polymer Derived SiOC." *Journal of the American Ceramic Society*, 339-345.
- S. R. Shah, R. Raj.** (2002) "Mechanical Properties of a Fully Dense Polymer Derived Ceramic Made by a Novel Pressure Casting Process." *Acta Materialia*,: 4093–103.
- S. Trassl, G. Motz, E. Rössler, G. Ziegler.** (2002) "Characterization of the free-carbon phase in precursor-derived Si-C-N ceramics: I, Spectroscopic methods." *Journal of the American Ceramic Society*, 239-244.
- S. Trassl, M. Puchingera, E. Rossler, G. Ziegler.** (2003) "Electrical properties of amorphous SiC_xNyHz-ceramics derived from polyvinylsilazane." *Journal of European Ceramic Society*, 781–789.
- S. Y. Seo, K. S. Cho, J. H. Shin.** (2004) "Intense blue–white luminescence from carbon-doped silicon-rich silicon oxide." *Applied Physics Letters*, 717-719.

- S. Yajima, J. Hayashi, M. Omori, K. Okamura.** 1976 "Development of a silicon carbide fibre with high tensile strength" *Nature*, 684–685.
- Sorarù, G. D.** (1994) "Silicon Oxycarbide Glasses from Gels." *Journal of Sol-Gel Science and Technology*, 843-848.
- T. Ishikawa, Y. Kohtoku, K. Kumagawa, T. Yamamura, T. Nagasawa.** (1998) "High-strength alkali-resistant sintered SiC fibre stable to 2,200 degrees C." *Nature*, 773-775.
- T.J. Cross, R. Raj, S. V. Prasad, T. E. Buchheit, D. R. Tallant.** (2006)"Synthesis and Tribological Behavior of Silicon Oxycarbonitride Thin Films Derived from Poly(Urea)Methyl Vinyl Silazane." *International Journal of Applied Ceramic Technology*, 113–126.
- T. J. Cross, R. Raj, S. V. Prasad, T. E. Buchheit, D. R. Tallant.** (2006(b)) "Mechanical and Tribological Behavior of Polymer-Derived Ceramics Constituted from SiC_xO_yN_z." *Journal of the American Ceramic Society*, 3706-3714.
- T. Rouxel, J. C. Sanglebœuf, J. P. Guin, V. Keryvin, G. D. Soraru.** (2001) "Surface Damage Resistance of Gel-Derived Oxycarbide Glasses: Hardness, Toughness and Scratchability." *Journal of the American Ceramic Society*, 2220-2224.
- T. Tharigen, G. Lippold, V. Riede, M. Lorenz, K. J. Koivusaari, D. Lorenz, S. Mosch, P. Grau, R. Hesse, P. Streubel, R. Szargan.** (1999) "Hard Amorphous CSixNy Thin Films Deposited by RF Nitrogen Plasma Assisted Pulsed Laser Ablation of Mixed Graphite/Si3N4-Targets." *Thin Solid Films*, 103–113.
- V. Belot, R. J. P. Corriu, D. Leclercq, P. Lefe`vre, P. H. Mutin, A. Vioux, A. M. Flank.** (1992) "Characterization of Silicon Sesquioxide and Thermal Behavior of Hydrosilsesquioxane Gels." In *Chemical Processing of Advanced Materials Vol. 14.*, by L. L. Hench and J. K. West, 143–58. New York:Wiley.
- V. Grivickas, J. Linnros.** (1995) "Free carrier absorption and luminescence decay of porous silicon." *Thin Solid Films*, 70-73.
- W. Verbeek,** (1974) "Production of Shaped Articles of Homogeneous Mixtures of Silicon Carbide and Nitride " U.S. Patent Patent 853, 567.

Verbeek, W. (1973) "Shaped articles of silicon carbide and silicon nitrate", German Offen Patent 2218960.

Wegner, G. (2000) "Thin film science." In *European White Book on fundamental Research in Materials science*, 197-200. Stuttgart: max-planck institute.

X. Liu, Y. L. Li, F. Hou. (2009) "Fabrication of SiOC Ceramic Microparts and Patterned Structures from Polysiloxanes via Liquid Cast and Pyrolysis." *Journal of the American Ceramic Society*, 49-53.

Y.-L. Li, E. Kroke, R. Riedel, C. Fasel, C. Gervais, F. Babonneau. (2001) "Thermal cross-linking and pyrolytic conversion of poly(ureamethylvinyl)silazanes to silicon-based ceramics." *Applied Organometallic Chemistry*, 820–832.

Young, T. (1805) "An Essay on the Cohesion of Fluids." *Philosophical Transactions of the Royal Society of London*, 65-87.

Appendix

As it is indicated before, optical measurements were performed in Physics Department in University of Trento by Romain Guider with the supervision of Prof. Lorenzo Pavesi. Photoluminescence as well as lifetime measurements were done to understand the optical properties of the films deeply and the results were discussed in the thesis. However, due to the complexity of these measurements, the experimental details of the measurements were not included in the main chapters and given as an appendix. The following chapters are taken from thesis of Romain Guider [Guider, 2009] in order to clarify the measurement conditions and improve the understanding of the analyses.

I. External Quantum Efficiency of SiOC samples

The luminescence properties of conjugated polymers are of considerable interest, both because of the fundamental information that can be obtained about exciton formation and decay, and because of the potential applications for conjugated polymers as the emissive material in light-emitting diodes LED [J.H. Burroughes, 1990; H. Sirringhaus, 1998]. Measurements of the photoluminescence quantum yield of high refractive index samples, such as thin films of polymeric semiconductors, are problematic owing to difficulties in determining the angular distribution of the emission, reflectivity, and absorbance. In the context of conjugated polymers, there is great interest in establishing the absolute quantum efficiency for PL as this is considered to determine the limits to the efficiency of electroluminescent diodes. A quantitative measurement of external PL efficiency is useful for a number of other reasons. For instance, in conjunction with time-resolved PL measurements, it provides a means of determining the radiative and non radiative decay constants [I. D. W. Samuel, 1993]. Luminescence in conjugated polymers is believed to be the result of radiative decay of singlet excitons. Competing non-radiative processes provide additional means of decay, and therefore reduce the efficiency of luminescence. Possible non-radiative mechanisms in the solid state include inter-chain processes (e.g. excimer formation), and quenching of excitons by extrinsic or conformational defects. If radiative and non-radiative decay are monomolecular processes with rates τ_r and τ_{nr} , respectively, the overall luminescence decay will be exponential, with a lifetime, τ , given by

$$\tau^{-1} = \tau_r^{-1} + \tau_{nr}^{-1} \quad \text{Eq. 1}$$

The efficiency for radiative decay of singlet excitons is then given by

$$q = \frac{\tau}{\tau_r} \quad \text{Eq. 2}$$

The efficiency of radiative decay of singlet excitons, q , sets an upper limit on the quantum efficiency which can be obtained in a polymer LED.

In a photoexcitation experiment, a useful figure which can be measured is the photoluminescence (PL) efficiency, defined as the number of photons emitted in photoluminescence per absorbed photon. This figure depends both on q and on the fraction a of absorbed photons which lead to the formation of singlet excitons. a is called the branching index. The PL efficiency, or external radiative quantum efficiency, η , is defined by Equation 3.

$$\eta = \frac{n_e}{n_a} = q \cdot a \quad \text{Eq. 3}$$

Where n_e is the number of photons emitted and n_a is the number of photons absorbed. PL efficiency measurements in solution are relatively simple because it is usually appropriate to assume an isotropic angular distribution for the emission. However, this is not true for thin solid films. For molecular and polymeric materials, anisotropy in the distribution of chromophores leads to an anisotropy in the emission dipole-moment. In addition, waveguiding effects also modify the angular distribution of the emission. In order to apply the method described above, it would be necessary to map out the angular distribution for the emission. This is inconvenient and is not always possible. A standard technique for measuring thin-film PL quantum efficiencies involves the use of an integrating sphere.

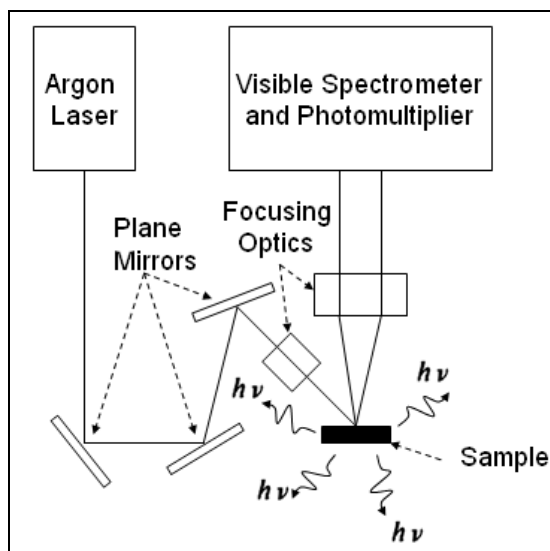


Figure 1.1. Schematic description of the experimental set-up for PL measurements.

In order to evaluate the potential of our films, we measured their external quantum efficiency (EQE). To measure the photon flux emitted from our samples, we calibrated the collection system described in **Figure 1.1** (collecting lenses, monochromator, photomultiplier, photon counting unit) with a red LED whose responsivity is known. By using this calibration, we measured the spectrally integrated luminescence intensity emitted by our films under photo-excitation and converted it into an emitted photon flux. The so-evaluated photon flux was corrected by the numerical aperture of the collecting system by assuming that the film is a lambertian point source. We considered that the total absorbed power by the active thin film is equal to the total laser power incident on the sample (E_{laser}) less the power transmitted by the sample (E_{trans}), the power reflected by the sample (E_{refl}) and the power absorbed by the quartz substrate (E'_{refl}). We illustrated all these energy in **Figure 1.2**.

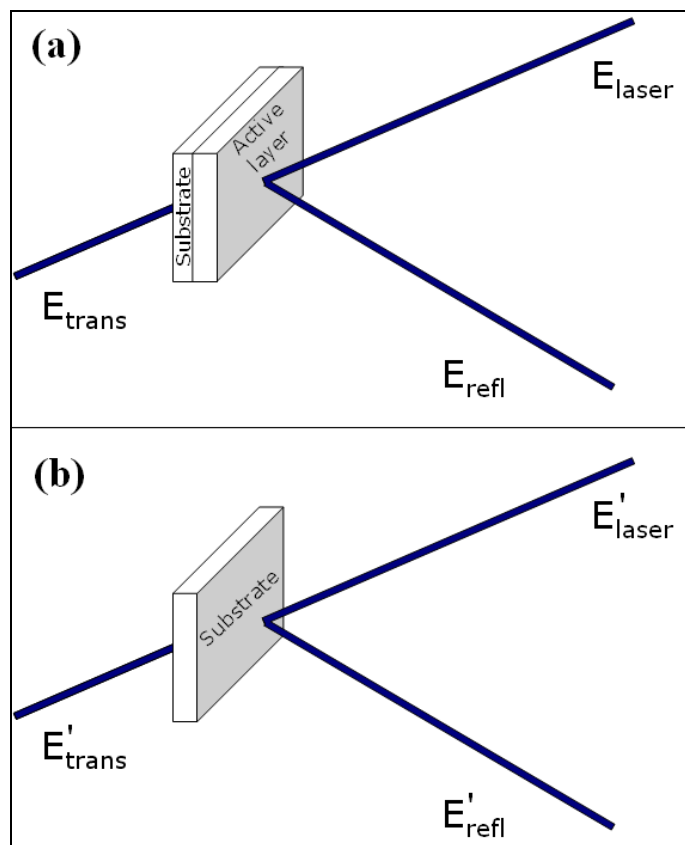


Figure 1.2. Schema of absorption, transmission and reflection energy in a case of (a) a thin film and (b) of a substrate.

We measured all these values with a power-meter calibrated at 365nm. Knowing the wavelength of the laser, we deduced the absorbed photon flux. The ratio between the emitted and the absorbed photon fluxes yields the external quantum efficiency of the film.

The first step of our measurements was the calibration of the spectrometer with a visible LED. In our case, we used a red LED. After measuring the power emitted at a know intensity, we made the spectrum of the LED at the spectrometer. On **Figure 1.3**, we show the spectrum of the LED. Before making a relation between the area of the spectrum and the power emitted, we corrected the spectrum by the fact that no all the light emitted enter in the spectrometer. In fact, the focusing optics is collecting the light only in an angle of 10° in front of our emitting device. In the case of our LED, it means that only 90% of the total emitting power is entering into our spectrometer. So we multiplied our measured emitted power by 0.9.

In our case, we measured a power of 9nW corresponding to an area of 2.1×10^6 for our spectrometer.

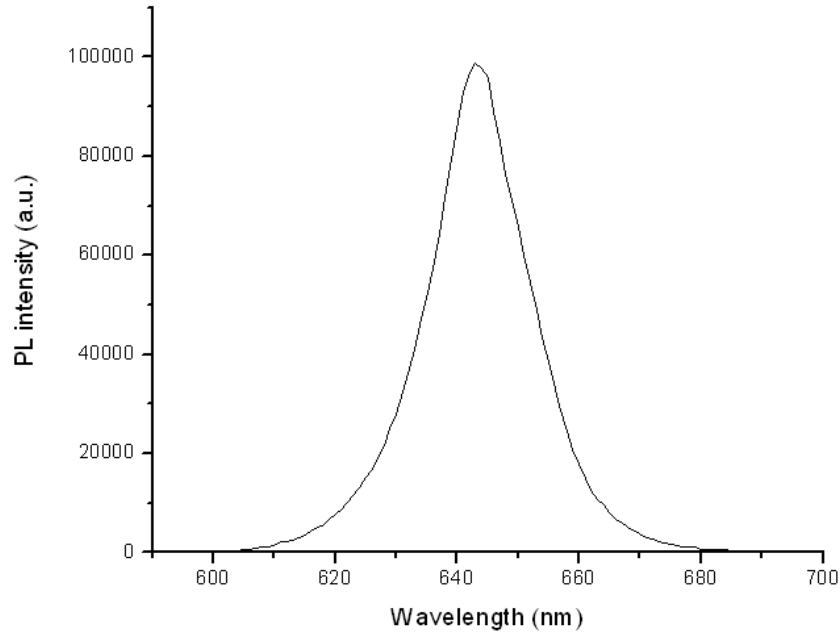


Figure 1.3. Luminescence Spectrum of red LED.

The first measurement of External Quantum Efficiency that we made was on colloidal suspension of Silicon Nanocrystals. Samples of *n*- or *p*-type Si that have been electrochemically etched to form porous Si can be ultrasonically dispersed into methylene chloride, acetonitrile, methanol, toluene, or water solvents, forming a suspension of fine Si particles that is luminescent, due to quantum confinement effects. In our case, these samples will be use as a reference and will help us to understand if our measurements are relevant or not. We measured first the power absorbed by the substrate of our suspension, in our case ethanol. As for a thin film in figure 3.8, we measured the energy of the laser incident on our sample, the energy reflected by our sample and the energy transmitted by our sample. The difference between the first one and the two others gave us the energy absorbed by our substrate (E'_{abs}). We made the same measurements for a sample including our silicon nanocrystals and we can deduce the energy absorbed by our nanocrystals using equation 1.4.

$$E_{abs} = E_{laser} - E_{trans} - E_{refl} - E'_{abs} \quad \text{Eq. 1.4}$$

Now, we measure the energy emitted by these nanocrystals. We made a spectrum in the same conditions as the measurements before. **Figure 1.4** represents the spectrum of various colloidal suspensions of Silicon Nanocrystals with different concentration of nanocrystals.

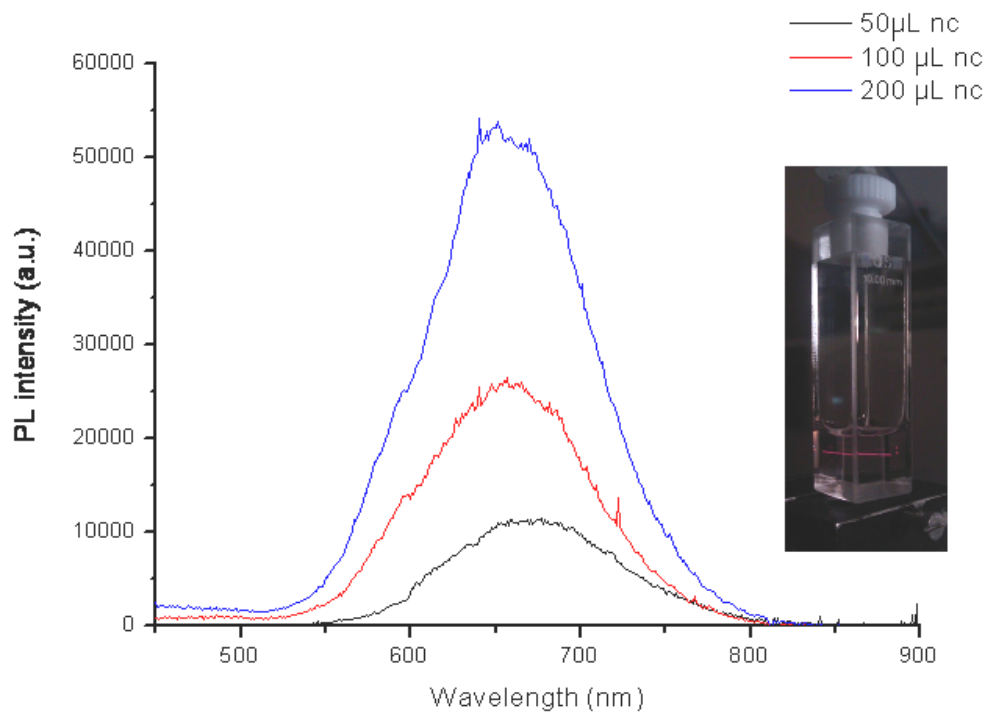


Figure 1.4. PL spectra of colloidal suspension of Si_{nc} in ethanol at different concentration. (inset) Photography of the sample under UV laser beam.

Before correlated these spectra with certain energy, we should measure how many emitted light is going into our spectrometer. We supposed that our nanocrystals in suspension have a spherical emission. It means that only 0,88% of the light emitted by our sample is going inside our spectrometer. We should by consequence correct the area of our spectrum by this number. We made multiples measurements with various concentrations of nanocrystals, to have a better value of our external quantum efficiency. **Table 1.1** resumed the results.

Table 1.1. External Quantum Efficiency of colloidal suspension of Si_{ncs} in function of their concentration

Concentration of nanocrystals (μL) in 1mL ethanol solution	E_{abs} (μW)	$E_{emitted}$ (μW)	E.Q.E.
50 μL	14,7	0,7	4,6%
100 μL	31,8	1,4	4.3%
200 μL	53,9	2,8	5,2%

To conclude, we found an external Quantum Efficiency around 5% for this colloidal suspension of Silicon Nanocrystals. This result is very close to various results found in the literature, which oscillate between 1% and 10% [L.B. Ma, 2006, D. Jurbergs, 2006].

The use of a spectrometer in these efficiency measurements provides several advantages over methods described previously in the literature. Absorption and PL are measured simultaneously, so the effects of sample degradation are minimized. We consider that the major advantage of this method is that it provides a means of determining quantum efficiencies for highly luminescent samples in a very fast way. With this method, we are able to make a reliable measurement of the luminescent properties of the sample. The method therefore greatly extends the range of materials which can be investigated.

After the demonstration of the procedure, we can no measure the external quantum efficiency of our SiOC samples. To verify that our substrate is not influencing our luminescence measurements, we made a spectrum of it to verify that it has no luminescence in the luminescence range of our SiOC samples.

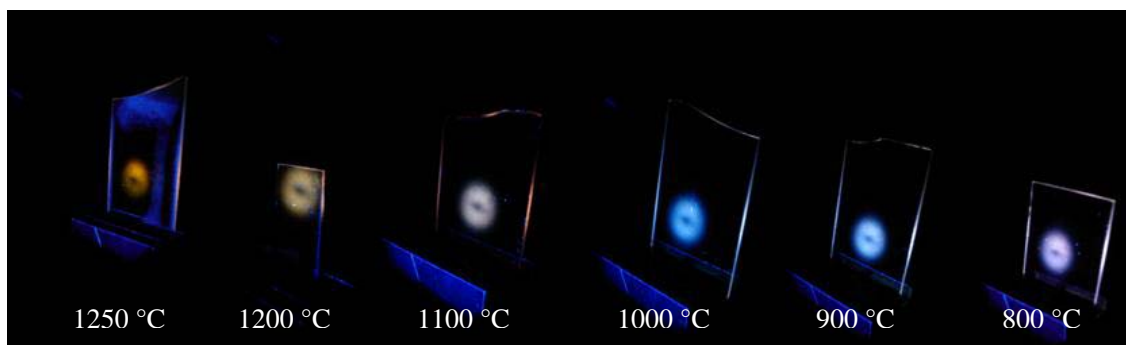


Figure 1.5. Photograph of the T^H films pyrolysed from 800 °C to 1250 °C under UV laser excitation.

We found a value of about 5% for the film annealed at 1200°C. This value is encouraging as it compares to the best results reported in the literature about Si nanomaterials so far [C. Turquat, 2001; J. C. Pivin M. S.-V., 1998].

Photographs of the T^H films pyrolyzed at different temperatures from 800 to 1250°C under blue light excitation are shown in **Figure 1.5**. The strong emission from the edges of the samples is caused by waveguide effects of the quartz substrate. The colours of the visible photoluminescence range from UV-violet for 800 °C to blue at 1000 °C and yellow-orange for 1250 °C. At 1250 °C the substrate starts to show an opaque appearance which could be indicative of thermal stability-related problems and can be the reason of the sudden PL intensity decrease at this temperature.

The external quantum efficiency of the T^H films pyrolysed at 1200 °C was 11.5 %; whereas, T^HD^H2 films showed 5% efficiency. Since T^HD^H1 films did not show noticeable luminescence, they had relatively low quantum efficiency. These external quantum efficiency values are very promising and make SiOC a potential material for LED applications.

II. Lifetime measurements

The time-resolved photoluminescence (TRPL) technique is a contactless method to characterize recombination and transport in photovoltaic materials. TRPL is measured by exciting luminescence from a sample with a pulsed light source, and then measuring the subsequent decay in photoluminescence (PL) as a function of time. A wide variety of experimental configurations can accomplish this. Most experiments excite the sample with a pulsed laser source, and detect the PL with a photodiode, streak camera, or photomultiplier tube (PMT) set up for upconversion or single-photon counting. The system response time, wavelength range, sensitivity, operational difficulty, and cost vary widely for each configuration.

The temporal behaviour of the observed PL from porous Si, following a short excitation pulse, exhibits a “stretched exponential” decay line shape explained in Equation 2.1 [L. Pavesi, 1994; J. Linnros, 1999]:

$$I(t) = I_0 \exp\left[-\left(\frac{t}{\tau}\right)^\beta\right] \quad \text{Eq. 2.1}$$

where $I(t)$ and I_0 are the PL intensity during the decay and at $t = 0$, respectively. Decay time τ and dispersion factor β are characteristic *wavelength-dependent* constants of the decay, β being related to the curvature of the decay. In general, $\beta < 1$ represents a distribution of independent single exponentials (from nanocrystals of a certain size as determined by the observation wavelength) with different lifetimes. Pavesi et. al. [L. Pavesi, 1994] argues that the stretched decay line shape follows, generally, from a disordered system of interconnected crystals in which *migration of excitons* is possible, accompanied by capture and delayed release of excitons. The observed PL intensity is a probe of the decaying carrier concentration where nonradiative recombination is believed to dominate at room temperature [V. Grivickas, 1995].

Applying this model to a colloidal suspension of Si nanocrystals embedded in water, samples that we used before to test our measurements of external quantum efficiency, one would argue that a *single exponential decay* would be expected as such a system

would be equivalent, in a first approximation, to a system of isolated luminescent centers surrounded by infinite oxide barriers.

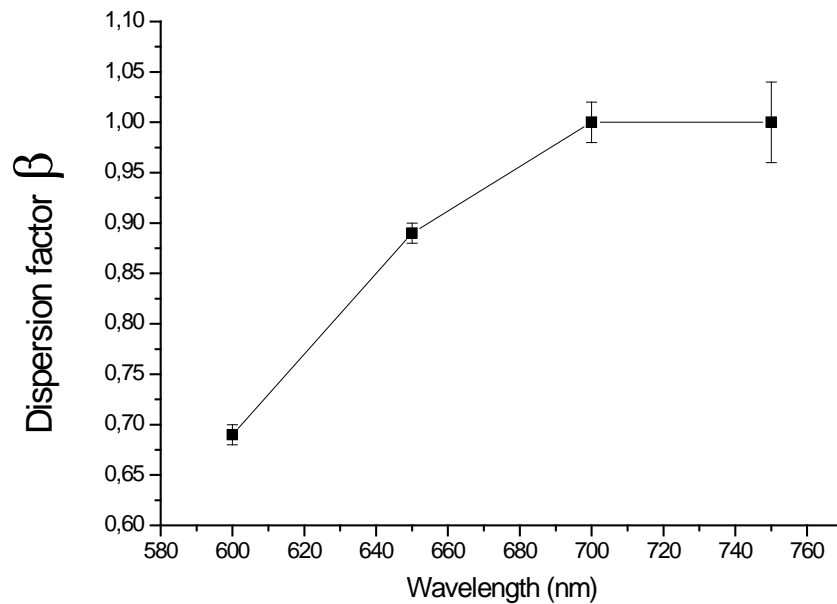


Figure 2.1. Dispersion factor β extracted from PL decay data by fitting a stretched exponential line shape to the data for a colloidal suspension of Si nanocrystals

As we can see on **Figure 2.1**, the “stretched exponential” model yielded higher β values for decreasing nonradiative lifetimes. In other words, the decay parameter β signifies the amount of exciton diffusion and trapping in the system in relation to a characteristic recombination time, $\beta=1$ being characteristic of a system behaving as isolated crystals. Indeed, this behaviour should be observed for low nanocrystal densities and, at high densities, for some smaller fraction of crystals being isolated. Comparing with our experiment, we found very similar results, with a β value very close to one when we are in a configuration of smaller fraction of Silicon crystals being isolated.

Examples of time resolved decays of the dominant emission (550nm) from a SiOC sample at low (800°C) and high temperature annealing (1200°C) are displayed in **Figure 2.2**. The solid lines show the “stretched exponential” fitting results to the experimental data. Two decay time constants of 13.9 and 16.2 ns were obtained. It

should be noted that the decay times of about 16 ns are at least one order of magnitude slower than thus found in the literature.

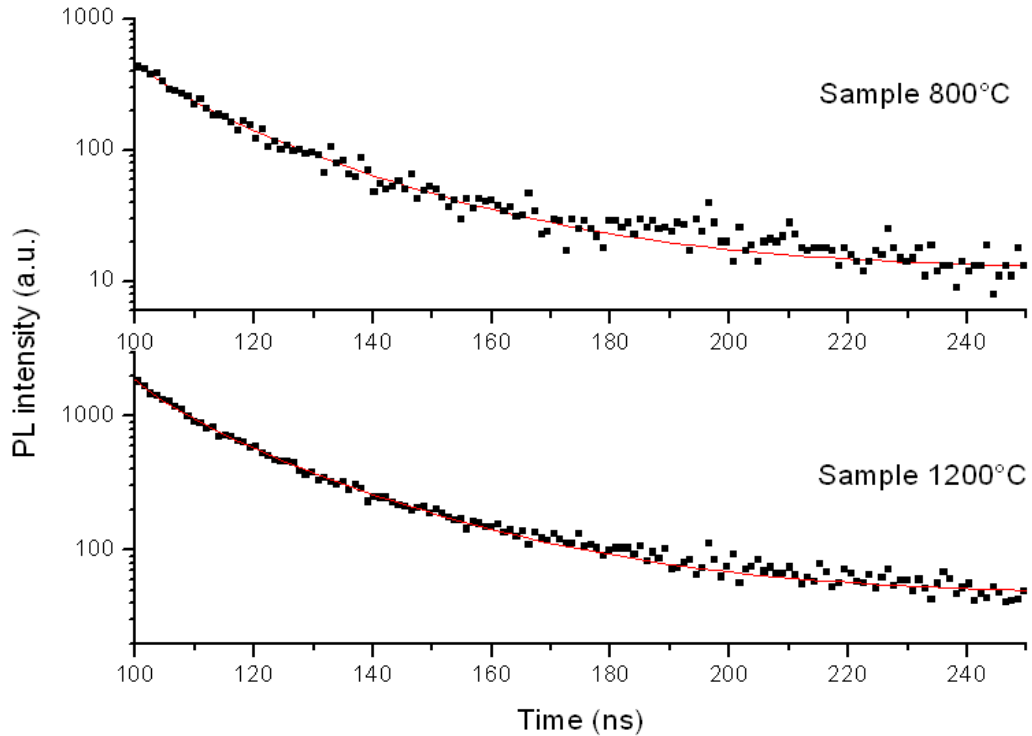


Figure 2.2. Time resolved PL decays curves of SiOC samples annealed at 800°C and 1200°C. Red solid lines are stretched exponential fits to the decays.

To have a better value of our lifetime, an average lifetime $\langle \tau \rangle$ was calculated with Equation 2.2, where Γ represents the gamma function [C. P. Lindsey, 1980].

$$\langle \tau \rangle = \frac{\tau}{\beta} \Gamma\left(\frac{1}{\beta}\right) \quad \text{Eq. 2.2}$$

Low β values indicate a highly skewed distribution of rates, and thus the average lifetimes can be up to an order of magnitude greater than τ . The best-fit parameters τ and β were determined and the corresponding average lifetime calculated (**Table 2.1**).

Table 2.1. τ , β and the corresponding average lifetime $\langle \tau \rangle$ calculated with equation 6.

Sample	τ	β	$\langle \tau \rangle$
800°C	13.9	0.76	16.4
1200°C	16.2	0.76	16.8

The observed decay time is in the order of that for known bands of SiO₂. In fact, for the 2.2 eV band, the decay times are around 25 ns [I. A. Movtchan, 1996]. Another very important observation is that we did not see any difference between sample annealed at 800°C and 1200°C, whereas the luminescence of the two samples is very different, and as we suppose the SiC contents also. But as SiC lifetime is in the order of the nanoseconds [S. J. Xu, 2000], and as we are working in a SiO₂ matrix with a higher lifetime, it is impossible for us to confirm the presence of SiC nanocrystals in our sample with this method.

Finally, this method confirms the fact that we do not have any presence of Si nanocrystals in our sample. As everybody know, lifetime of Si nanocrystals are in the order of 10-150 μ s [J. Linnros, 1999], which is much slower than the one that we found in our samples. It confirms our hypothesis about the origin of the photoluminescence due to interaction between SiC and C clusters.

Acknowledgement

This Research is supported by European Community FP6 through MCRTN-019601, PolyCerNet. Three years has passed with many memories of the schools, conferences, courses and joy. It was a pleasure for me to work, discuss and travel together with friends in the network. I would like to especially thank to Dr. Florence Babonneau, Dr. Cristina Fernandez Martin, Dr. Amir Hossein Tavakoli and Dr. Tomáš Plachký for their kind support.

Some optical analyses and AFM measurements were done in Physics department in University of Trento by Dr. Romain Guider. Therefore, I am pleased to acknowledge him for his patience and Prof. Lorenzo Pavesi for helpful discussions. Meanwhile, I am grateful to Dr. Mariangela Fedel for FE-SEM analysis, Dr. Cedric Boissiere and Dr. Laurent Binet for Ellipsometer & EPR measurements, Dr. Emanuela Callone for NMR, Dr. Mirco Dincau for XRD, Guisti Giovanni for some SiOCN analyses.

I would like to express my sincere thanks to my friends and colleagues in ceramic laboratory for their consideration. Especially, I feel lucky to work together with some talented researcher friends like Dr. Philippe Dibandjo, Dr. Raquel De La Pena Alonso, Dr. Aravind Ramaswamy and Dr. Marco Cologna.

I owe much to my tutor Prof. Gian Domenico Sorarù. It was a great pleasure for me to work with him and know him personally. He was not only an encouraging advisor but also a very kind friend to listen to my daily problems. I particularly appreciated his energy to teach me even the basic concepts of chemistry and his time for valuable discussions.

Clearly, I would like to acknowledge the loving support of my family and friends. Many thanks to my dear friends Anna Rita Contino, Dr. Lorenzo Tognana and Vincenzo Catania, who made me feel like at home in Italy. In this three years period, I almost have no memories without them. They supported me continuously and brought happiness to my life. Meanwhile, my mother, my father, my brother and Gamze were always behind me and always been a source of support in many forms. This work could

not been written without their encouragement. Finally, this work is dedicated to my loving grandmother and grandfather, whom I lost during my doctorate study. It was an honor for me to be their granddaughter.

Curriculum Vitae

SCIENTIFIC BACKGROUND

PhD: Department of Materials Engineering, University of Trento, Trento, Italy (2006-2010)

Dissertation: “Synthesis and Characterization of Nanostructured SiOC Thin Films

Containing SiC_n and Si_n”

MSc: Department of Metallurgical and Materials Engineering, Middle East Technical University, Ankara, Turkey (2005-2006)

Thesis: “Characterization of Maghemite Thin Films Prepared by Sol-Gel Processing”

BSc: Department of Metallurgical and Materials Engineering, Middle East Technical University, Ankara, Turkey (2001-2005)

EXPERIENCE

Early Stage Researcher (ESR) in Marie Curie Research Training Network on Tailored Multifunctional Polymer-Derived Nanoceramics (PolyCerNet), Trento, Italy (2006-2009)

Project Assistant in TÜBİTAK (The Scientific and Technological Research Council of Turkey), Ankara, Turkey (2005-2006)

TEACHING EXPERIENCE

Assistant supervisor of graduate student Giusti Giovanni on his thesis “Characterization of ceramic films for optical devices made from polymer precursor”

PUBLICATIONS/PROCEEDINGS/BOOK CHAPTERS

A. Karakuscu and G. D. Sorarù “Si and SiC nanocrystals by pyrolysis of sol-gel-derived precursors” Silicon Nanocrystals, ed by Pavesi, Turan, Wiley-VCH (2010)

A. Karakuscu, R. Guider, L. Pavesi and G. D. Sorarù “White luminescence from sol-gel derived SiOC thin films” Journal of American Ceramic Society 92 (2009) 2969–2974

A. Quaranta, **A. Karakuscu** and G. D. Soraru “Optical Properties” in: Polymer Derived Ceramics, ed by P. Colombo, R. Riedel, G.D. Sorarù and A. Kleebe, DEStech Publications (2009) 253-261

A. Karakuscu, R. Guider, L. Pavesi and G. D. Sorarù “Synthesis and Optical Properties of SiC_n/SiO₂ Nanocomposite Thin Films” Nanostructured Materials and Nanotechnology II, Ceramic Engineering and Science Proceedings ed by Mathur S. and Singh M., American Ceramic Society, **29** (2008) 85-91

A. Karakuscu and M. Özenbas, “Characterization of iron oxide thin films prepared by sol-gel processing” Journal of Nanoscience and Nanotechnology, **8** (2008) 901-906

PRESENTATIONS

A. Karakuscu, R. Guider, L. Pavesi and G. D. Sorarù "SiCO Thin Films: a Novel LED Material" 33rd International Conference & Exposition on Advanced Ceramics and Composites, Daytona Beach, USA (2009)

A. Karakuscu, R. Guider, L. Pavesi and G. D. Sorarù "Intense white luminescence from SiOC ceramics containing Si, C and SiC clusters" 8th Pacific Rim Conference on Ceramic and Glass Technology, Vancouver, Canada (2009)

M. Affatigato, **A. Karakuscu**, A. Marquardt and G. D. Sorarù “Laser Ionization Time of Flight Mass Spectrometry Study of Silicon Oxycarbide Glasses” 8th Pacific Rim Conference on Ceramic and Glass Technology, Vancouver, Canada (2009)

A. Karakuscu, R. Guider, L. Pavesi and G. D. Sorarù “Synthesis and Optical Properties of SiC_n/SiO₂ Nanocomposite Thin Films”, 32nd International Conference & Exposition on Advanced Ceramics and Composites, Daytona Beach, USA (2008)

A. Karakuscu, R. Guider, L. Pavesi and G. D. Sorarù “Compositional Effects on Optical Properties of SiOC Thin Films” 2nd Forum Nazionale dei Giovani Ricercatori di Scienza e Ingegneria dei materiali, Genova, Italy (2008)

A. Karakuscu, R. Guider, L. Pavesi and G. D. Sorarù “Optical Properties of Sol-Gel Derived SiOC Thin Films” VI Workshop Italiano Sol-Gel, Lecce, Italy (2008)

A. Karakuscu, R. Guider, L. Pavesi and G. D. Sorarù “Synthesis and Optical Properties of SiBOC Thin Films” 8th Conference on Solid State Chemistry, Bratislava, Slovakia (2008)

R. Guider, **A. Karakuscu**, L. Pavesi and G. D. Sorarù “Compositionnal Effects on Optical Properties of SiOC Thin Films” 8th Conference on Solid State Chemistry, Bratislava, Slovakia (2008)

POSTERS

A. Karakuscu, R. Guider, L. Pavesi and G. D. Sorarù “Synthesis and Optical Properties of (SiC_{nc}+Si_{nc})/SiO₂ Nanocomposite Thin Films” 2nd Forum International Congress on Ceramics, Verona, Italy (2008)

A. Karakuscu, R. Guider, L. Pavesi and G. D. Sorarù “Luminescence of SiOC Thin Films and Their Possible Applications as LED” Marie Curie Conference, Barcelona, Spain (2008)

R. Guider, **A. Karakuscu**, L. Pavesi and G. D. Sorarù, “Compositionnal effects on optical properties of SiOC thin films” SEDWAL (Sensitized Err doped waveguide amplifier/laser) workshop, Levico Terme, Italy (2008)

M. Özenbas, **A. Karakuscu** “Characterization of iron oxide thin films prepared by sol-gel processing” Third Seeheim Conference on Magnetism, Frankfurt, Germany (2007)

A. Karakuscu, M. Özenbas “Characterization of iron oxide thin films prepared by sol-gel processing” 13th International Metallurgy-Materials Congress, Istanbul, Turkey (2006)

M. Özenbas, **A. Karakuscu** “Characterization of iron oxide thin films prepared by sol-gel processing” Materials Research Society Fall Meeting, Boston, USA (2006)

CERTIFICATES AND PARTICIPATION IN SCHOOLS

ISGS -Summer School 2008: Sol-Gel in Small Dimensions: Nanoparticles and Thin Films, Alghero (Sardinia), Italy (2008)

PolyCerNet Rheology School Bucharest - Iassy, Romania (2007)

International/European Welding Engineering Certificate, METU Welding Technology Center/SLV München (2005)